ABSTRACT

LIU, XIAOMING. Numerical Simulations of Gulf Stream Meanders and Eddies and Their Effects on the Cross-Shelf Transport off the Carolina Coast. (Under the direction of Dr. Lian Xie.)

Gulf Stream meanders and eddies off the Carolina coast are studied using an ocean numerical model. Numerical simulation results show that the isobathic curvature in the vicinity of the Charleston Bump has great effect on the development and evolution of Gulf Stream meanders and eddies, and the formation of the Charleston Trough, a Gulf Stream meander that appears as a low pressure or depressed water surface region downstream of the bump, is the result of the combined effect of the Charleston Bump and the isobathic curvature in the region. The isobathic curvature plays a major role in enhancing the baroclinic and barotropic energy transfer rates, whereas the bump provided a localized mechanism to maximize the energy transfer rate downstream of the Charleston Bump.

The effects of the Gulf Stream meanders and eddies on the cross-shelf transport near the Carolina coast are also studied in the ocean numerical model. There are two factors that affect the ocean circulations on the continental shelf off the North and South Carolina coast: wind and the Gulf Stream meanders and eddies. It is concluded that the combination of the wind effect and the effect of the Gulf Stream meanders and eddies caused the red tide bloom event in the North Carolina near shore waters in October 1987. Neither wind alone nor the Gulf Stream meander/eddy alone is sufficient to transport the passive tracer to the near-shore area.

NUMERICAL SIMULATIONS OF GULF STREAM MEANDERS AND EDDIES AND THEIR EFFECTS ON THE CROSS-SHELF TRANSPORT OFF THE CAROLINA COAST

by
XIAOMING LIU

A dissertation submitted to
the Graduate Faculty of North Carolina State University
in partial fulfillment of the requirements for the
Degree of Doctor of Philosophy

MARINE, EARTH AND ATMOSPHERIC SCIENCES

Raleigh

2006

APPROVED BY:

Dr. Leonard J. Pietrafesa	**Dr. John M. Morrison**
Dr. Daniel L. Kamykowski	**Dr. Lian Xie** **(Chair of Advisory Committee)**

BIOGRAPHY

Xiaoming Liu was born in Linshu county, Shandong province, People's Republic of China. He Graduated from No. 1 Linshu High School in 1987. He attended Ocean University of Qingdao at Qingdao, China, receiving Bachelor of Science degree in Physical Oceanography in 1991, and Master of Science degree in Environmental Oceanography in 1994. From 1995 to 1998, he studied at the Department of Marine, Earth and Atmosphere sciences, North Carolina State University, Raleigh, NC, and received a Master of Science degree in Marine Science. From 1998 to 2000, He studied in the Department of Computer Science, Dalhousie University, Halifax, Nova Scotia, Canada, and received a degree of Master of Computer Science in May 2000.

ACKNOWLEDGMENTS

I wish to thank Dr. Lian Xie, the chair of the advisory committee, for his guidance, support and encouragement on this research. I appreciate that Dr. Xie provides me a very flexible research environment that is suitable for my research interests and strength. I always have freedom to explore some new ideas with available resources. I also benefit a lot from his methodology in ocean numerical modeling, his many thoughtful ideas that keep my research topic in step with current active research in this area.

I want to express my appreciation to the advisory committee members, Dr. Leonard Pietrafesa, Dr. John Morrison and Dr. Daniel Kamykowski for their support, thoughtful input and advice on this research. They are also very helpful in providing me with various resources for the study. Special thanks for Dr. Morrison for his endless support and kindness since I first came to Raleigh from China in September 1995.

I also want to thank Dr. Gerald Janowitz, Dr. Fred Semazzi, Dr. Xiang San Liang and Dr. Alan Wallcraft for their help in this study. Thank all people in the Coastal Fluid Dynamics Lab, Dr. Machuan Peng, Dr. Shaowu Bao, Dr. Jing Lin, Dr. Shiqiu Peng, Dr. Tingzhuang Yan, Dr. Changlong Guan, Xuejin Zhang, Huiqing Liu, Kristen Foley, Binyu Wang, Meng Xia, Peng Su, Joshua Palmer, Meredith Croke and Yanyun Liu.

Special thanks for my wife, Changjian Chen, and my parents for their support, encouragement and patience.

TABLE OF CONTENTS

LIST OF TABLES ..... **vi**

LIST OF FIGURES ..... **vii**

CHAPTER 1 INTRODUCTION **1**

1. Background 1
2. Brief Description of the Research Topics 4
2.1 Sensitivity Test 4
2.2 Bathymetry Effect on the Gulf Stream Meanders and Eddies 5
2.3 Cross-shelf and Along-shelf Transport 6
3. Organization of the Dissertation 7
4. References 7

CHAPTER 2 DATA AND OCEAN NUMERICAL MODEL **10**

1. Data 10
1.1 ECMWF 40-year Reanalysis Data 10
1.2 North America Regional Reanalysis Data 11
1.3 COADS Climatology Data 12
1.4 Levitus Ocean Data 12
1.5 ETOP02 13
2. Ocean Numerical Model 13
3. References 15

CHAPTER 3 SENSITIVITY TEST **16**

1. Objectives and Tests 16
2. Results 18
2.1 0.54°, 0.45°, 0.36°, 0.27°, 0.18° simulations 18
2.2 0.06° resolution simulation 20
2.3 0.027° simulation 21
2.4 Sensitivity to High-frequency Atmospheric Forcing 22
3. Conclusions 23
4. References 24

CHAPTER 4 EFFECT OF BATHYMETRY CURVATURE ON THE GULF STREAM INSTABILITY IN THE VICINITY OF THE CHARLESTON BUMP **52**

1. Introduction 52
2. Brief Description of the Numerical Model and Numerical Experiments 57
3. Results 59
3.1 Manifestation of Gulf Stream meanders depicted by SST 59
3.2 Temperature anomaly at 125 meter depth 60
4. Diagnostics of Energy Conversion 62
4.1 Energy Analysis using Brooks and Niiler (1977) Energy Equation for Case IV 63
4.2 Analysis with MS-EVA for Case IV 66
4.3 MS-EVA analysis for Cases II and III 71
5. Discussions and Conclusions 73
6. References 76

CHAPTER 5 NUMERICAL SIMULATION OF THE NUMERICAL SIMULATION OF THE TRANSPORT OF KARENIA BREVIS CELLS FROM GULF OF MEXICO TO NORTH CAROLINA COAST USING PASSIVE TRACER 100

1. INTRODUCTION 100
2. BACKGROUND OF PHYSICAL OCEANOGRAPHY OF STUDY AREA 103
2.1 SOUTH ATLANTIC BIGHT 103
2.2 WEST FLORIDA SHELF 106
3. NUMERICAL MODEL, WIND FORCING AND SIMULATIONS 109
4. RESULTS 113
4.1 RESULTS OF SIMULATIONS IN THE OUTER DOMAIN 113
4.2 RESULTS OF THE INTERMEDIATE DOMAIN SIMULATION 116
4.3 RESULTS OF THE INNER DOMAIN SIMULATIONS 118
5. SUMMARY AND CONCLUSIONS 123
6. REFERENCES 124

CHAPTER 6 FUTURE WORK 156

1. DATA ASSIMILATION 156
2. BIOLOGICAL MODELING 157
3. OCEAN PREDICTION 159
4. REFERENCES 160

LIST OF TABLES

CHAPTER 4

1. LIST OF NUMERICAL SIMULATIONS 81

CHAPTER 5

1. LIST OF NUMERICAL SIMULATIONS 112

LIST OF FIGURES

CHAPTER 3

1. MIXED LAYER VELOCITY IN (A) 0.54° (B) 0.45° (C) 0.36° (D) 0.27° (E) 0.18° SIMULATIONS 25
2. MIXED LAYER TEMPERATURE IN (A) 0.54° (B) 0.45° (C) 0.36° (D) 0.27° (E) 0.18° SIMULATIONS..... 29
3. SIMULATED (A AND B) AND OBSERVED (C) TEMPERATURE VERTICAL CROSS-SECTION AT 27°N 33
4. SIMULATED AND OBSERVED GULF STREAM TRANSPORT AT 27°N..... 34
5. HORIZONTAL VELOCITY IN 0.06 DEGREE SIMULATION 35
6. SEA SURFACE TEMPERATURE IN 0.06 DEGREE SIMULATION..... 36
7. MIXED-LAYER SST IN THE 0.08 DEGREE SIMULATION ON NOV. 11 37
8. MIXED-LAYER SST IN THE 0.027 DEGREE SIMULATION ON NOV. 11 38
9. SST OF 0.027° SIMULATION FROM OCT. 30 TO NOV. 15..... 39
10. COMPARISON OF SATELLITE SST IMAGE AND SIMULATED MIXED LAYER SST ON FEB. 10, 1996..... 42
11. COMPARISON OF SATELLITE SST IMAGE AND SIMULATED MIXED LAYER SST ON APRIL 4, 1996 43
12. COMPARISON OF SATELLITE SST IMAGE AND SIMULATED MIXED LAYER SST ON APRIL 11, 1996 44
13. COMPARISON OF SATELLITE SST IMAGE AND SIMULATED MIXED LAYER SST ON APRIL 16, 1996 45
14. COMPARISON OF SATELLITE SST IMAGE AND SIMULATED MIXED LAYER SST ON APRIL 22, 1996 46
15. COMPARISON OF SATELLITE SST IMAGE AND SIMULATED MIXED LAYER SST ON MAY 1, 1996..... 47
16. COMPARISON OF SATELLITE SST IMAGE AND SIMULATED MIXED LAYER SST ON MAY 5, 1996..... 48
17. MODIS SST OF SAB FROM JAN. 12 TO JAN. 17, 2004..... 49
18. SST OF NAOPS WITHOUT NESTING..... 50
19. SST OF 0.027-DEGREE NESTED NAOPS SIMULATION..... 51

CHAPTER 4

1. BATHYMETRY OF SOUTH ATLANTIC BIGHT FROM ETOPO2 82
2. MODIS SST OF SAB FROM JANUARY 12 TO JANUARY 17, 2004. AN EDDY ON THE WEST EDGE OF THE GULF STREAM AT 32°N IS AMPLIFIED 83

3. Bathymetry contour: a) small curvature without a bump; b) small curvature with a bump; c) large curvature without a bump; d. large curvature with a bump (units: m) 84

4. SST (7.5 m depth) of January 23, 25 and 27 for Case I (panel I a-c), Case II (panel II a-c), Case III (panel III a-c) and Case IV (panel IV a-c) 85

5. Water temperature anomaly (TA) at 125 meter depth of January 23, 25 and 27 for Case I (panel I a-c), Case II (panel II a-c), Case III (panel III a-c) and Case IV (panel IV a-c)..... 86

6. a) x-component of density flux $\overline{\rho' u'}$; b) y-component of density flux $\overline{\rho' v'}$ of Case IV at 125 meter depth (units: Kg $m^{-2}s^{-1}$) 87

7. Momentum fluxes: a) $\overline{u'v'}$; b) $\overline{u'u'}$; and c) $\overline{v'v'}$ of Case IV at 125 meter depth..... 88

8. Baroclinic transfer rate of Case IV at 7.5, 25, 47.5, 80, 125, 190, 305, 495, and 760 meter depth. (units: m^2s^{-3}) 89

9. Barotropic transfer rate of simualtion IV at 7.5, 25, 47.5, 80, 125, 190, 305, 495, and 760 meter depth. (units: m^2s^{-3})..... 90

10. Eddy energy budget of Case IV at 25 m depth: a) total rate change of energy; b) baroclinic transfer rate; c) barotropic transfer rate; d) pressure work. (units: m^2s^{-3}) 91

11. Eddy energy budget of Case IV at 125 m depth: a) total rate change of energy; b) baroclinic transfer rate; c) barotropic transfer rate; d) pressure work. (units: m^2s^{-3}) 92

12. MS-EVA baroclinic transfer rate of Case IV on January 27 at 25, 47.5, 80, 125, 190, 305 m depth (panel a 1-6 respectively) and barotropic transfer rate of Case IV on January 27 at 25, 47.5, 80, 125, 190, 305 m depth (panel b 1-6 respectively) (units: m^2s^{-3}) 93

13. Baroclinic transfer rate of Case IV at 125 m depth from January 23 to 31 (units: m^2s^{-3}). Panels a) through h) correspond to January 23 through 31, respectively 94

14. Barotropic transfer rate of Case IV at 125 m depth from January 23 to 31 (units: m^2s^{-3}). Panels a) through h) correspond to January 23 through 31, respectively 95

15. a) Eddy available potential energy (APE, units: m^2s^{-2}); b) APE budget (units: m^2s^{-3}) at (77.9°W, 32.2°N) 96

16. a) Eddy kinetic energy (KE, units: m^2s^{-2}); b) Eddy kinetic energy budget (units: m^2s^{-3}) at (77.9°W, 32.2°N) 97

17. Baroclinic and barotropic transfer rates at the 125 m depth on January 25 of Cases II and III: (a) barotropic transfer rate of Case II; (b) baroclinic transfer rate of Case II; (c) barotropic transfer rate of Case III; (d) baroclinic transfer rate of Case III..... 98

18. Potential vorticity balance in Case I (panel a) and Case III (panel b)..... 99

CHAPTER 5

1. Sea Surface Height in Simulation I for September 11, 15, 20 and 25 respectively 132
2. Initial condition of passive tracers 135
3. Passive tracer concentrations on September 17, 23, 29 and October 5, 11, 17 136
4. Wind on September 16 from (a) NARR and (b) ECMWF 137
5. Passive tracer concentration in (a) Simulation I, and (b) Simulation II 138
6. NARR monthly mean wind for October 1987 139
7. SSH on October 7, 12, 18 and 23 in Simulation III 140
8. SST on October 7, 12, 18 and 23 in Simulation III 141
9. Passive tracer concentration on October 7, 12, 18 and 23 in Simulation III 142
10. SSH on October 21, 23, 25, 27, 29 and 31 in Simulation IV 143
11. SST on October 21, 23, 25, 27, 29 and 31 in Simulation IV 144
12. Passive tracer concentration on October 21, 23, 25, 27, 29 and 31 in Simulation IV 145
13. SSH on October 21, 23, 25, 27, 29 and 31 in Simulation V 146
14. SST on October 21, 23, 25, 27, 29 and 31 in Simulation V 147
15. Passive tracer concentration on October 21, 23, 25, 27, 29 and 31 in Simulation V 148
16. SSH on October 21, 23, 25, 27, 29 and 31 in Simulation VI 149
17. SST on October 21, 23, 25, 27, 29 and 31 in Simulation VI 150
18. Passive tracer concentration on October 21, 23, 25, 27, 29 and 31 in Simulation VI 151
19. SSH on October 21, 23, 25, 27, 29 and 31 in Simulation VII 152
20. SST on October 21, 23, 25, 27, 29 and 31 in Simulation VII 153
21. Passive tracer concentration on October 21, 23, 25, 27, 29 and 31 in Simulation VII 154
22. Mixed-layer horizontal velocity on October 29, 1987 in Simulation IV 155

Chapter 1

Introduction

1. Background

On October 31, 1987, shelf waters in the Onslow Bay, North Carolina became infested with *Karenia Brevis* (formerly *Gymnodinium Breve*) red tide bloom, which continued for 4-5 months. Shellfish such as clams, scallops and oysters became infected and were rendered inedible. Shellfishing was banned from Avon to Long Beach. Beachcombers felt burning eyes and lungs, and became nauseous and dizzy. This bloom resulted in 48 documented cases of neurotoxic shellfish poisoning, closure of up to 1480 km^2 of North Carolina waters to shellfish harvesting, and economic losses exceeding $24 million (Tester and Fowler 1990). This red tide bloom occurred at Onslow Bay, North Carolina is the first record of *K. Brevis* north of Jacksonville, Florida (Tester et. al, 1991).

Pietrafesa et al. (1988) reported that the dinoflagelate found off the coast of North Carolina in the 1987 red tide bloom event was accompanied by marine blue-green algae indigenous to subtropical waters. It became suspicious that the dinoflagelate was transported to the North Carolina from the south. They analyzed the National Weather Service atmospheric pressure map, and found that the winds associated with the weather system on the west Florida shelf were affecting an offshore transport of surface waters from the shelf into the Loop Current during a red tide breakout event off the coast of Naples, Florida. Pietrafesa et al (1988) also analyzed the sea surface temperature imagery off the North Carolina coast collected via the NOAA-9 Advanced Very High Resolution Radiometer (AVHRR) sensor, and found that there were frontal warm filaments

associated with Gulf Stream meanders and eddies off the North Carolina coast. The wind field as observed at the Cape Hatteras Lighthouse station was then further analyzed and it was found that from Oct. 9 through Nov. 9, the wind velocity was directed towards the southwest to south sector. The observed wind fields were then applied to Ekman transport theory to estimate the Ekman transport and concluded that the wind was strong enough to transport the *K. Brevis* cells out of the filaments and across the shelf in Onslow Bay.

The red tide bloom event was a complicated coupled physical-biological process. The physical process included wind-driven ocean current and Ekman transport, continental shelf circulation, Gulf Stream meanders and eddies, upwelling induced by the Gulf Stream meander, warm filament associated with Gulf Stream meanders and eddies, and mixing process of the Gulf Stream water with continental-shelf water. The biological processes included nutrient source, nutrient uptake, photosynthesis, food-chain (phytoplankton->zooplankton->fishes). The impact of physical process on the biological processes was two folds. First, the ocean current and mixing process could transport nutrient and biological cells both horizontally and vertically. The physical processes described by Pietrafesa et al (1988) fall into this category. Secondly, temperature can also have great effect on the biological process. Although the temporal and spatial variations of the temperature are physical processes, water temperature can have a great effect on the biological cell division rate, phytoplankton growth rate etc. Tester et al (1991) analyzed the cell count sampling during the red tide bloom event, along with satellite SST images and observed wind. It was found that the transport of cells onto the inner continental shelf might have resulted from the large meanders of the Gulf Stream. The warm filament associated with this meander persisted on the continental shelf for at least

19 days, and inshore surface waters of both Onslow and Raleigh Bays were warmed. Both wind speed and direction were important in determining its distribution. It was concluded that the persistence of the filament in the inshore area for nearly 3 weeks in October-November 1987 was the key factor that could have provided ample time for cell division and bloom development.

In this research, we will use ocean numerical model to study the above mentioned physical processes, which include the continental shelf circulations on the West Florida Continental Shelf and the Southeastern U.S. Continental Shelf, Gulf Stream and its meander and eddy, and wind effects on the cross-shelf and along-shelf circulation. Specifically, we are trying to answer these questions:

a) What is the horizontal resolution required to simulate the Gulf Stream meanders and eddies?

b) What is the limitation of the numerical model in the simulation of a particular Gulf Stream meander event using only atmospheric data without ocean data assimilation?

c) How does the bottom topography affect the Gulf Stream meander and eddy in the South Atlantic Bight?

d) What are the effects of the wind and eddies on the cross-shelf and along-shelf transport?

The objective of this study is to investigate the physical processes that contribute to the transport of the *K. Brevis* cells from the West Florida Shelf to the North Carolina coast. However, data assimilation and biological modeling are not in the scope of this

study, although they are both very important components in any ecological system prediction.

2. Brief Description of the Research Topics

2.1 Sensitivity Test

To find out the appropriate horizontal resolution required for simulation of the Gulf Stream, meso- and submeso-scale eddies, sensitivity of the numerical simulation to the horizontal resolutions will be tested. Basin-wide simulations with different horizontal resolutions will be run to test the minimum horizontal resolution requirement to simulate the Gulf Stream. Since basin-wide simulations cover a large area, the integration speed is slow and the computation cost is high. Triple-nesting approach will be taken to achieve higher resolutions with less computational cost. The inner-most domain will have the highest horizontal resolution of 0.027-degree. Another sensitivity study is to test the sensitivity of simulations to high-frequency atmospheric forcing. Gulf Stream meander and eddies are irregular and episodic. The purpose of this test is to see what is the model's capability in simulating the episodic Gulf Stream meander events using high-frequency atmospheric forcing without using ocean data assimilation.

North Atlantic Ocean Prediction System (NAOPS) is a HYCOM–based ocean forecast system. It is run in near real time at the Naval Oceanographic Office (NAVOCEANO) Major Shared Resource Center using a High Performance Computing Challenge Grant of computer time provided by the Defense Department High Performance Computing Modernization Program. It uses atmospheric forcing from the Navy Operational Global Atmospheric Prediction System (NOGAPS) and it assimilates

satellite altimeter sea surface height data obtained via the NAVOCEANO Altimeter Data Fusion Center. The Atlantic model has 1/12° equatorial resolution and latitudinal resolution of 1/12° cos(lat) or ˜ 7 km for each variable at mid-latitudes. It has 26 coordinate surfaces in the vertical. A 0.027° simulation will be nested in the NAOPS and see if the model can predict a Gulf Stream meander and eddy event in high resolution simulations and with data assimilation.

2.2 Bathymetry Effect on the Gulf Stream Meanders and Eddies

At proximately 32°N, a submarine ridge called the Charleston Bump (referred to as CB here after) extends seaward from the continental slope offshore of Charleston, South Carolina. This topographic feature produces an eastward deflection in the Gulf Stream (Pietrafesa et al., 1978; Rooney, et al, 1978; Brooks and Bane, 1978), forming a quasi-permanent 10 to 150 km meander. It has also been reported that the lateral meanderings of the Gulf Stream undergo a dramatic 'amplification' (Knauss, 1969; Maul et al., 1978; Bane and Brooks, 1979; Bane, 1983; Hood and Bane, 1983; Olson et al., 1983) downstream from the CB. The triggering mechanism for the larger meanders and filaments downstream of the CB is presumably the topographic effect of the CB (Pietrafesa et al, 1978; Rooney et al, 1978; Brooks and Bane, 1978; Chao and Janowitz, 1979; Legeckis, 1979; Pietrafesa, 1983; Dewar and Bane, 1985). However, another characteristic of the bathymetry in the SAB is the curvature of the isobaths The isobaths are north-south oriented south of 30ºN, and turn sharply to northeast-southwest oriented around 31ºN. The CB is located in the region of large curve where the Gulf Stream turns from northward to northeast-ward. So, the question is, could the curvature of the isobaths

have an effect on development of Gulf Stream meanders and eddies? The radius of the curvature can be as small as 200-300 km, and the centrifugal force required for a current of approximately 2 m/s is of magnitude 10^{-5} N which is the same order of magnitude of the local Coriolis force. The vorticity created by the curvature is of the order of 10^{-5} s^{-1} which is of same order of magnitude of the planetary vorticity. Thus, two hypotheses to be tested are: isobathic curvature has a significant effect on the stability of the Gulf Stream; and the combined effects of isobaths curvature and the influence of the CB are responsible for the development of the CB. In this study, the numerical modeling methods will be used to study the effects of the bathymetry curvature and the bump on the Gulf Stream meanders and eddies.

2.3 Cross-shelf and Along-Shelf Transport

As concluded by Pietrafesa et al. (1988) and Tester et al (1991), both Gulf Stream meanders and wind effect are important for the cross-shelf transport of the *K. Brevis* cells from the Gulf Stream to the North Crolina inshore area. In this study, an ocean numerical model will be used to simulate the process of transportation of *K. Brevis* cell from the West Florida Shelf in Gulf of Mexico to the inshore area of the North Carolina coast. The numerical model used is the Hybrid Coordinate Ocean Model (HYCOM) with highest resolution of 0.02 degrees. Since the process covers a large area, it is very time-consuming to run the simulation in the whole area of interest. Therefore, a triple-nested approach was taken to achieve the high resolution: the outer domain covers the whole north and equatorial Atlantic, the intermediate domain covers the south east U.S. continental shelf, and the inner domain covers the North and South Carolina continental

shelf. The purpose of this part of research is to testify the hypothesis that the red tide bloom in the North Carolina coast was originated and transported from the West Florida Shelf. The individual and combined effect of the wind and Gulf Stream meander and eddy on transportation of the *K. Brevis* cell from the Gulf Stream to North Carolina inshore area will also be investigated.

3. Organization of the Dissertation

Data and ocean numerical model used in this research will be discussed in Chapter 2. The result of sensitivity tests on horizontal resolution and high-frequency atmospheric forcing will be included in Chapter 3. In Chapter 4, the study of the effect of bathymetry curvature on the Gulf Stream instability in the vicinity of the Charleston Bump will be presented. In Chapter 5, numerical Simulation of the transport of *K. Brevis* cells from Gulf of Mexico to North Carolina coast using passive tracer will be presented. Finally, future work will be discussed in Chapter 6.

4. References

Bane, J. M., Jr., and D. A. Brooks, 1979: Gulf Stream meanders along the continental margin from the Florida Straits to Cape Hatteras, Geophys. Res. Lett., 6, 280-282.

Bane, J. M., Jr., 1983: Initial observation of the subsurface structure and short-term variability of the sea-ward deflection of the Gulf Stream off Charleston, South Carolina, J. Geophys. Res., 88(C8), 4673-4684.

Brooks, D. A. and J. M. Bane, Jr., 1978: Gulf Stream deflection by a bottom feature off Charleston, SC, Science, 201, 1225-1226.

Chao, S. Y. and G. S. Janowitz, 1979; The effect of a localized topographic irregularity on the flow of a boundary current along the continental margin, J. Physical Oceanogr., 9, 900-910.

Dewar, W. K., and J. M. Bane Jr., 1985: Subsurface energetics of the Gulf Stream near the CB. J. Physical Oceanogr., 15, 1771-1789.

Hood, C. A. and J. M. Bane, Jr., 1983; Subsurface energetics of the Gulf Stream cyclonic frontal zone off Onslow Bay, North Carolina, J. Geophys. Res., 88(C8), 4651-4662

Knauss, J. A., 1969: A note on the transport of the Gulf Stream. Deep Sea Res., 16(Suppl.), 117-123.

Legeckis, R. V., 1975: Application of synchronous meteorological data to the study of time-dependent sea surface temperature changes along the boundary of the Gulf Stream. Geophys. Res. Lett., 24, 435-438.

Maul, G. A., P. W. deWitt, A. Yanaway, and S. R. Baig, 1978: Geostationary satellite observations of Gulf Stream Meanders: Infrared measurements and time series analysis, J. Geophys. Res., 83, 6123-6135.

Olson, D. B., O. B. Brown, and S. R. Emmerson, 1983: Gulf Stream frontal statistics from Florida Straits to Cape Hatteras derived from satellite and historical data, J. Geophys. Res., 88(C8), 4569-4577

Pietrafesa, L. J., J. O. Blanton, and L. P. Atkinson, 1978: Evidence for deflection of the Gulf Stream at the Charleston Rise, Gulf Stream, 4(9), 3 and 6-7

Pietrafesa, L. J., G. S. Janowitz, K. S. Brown, F. Askari, C. Gabriel, and L. A. Salzillo, 1988: The invasion of the Red Tide In North Carolina Coastal Waters, UNC Sea Grant Publication UNC-SG-WP-88-1, August 1988

Pietrafesa, L. J., 1983; Survey of a Gulf Stream frontal filament, Geophys. Res. Lett., 10, 203-206.

Rooney, D. M., G. S. Janowitz and L. J. Pietrafesa, 1978: A simple model of deflection of the Gulf Stream by the Charleston rise, Gulf-stream, 4(11), 3-7

Tester, P. A. and S. Fowler, 1990: Brevetoxin contamination of Mercenaria and Crassostrea virginica: A management issue, p499-503. In Toxic marine phytoplankton. Proc. 4th Int. Conf. Elsevier.

Tester, P. A. and K. A. Steidinger, 1997:Gymnodinium breve Red Tide Blooms: Initiation, Transport, and Consequences of Surface Circulation, Limnology and Oceanography, 42, 1039-1051.

Tester, P. A., R. P. Stumpf, F M. Vukovich, P. K. Flower, J. T. Turner, 1991: An expatriate Red Tide Bloom: Transport, Distribution, and Persistence, Limnology and Oceanography, 36, 1053-1061.

Chapter 2

Data and Ocean Numerical Model

1. Data

The data used in this research include ECMWF 40-year reanalysis data, North America Regional Reanalysis data, COADS climatology, Levitus ocean data, and ETOP02 bathymetry. They are briefly described as below.

1.1 ECMWF 40-year reanalysis data (ERA-40)

The European Center for Medium-Range Weather Forecasting (ECMWF) carried out this 40-year atmospheric reanalysis project. ERA-40 provides a comprehensive set of global analyses describing the state of the atmosphere and land and ocean-wave conditions from mid-1957 to 2001. It uses a variational data assimilation system to make a new synthesis of the in-situ and remotely-sensed measurements made over the period since mid-1957, when a major improvement was made to the atmospheric observing system in preparation for the International Geophysical Year, 1958. ERA-40 produces analyses with six hourly frequency throughout the period, supplemented by intermediate three-hour forecasts. The products are of high temporal and spatial resolution, with a grid-spacing close to 125km in the horizontal and with sixty levels in the vertical located between the surface and a height of about 65km. The basic analyzed variables include not only the conventional meteorological wind, temperature and humidity fields, but also stratospheric ozone and ocean-wave and soil conditions. Additional information estimates the quality of both the observations used and the analyses generated.

1.2 North America Regional Reanalysis data (NARR)

The dataset was originally produced at NOAA's National Center for Atmospheric Prediction (NCEP). It is a long-term set of consistent climate data on a regional scale, for the North American domain. The NARR is superior to the completed NCEP/NCAR Global Reanalysis (GR), in both resolution and accuracy. This was achieved using the GR to drive the Regional Reanalysis (RR) system, and taking advantage of the regional Eta Model, and of the various advances that have been made in regional modeling and data assimilation since the GR system starting time of 1995. These advances include assimilation of precipitation, direct assimilation of radiances, the use of additional data as well as improved data processing efforts, and several Eta Model developments, in particular those arrived at within the NCEP's land-surface effort. Thus, the NARR data are the premier North American data set for a variety of climate, NWP, predictability, water resources, and numerous other application purposes.

The resolution of the RR is 32 km/ 45 layers, and the domain used covers most of North America and large parts of the adjacent oceans. The native model grid is converted to a Northern Lambert Conformal Conic grid for archive. The products archived consist of analysis and first guess fields, as well as free forecasts, to 72 h every 2.5 days. The initial period covered is 25 years, 1979-2003, but the RR has been running continuously in real-time after the initial period.

1.3 COADS climatology

The Comprehensive Ocean-Atmosphere Data Set (COADS) was created by National Climatic Data Center (NCDC), Environmental Research Laboratories, the cooperative Institute for Research in Environmental Sciences and the National Center for Atmospheric Research (NCAR). Products include fully quality-controlled reports and summaries. Global marine data observed during 1854-1979, primarily by ships-of-opportunity, have been collected, edited, and summarized statistically for each month of the period, using 2 degree latitude x 2 degree longitude boxes. Each of the 70 million unique reports contain 28 elements of weather, position, etc., as well as flags indicating which observations were statistically trimmed. The summaries give l4 statistics, such as the median and mean, for each of eight observed variables of air and sea surface temperatures, wind, pressure, humidity, and cloudiness, plus ll derived variables. Relatively noisy (untrimmed) individual reports and summaries (giving l4 statistics for each of the eight observed variables) are available for investigators who prefer their own quality control. Two other report forms, inventories, and decade-month summaries are among the other products available.

1.4 Levitus ocean data

This dataset is produced by NOAA National Oceanic Data Center (NODC). The atlas contains annual and monthly long term means for temperature and salinity at multiple depths as well as mixed layer depths as monthly long term means, the last derived both from potential temperature and potential density. The Levitus Climatology provides a raw

field of data (Temperature,Salinity,etc) from which specific seasons and years can be extracted. Data which contain any of several documented errors are flagged, so these can be discarded as we have done when using the raw data. An analyzed field for all years and individual seasons is also provided. This method is similar to our optimal interpolation scheme in that a correlation length scale is specified, a weighting function is chosen and a first guess field is used.

1.5 ETOP02

This data set is from National Geographical Data Center (NGDC). It contains digital data bases of seafloor and land elevations on a 2-minute latitude/longitude grid.

2. Ocean Numerical Model

HYCOM is a primitive equation ocean general circulation model that evolved from the Miami Isopycnic-Coordinate Ocean Model (MICOM). It was developed to address known shortcomings of the MICOM vertical coordinate scheme. MICOM vertical coordinates are isopycnic except for model layer 1, which is a non-isopycnic slab mixed layer. This leads to two significant problems: First, slab models must be used to govern mixed layer entrainment and detrainment. MICOM was equipped with a Kraus-Turner type model as described in Niiler and Kraus (1977), but using the modified turbulent kinetic energy balance parameterization of Gaspar (1988). Second, vertical coordinates are “wasted” because all model layers less dense than the mixed layer (layer 1) exist as zero-thickness layers at the mixed layer base. Although MICOM has produced good scientific results, improvements in the representation of vertical mixing, and the

representation of oceanic flow in shallow-water and weakly stratified regions are constrained by these vertical coordinate limitations.

Vertical coordinates in HYCOM remain isopycnic in the open, stratified ocean. However, they smoothly transition to z coordinates in the weakly-stratified upper-ocean mixed layer, to terrain-following sigma coordinate in shallow water regions, and back to level coordinates in very shallow water. The latter transition prevents layers from becoming too thin where the water is very shallow. The vertical coordinates that were "wasted" in MICOM are used to provide vertical resolution within the surface mixed layer. This enables the use of more sophisticated non-slab closure schemes. One important goal for HYCOM is to provide the capability of selecting among several different vertical mixing schemes for both the surface mixed layer and the comparatively weak interior diapycnal mixing. In the most recent release of version 2.1, four mixed layer models has been included in HYCOM: the K-Profile Parameterization (KPP, Large et al., 1994; 1997), the Kraus-Turner slab model, the dynamical instability model of Price *et al.* (1986), and the Mellor-Yamada level 2.5 turbulence closure used in the Princeton Ocean Model (Mellor and Yamada, 1982; Mellor, 1998). Other mixed layer models will be included in the near future, such as the model developed recently by Canuto (2000).

HYCOM is fully parallelized with MPI and OpenMP standard, and it is designed to be portable among all UNIX-based systems such as SGI Origin, IBM SP, Cray T3E and Linux-based PC Clusters.

3. References

Cooper, M. and K. Haines, 1996: Atimetric assimilation with water property conservation. J. Geophys. Res. 101, C3, 1,059-1,077.

Evensen G., 1994: Sequential data assimilation with a nonlinear quasi-geostrophic model using Monte Carlo methods to forecast error statistics. J. Geophys. Res., 99(C5), 10,143-10,162.

Gaspar, Ph., 1988: Modeling the seasonal cycle of the upper ocean. J. Phys. Oceanogr., 18, 161-180.

Large, W. G., J. C. Mc Williams, and S. C. Doney, 1994: Oceanic vertical mixing: a review and a model with a nonlocal boundary layer parameterization. Rev. Geophys. 32, 363-403.

Large, W. G., G. Danabasoglu, S. C. Doney, and J. C. McWilliams, 1997: Sensitivity to surface forcing and boundary layer mixing in a global ocean model: annual-mean climatology. J. Phys. Oceanogr., 27, 2418-2447.

Levitus, S., 1997: World Ocean Atlas, Washington DC, NOAA

Mariano, A.J. and O.B. Brown, 1992: Ecient objective analysis of dynamically heterogeneous and nonstationary fields via the parameter matrix. Deep-Sea Res., 39, 1255-1271.

Mellor, G. L. and Yamada, T., 1982: Development of a turbulence closure model for geophysical fluid problems. *Rev. Geophys. Space Phys.*, **20**, 851-875.

Mellor, G. L., 1998: Users Guide for a Three-Dimensional, Primitive Equation Numerical Ocean Model. Available on the Princeton Ocean Model web site.

Niiler, P.P. and E. B. Kraus, 1977: One-dimensional models. In Modeling and Prediction of the Upper Layers of the Ocean, E. B. Kraus, Editor. Pergamon, New York, 143-172

Price, J. F., R. A. Weller, and R. Pinkel, 1986: Diurnal cycling: Observations and models of the upper ocean response to diurnal heating, cooling, and wind mixing. *J. Geophys. Res.*, **91**, 8411-8427.

Pham D.T., J. Verron, M.C. Roubaud, 1998: Singular evolutive extended Kalman filter with EOF initialization for data assimilation in oceanography. J. Marine Systems, 16 (3-4), 323-340.

Chapter 3

Sensitivity Test

1. Objectives and Tests

Two types of sensitivity test will be conducted. First, we need to test the sensitivity of simulation to the horizontal resolution. The purpose of these tests is to find out the appropriate horizontal resolution required for simulation of the Gulf Stream, meso- and submeso-scale eddies. The following tests will be performed:

1) Five simulations with horizontal resolution of 0.54º, 0.45º, 0.36º, 0.27º, 0.18º respectively will be run to test the minimum horizontal resolution requirement to simulate the Gulf Stream. Since Gulf Stream is generated on the basin-wide scale, the domain of these simulations should cover the whole north and equatorial Atlantic region. All these simulations will be driven by COADS monthly climatology.
2) A 0.06º simulation will be nested in the 0.18º simulation of basin-wind domain. The inner domain of the 0.06º nested simulation covers the entire SAB. This simulation is to test the model's capability in simulating meso-scale Gulf Stream meanders and eddies.
3) A triple-nested simulation (0.24º → 0.08º → 0.027º) will be performed to study the submeso-scale eddies at a finer resolution. The outermost domain should cover the whole north and equatorial Atlantic; the middle domain should cover SAB; the innermost domain should cover the coastal area off the

Carolina coast. The model grids of the simulation will be placed within the grids of the North Atlantic Ocean Prediction System (NAOPS), so that the 0.027º simulation can be nested within the NAOPS domain. This is to test the horizontal resolution required to simulate the submeso-scale eddies.

The second type of sensitivity test is to test the simulations with high-frequency forcing. Gulf Stream meander and eddies are irregular and episodic. A question one might ask is that given the high-frequency atmospheric forcing, can the model simulate a particular event? In this experiment, instead of using monthly averaged climatology forcing, we will use high frequency atmospheric forcing from the ECMWF reanalysis data to drive the ocean model. The 10m-wind speed, air temperature, radiation daily average data were calculated on ECMWF reanalysis grid and then interpolated on to the model grid. A numerical simulation will be done using the atmospheric forcing of year 1996 and the result will be compared with 1996 satellite SST image. The purpose of this test is to determine the model's capability in simulating the episodic Gulf Stream meander events without using ocean data assimilation.

Since NAOPS has the data assimilation of remotely sensed SSH and SST data, it's ability in predicting the Gulf Stream meanders and eddies are greatly improved. A 0.027º simulation will be nested in the North Atlantic Ocean Prediction System (NAOPS: http://www7320.nrlssc.navy.mil/ATLhycom1-12/skill.html) as a hindcast case study of the Gulf Stream meanders and eddies. The model-predicted oceanic data from 12 – 17 January 2004 will be downloaded from the NAOPS data server and be used as the initial and boundary condition. The simulation result will be compared with satellite SST observation.

2. Results

2.1 0.54º, 0.45º, 0.36º, 0.27º, 0.18º simulations

In this sensitivity test, simulations were conducted using five horizontal resolutions: 0.54º, 0.45º, 0.36º, 0.27º, 0.18º. In the five simulations, the computation domain is the whole north Atlantic (97ºW-15ºE, 17ºS-51ºN), the atmospheric forcing is from COADS monthly climatology dataset, and the model is initialized with Levitus dataset. The bathymetry is from ETOPO2 and interpolated on the model grids of different resolutions. The model is spun up for one year, and the result presented in the following is from the simulation of the second year.

Figures 1a-e show the horizontal velocity in the mixed layer for the five simulations. In the 0.54º-, 0.45º- and 0.36º-resolution simulations, the Gulf Stream is not very well resolved (the boundary between the Gulf Stream and the adjacent continental shelf circulation is not clear). However, in the 0.27º- and 0.18º-resolution simulations, the Gulf Stream is clearly separated from the continental shelf circulations. The Gulf Stream appears to be broader in the low-resolution (0.54º, 0.45º and 0.36º) simulations than in the high-resolution (0.27º and 0.18º) simulations. The maximum velocity near the Gulf Stream axis in the 0.54º-resolution simulation is about 75cm/s, but in the 0.18º-resolution simulation, the maximum velocity can reach to 150cm/s. Therefore, the high-resolution simulations are more energetic.

In the real ocean, eddies occur on both sides of the Gulf Stream edge. In the sensitivity test, eddies on the sea-ward edge of the Gulf Stream can be resolved in the 0.18º-resolution simulation, but can only be marginally resolved in the 0.27º-resolution

simulation. However, shore-ward eddies and the Gulf Stream filaments on both sides of the Gulf Stream cannot be resolved at these two resolutions. In low-resolution (0.36º, 0.45º and 0.54º) simulations, no eddies or filaments can be resolved at all.

The mixed-layer horizontal velocity shows off-shore component near the Charleston bump in all of the five simulations (Figures 1a-e). Since the Gulf Stream is clearly separated from its adjacent continental shelf circulations in the 0.27° and 0.18° simulations, sea-ward deflection of the Gulf Stream path near the Charleston bump can also be seen in the horizontal velocity field of these two simulations (Figures 1d-e). The deflection of the Gulf Stream can be seen more clearly in the mixed-layer temperature in all of the five simulations (Figures 2a-e).

Figure 3 (a) and (b) show the northward velocity (cm/s) and temperature respectively at 27ºN in the 0.18-dgree simualtion. We can see that the maximum northward velocity at the Gulf Stream axis reach at the speed of 1.5 m/s, and the Gulf Stream temperature front can also be simulated very well. Figure 3 (c) shows the annual mean of the observed northward velocity from Tomczak and Godfrey (2003). We can see that the simulation is in good agreement with observation. Figure 4 show the simulated and observed monthly-averaged total transport of Florida current at 27ºN. We can see that the seasonal variation of the total transport is simulated very well, however, the model result are systematically smaller that the observation. The reason maybe due to the climatology atmospheric forcing used in the 0.18-degree simulation.

In summary, horizontal resolution has effect on the simulation of Gulf Stream itself and its associated eddies. At least 0.27°-resolution is need to resolve the Gulf Stream. Gulf Stream deflection near the Charleston bump can be seen in the horizontal velocity

field in all of the five simulations. Eddies on the sea-ward edge of the Gulf Stream can be resolved in the 0.18° simulation. However, to simulate the eddies on the shore-ward edge of the Gulf Stream, resolution higher than 0.18° is needed.

2.2 0.06° resolution simulation

As concluded in the last section, resolution higher than 0.18° is needed to resolve the eddies on the shore-ward edge of the Gulf Stream. However, to increase the horizontal resolution for the basin-wide Atlantic simulation is impractical with our current computation power. Therefore, a 0.06° resolution simulation is nested in the 0.18° simulation to achieve high resolution in the way that 0.18° simulation provides boundary condition for the 0.06° simulation (one-way nesting). The computation domain of the nested area covers 26°-41°N, 82°-70°W. The nested simulation time period in this experiment is from Jan. 1 to Feb. 20 of the second year.

Figure 5 and Figure 6 show the horizontal velocity and temperature of the mixed-layer of the 0.06° nested simulation on Feb. 13 of the second model year. Gulf Stream deflection near the Charleston bump is clearly simulated as shown in Figures 5 and 6, and a shore-ward eddy at 33º N can be identified in the mixed-layer horizontal velocity field in Figure 5, and the Gulf Stream filament associated with this eddy can be seen in the sea temperature field in Figure 6. Therefore, 0.06º resolution is sufficient for simulation of meso-scale eddies and their associate warm filaments. However, to simulate the submeso-scale eddies, finer resolution is required.

2.3 0.027° simulation

0.06° resolution is not sufficient for simulation of the submeso-scale eddies. Therefore, a 0.027° degree resolution is implemented using triple nested simulations. The outer domain has a 0.24 degree resolution and covers the whole north and equatorial Atlantic; the middle domain has a 0.08 degree resolution and covers the coastal area off the Carolina coast (81.68° – 75.68° W, 29.24° – 35.62° N); the inner domain has a 0.027 degree resolution and covers even smaller area (81.36° - 76.16° W, 30.18° - 35.23° N). The grids of 0.08 degree resolution are on the grids of NAOPS which is currently in operation at Naval Research Laboratory. One thing in our minds to design this kind of grids is that these grids will make it easier to have our 0.027° simulation nested in the NAOPS. NAOPS assimilates the satellite SST and SSH data and has the capability to simulate a particular Gulf Stream meander/eddy event, however, the submeso-scale eddies cannot be resolved, and coastal circulation features near-shore are missing.

Figure 7 shows mixed-layer SST in the 0.08 degree simulation on Nov. 11. There is an eddy at about 33° N, and its associated warm filaments are also simulated very well. Figure 8 show the mixed-layer SST in the 0.027 degree simulation on the same day. In this simulation, submeso-scale eddies that appear on the warm filaments are very well simulated. Figure 9 shows the SST of 0.027º simulation from Oct. 30 to Nov. 15. From this figure we can see the development of submeso-scale eddies on the warm filament. On Oct. 30, the warm filament is formed, but the isotherms are very smooth. Starting from Nov. 3, the isotherms show some wave-like oscillation, and by Nov. 9, the amplitude of oscillation is pretty large. The wavelength of these oscillations is about 20

Km which is in the same scale as the wave in Barth (1994) and Fukamachi (1992)'s theory. Therefore, 0.027 degree resolution can resolve both meso- and submeso-scale eddies.

2.4 Sensitivity to High-frequency Atmospheric Forcing

The one-year climatology result of 0.18-degree simulation was used as the initial condition in this test, and the 1996 daily forcing data was then used to drive the 0.18 degree run starting from January 1st (day 1) of 1996. The 0.06-degree simulation was then nested in the 0.18 degree 1996 simulation. All the following results are from the nested 0.06 degree 1996 simulation.

Since the purpose of this part of research is to test the model's capability to simulate the Gulf Stream meander/eddy events in 1996 using high frequency atmospheric forcing, the meander/eddy events in January to May 1996 that can be seen in the satellite AVHRR SST images were first found out, and then the simulated SST on the corresponding day were compared. Figure 10 to Figure 16 show seven Gulf Stream meander/eddies events that can be seen in the satellite SST images, and their corresponding simulated SST.

Of the seven Gulf Stream meander/eddy events as shown Figure 10 to Figure 16, we can see that only two of them (February 10 and April 22) are very well simulated, all other events are missed or not very well simulated. So even with high frequency atmospheric data, the model cannot simulate a particular Gulf Stream meander/eddy event very well. Two reasons may contribute to the model error. First, no data assimilation was used in the simulation. Secondly, horizontal resolution of the atmospheric forcing might be too low (currently, ECMWF 1.125°).

Figure 17 shows the AVHRR SST image of Jan 12-17, 2004. We can see that there are two eddies at 32°N and 33°N respectively on Jan. 12. These two eddies are amplified while passing through the Charleston Bump. Since NAOPS has the data assimilation of remotely sensed SST data and SSH data, these two eddies are simulated very well at the right time and location as we can see in Figure 18. However, since NAOPS has a resolution of 0.08 degree, the warm filament and near-shore process cannot be resolved very well. With the 0.027-degree simulation nested in the NAOPS, the warm filaments on the continental shelf are resolved very well, and the submeso-scale eddies can also be simulated (Figure 19).

3. Conclusions

Results of the test of sensitivity to horizontal resolution show that 0.18º resolution is sufficient to resolve the Gulf Stream, but not fine enough for the simulation of meso-scale eddies. Therefore, a 0.06º simulation was nested in the 0.18º simulation to reach a finer that is sufficient to resolve meso-scale eddies, and in the meantime, could save the computing cost. However, even finer resolution is required to resolve the submeso-scale eddies. A tipple nested simulation from 0.24º → 0.08º → 0.027º was done to resolve the submeso-scale eddy. The 0.027º resolution is sufficient to simulate the warm filaments and submeso-scale eddies.

4. References

Barth, J. A., 1989a: Stability of a coastal upwelling front: 1, Model development and a stability theorem. *J. Geophys. Res.,* **94,** 10 844–10 856.

Barth, J.A., 1989b: Stability of a coastal upwelling front: 2, Model results and comparison with observations. *J. Geophys. Res.,* **94,** 10 857–10 883.

Barth, J.A., 1994: Short-wavelength instabilities on coastal jets and fronts. *J. Geophys. Res.,* **99,** 16 095–16 115.

Fukamachi, Y., 1992: Instability of density fronts in layer and continuously stratified models. Ph.D. thesis, Nova University, 166 pp.

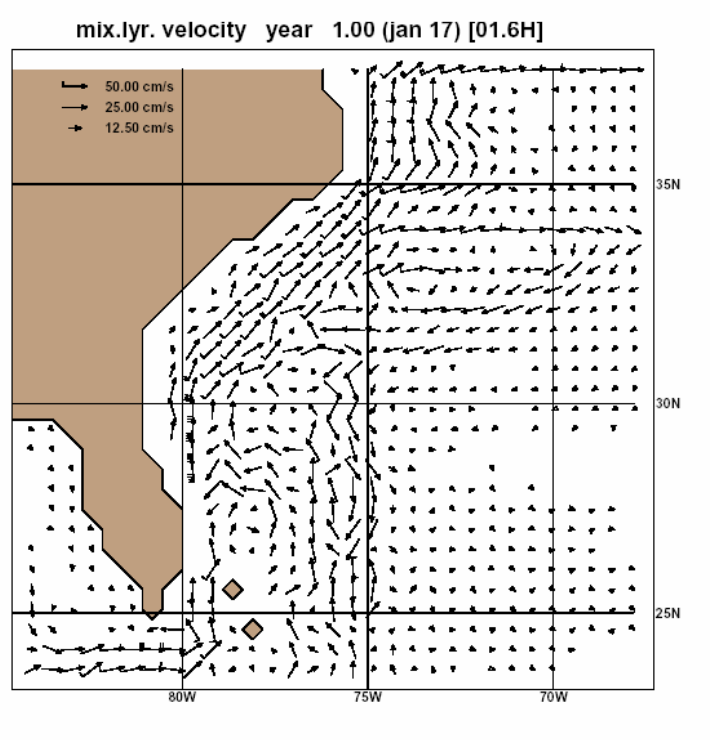
Fukamachi, Y., J. P. McCreary, and J. A. Proehl, 1995: Instability of density fronts in layer and continuously stratified models. *J. Geophys. Res.,* **100,** 2559–2577.

Gill, A. E., 1982: *Atmosphere–Ocean Dynamics.* Academic Press, 662 pp.

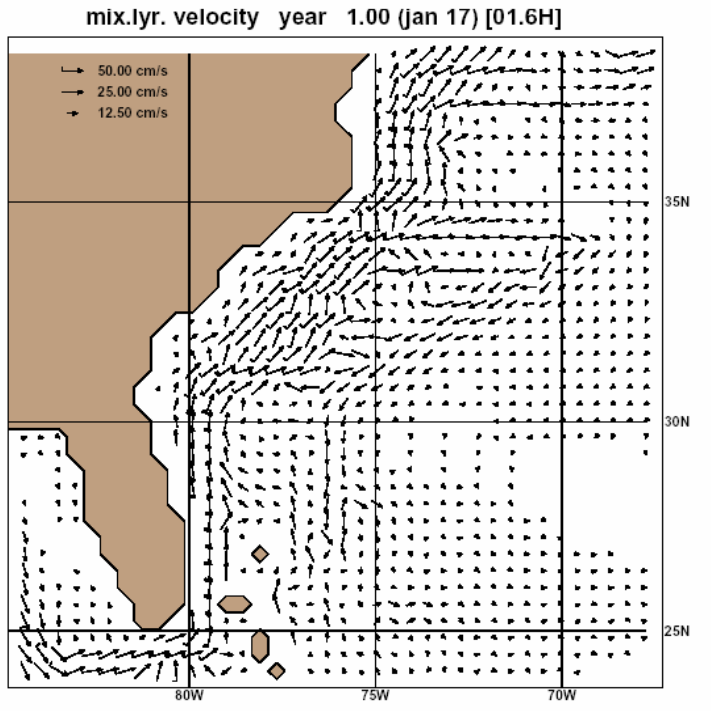
Tomczak, M and J. S. Godfrey, 2003: Regional Oceanography: an Introduction, 2nd edn, ISBN: 8170353068

Figure 1. Mixed layer velocity in (a) 0.54° (b) 0.45° (c) 0.36° (d) 0.27° (e) 0.18° simulations.

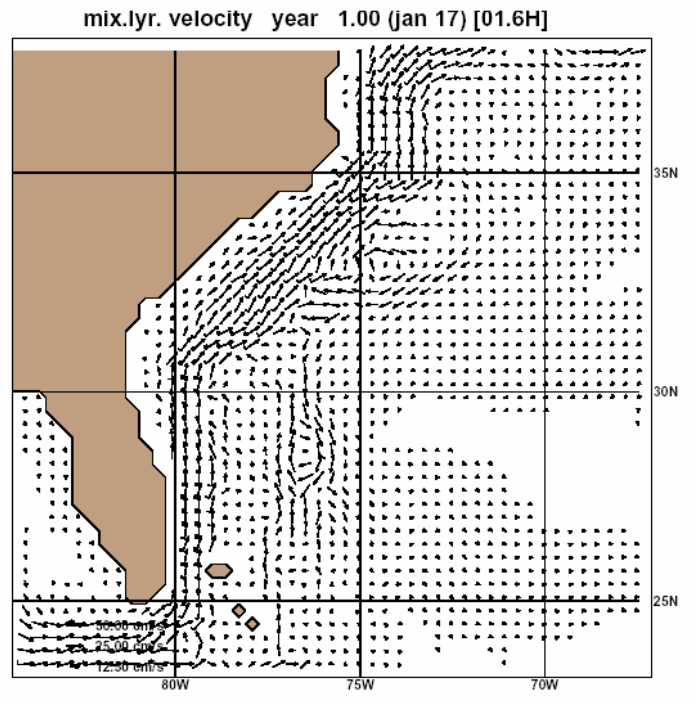
(a) 0.54 Degree Resolution



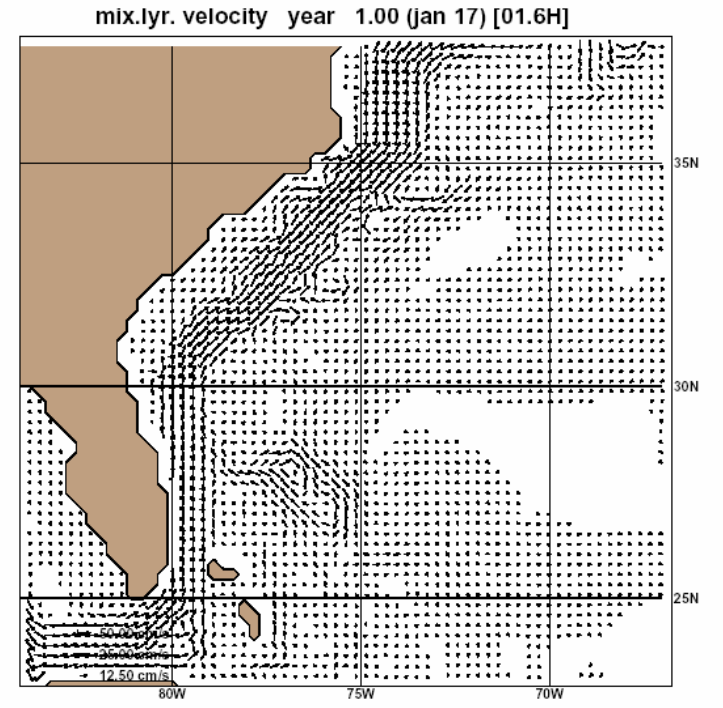
(b) 0.45 Degree Resolution



(c) 0.36 Degree Resolution



(d) 0.27 Degree Resolution



(e) 0.18 Degree resolution

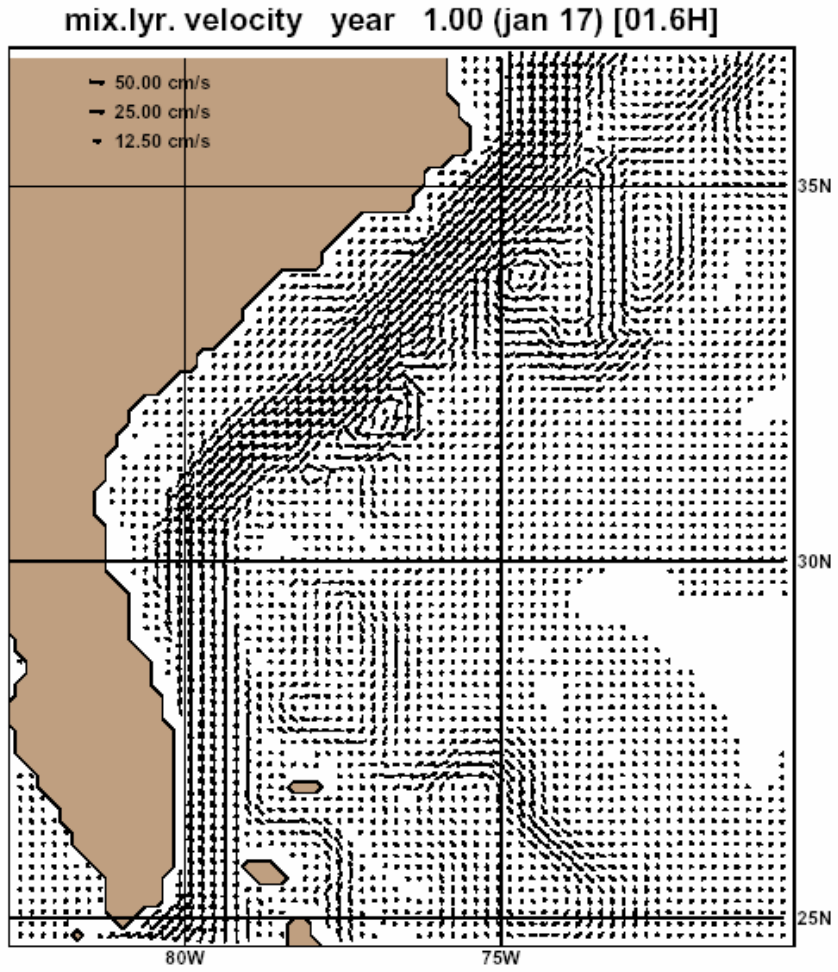
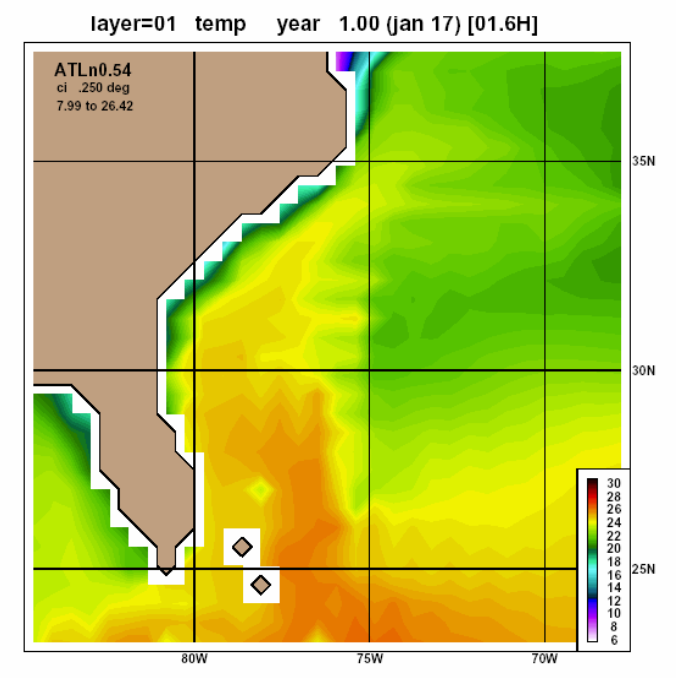
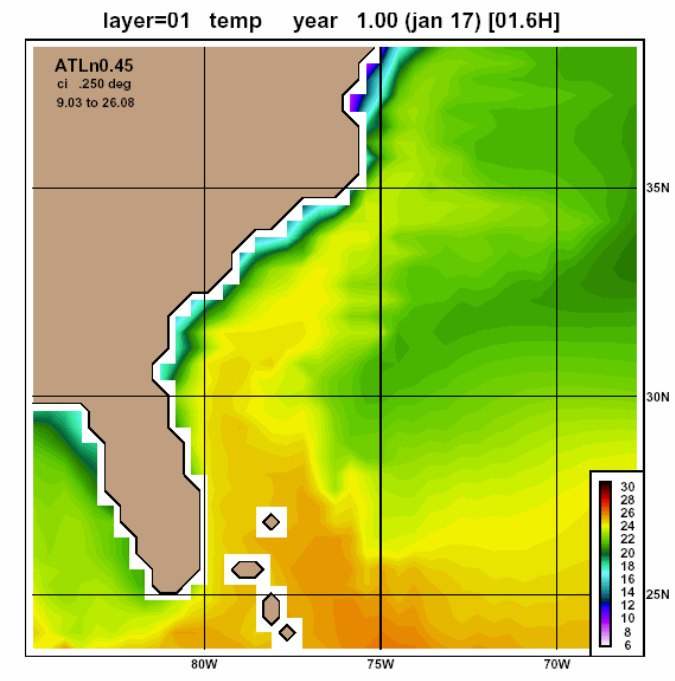


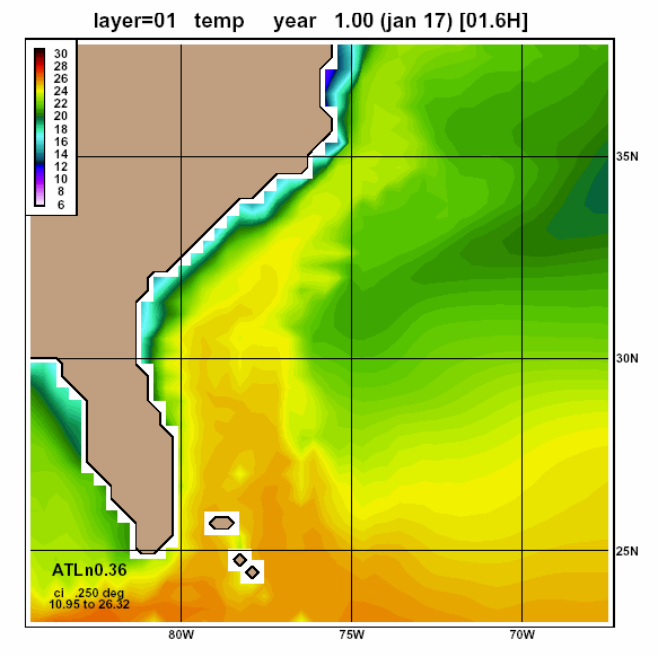
Figure 2 Mixed-layer temperature in (a) 0.54° (b) 0.45° (c) 0.36° (d) 0.27° (e) 0.18° simulations.



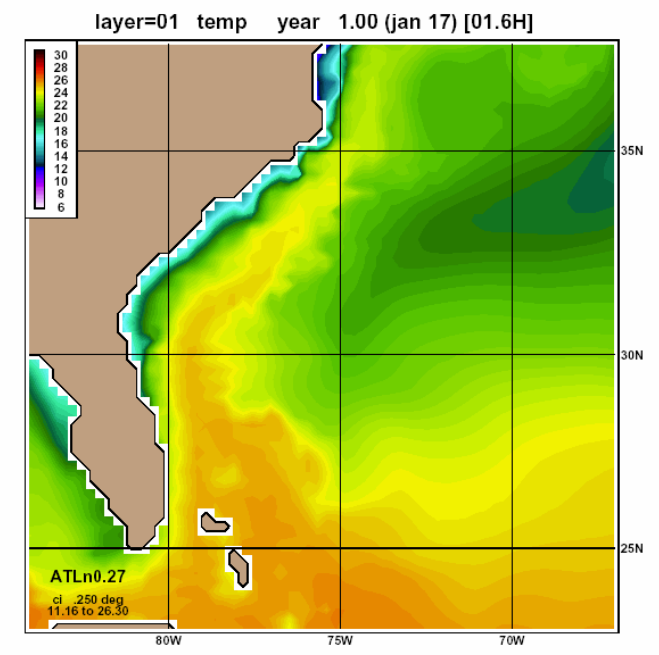
(a) 0.54 degree



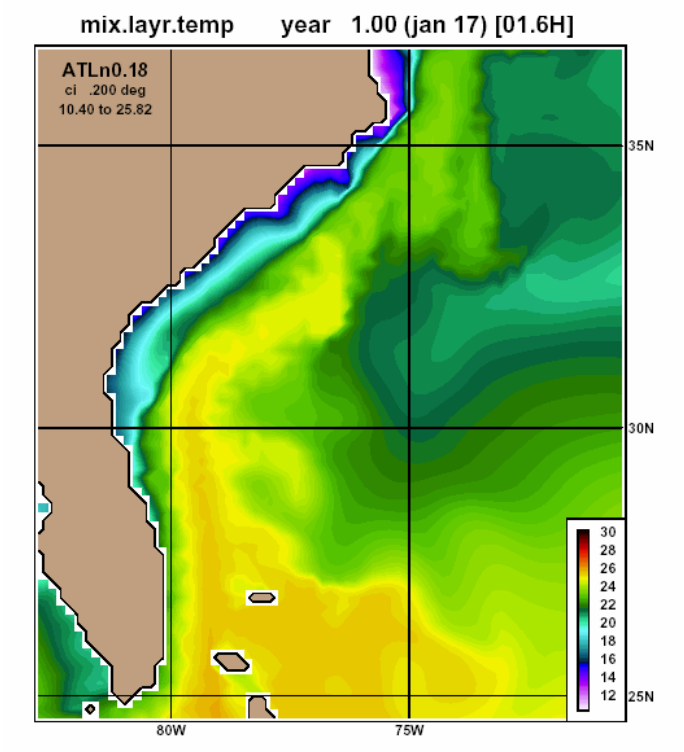
(b) 0.45 degree



(c) 0.36 degree

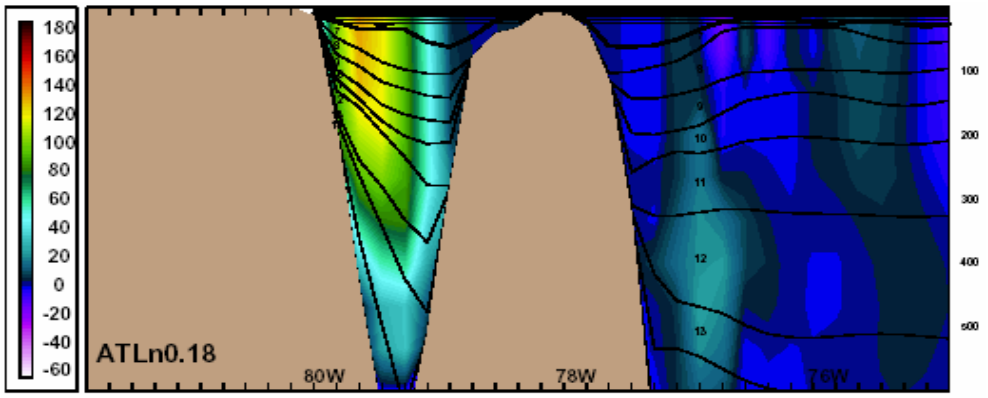


(d) 0.27 degree

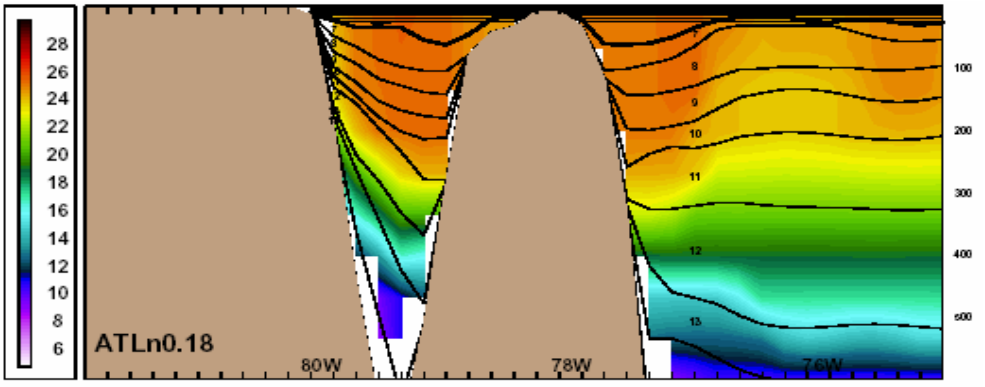

mix.layr.temp year 1.00 (jan 17) [01.6H]
ATLn0.18
ci .200 deg
10.40 to 25.82
35N
30N
25N
80W
75W
30
28
26
24
22
20
18
16
14
12

(e) 0.18 degree

(a)



(b)



(c)

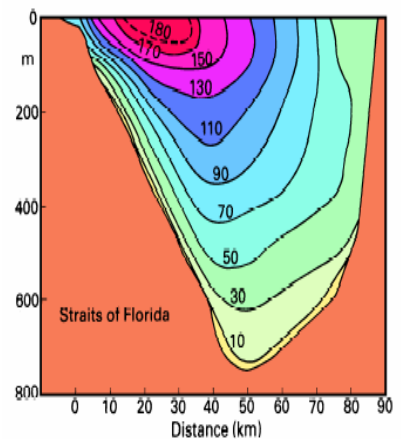


Figure 3 simulated (a and b) and observed (c) temperature vertical cross-section at 27°N

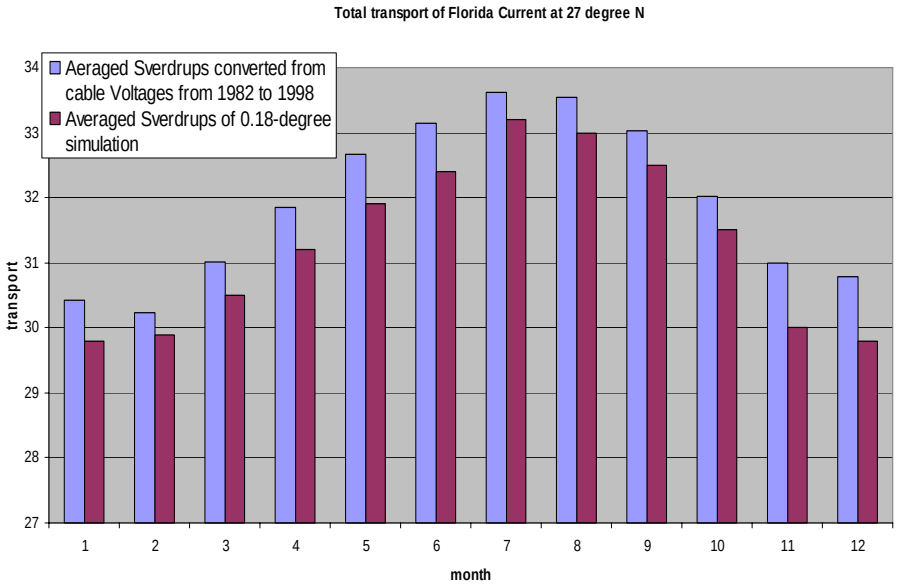


Figure 4 Simulated and observed Gulf Stream transport at 27°N

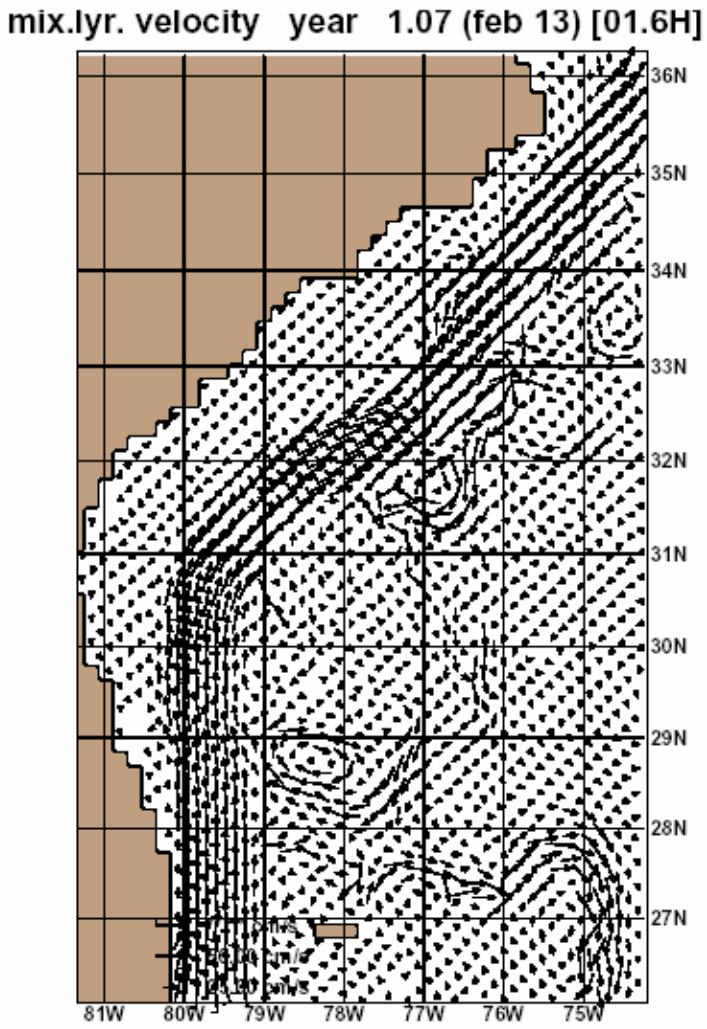


Figure 5 Horizontal velocity in 0.06° simulations

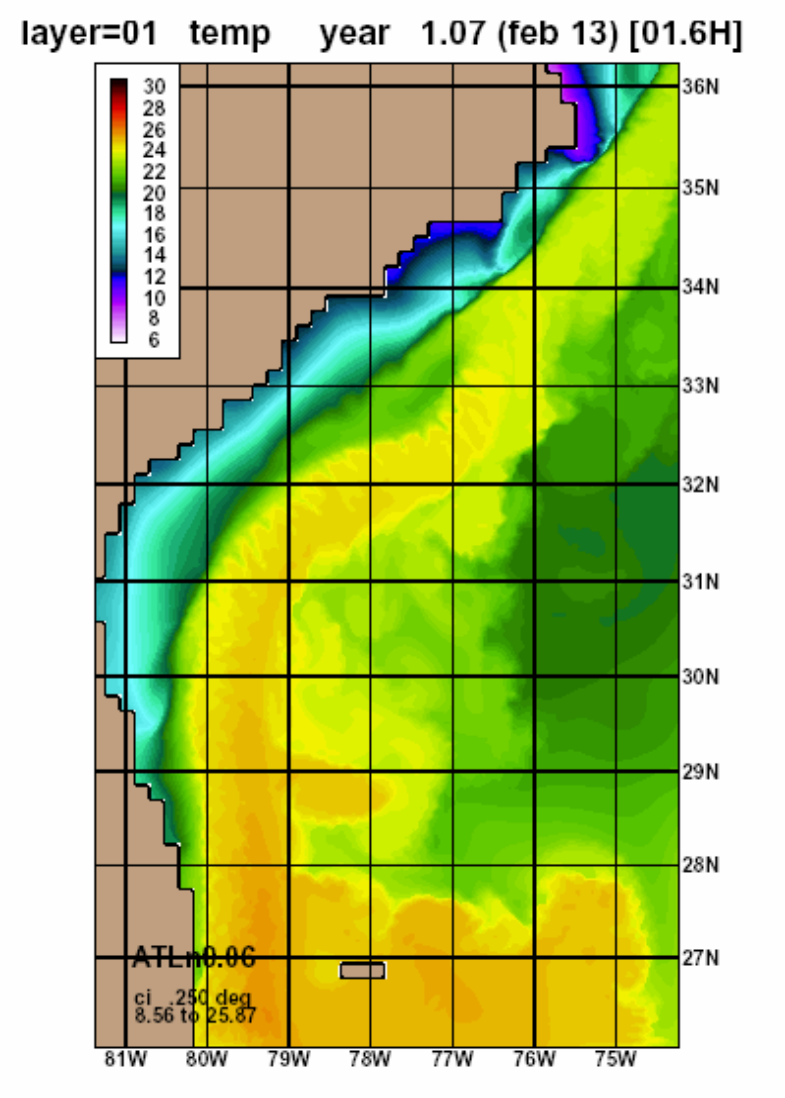


Figure 6 Sea surface temperature in 0.06° simulations

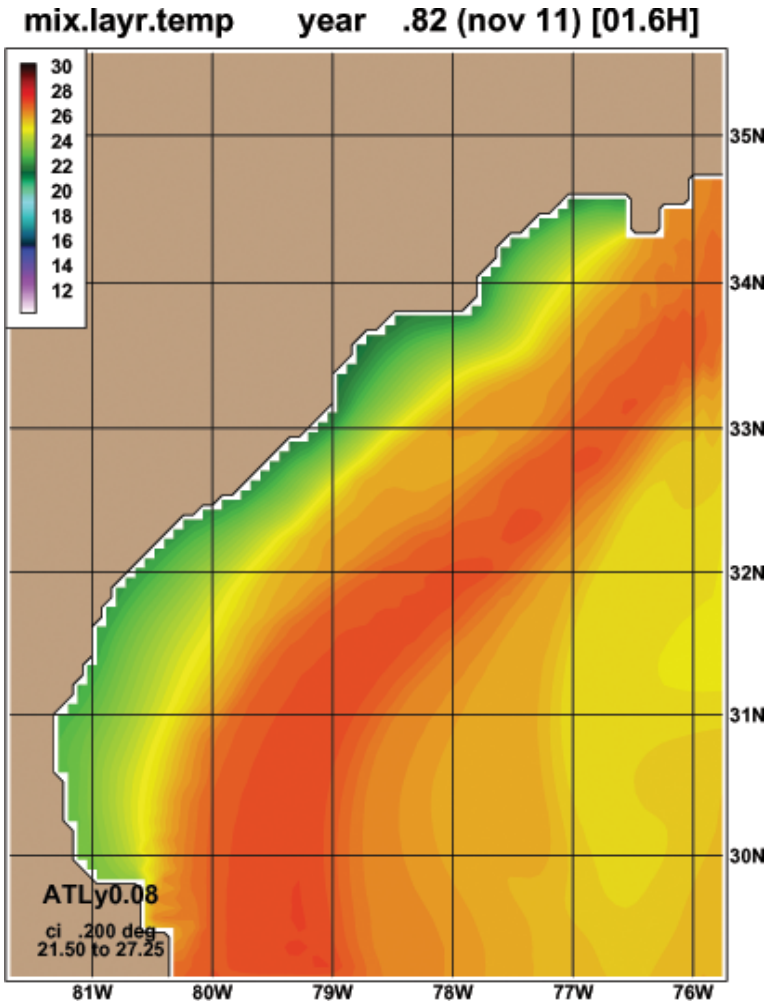


Figure 7 Mixed-layer SST in the 0.08 degree simulation on Nov. 11

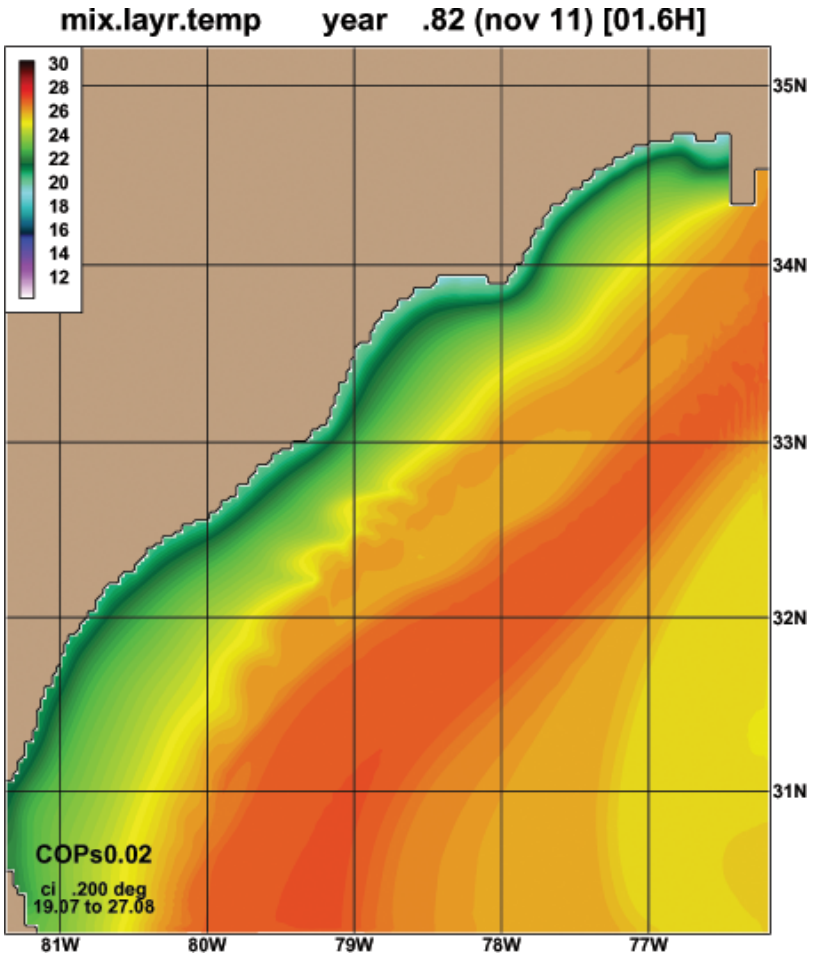
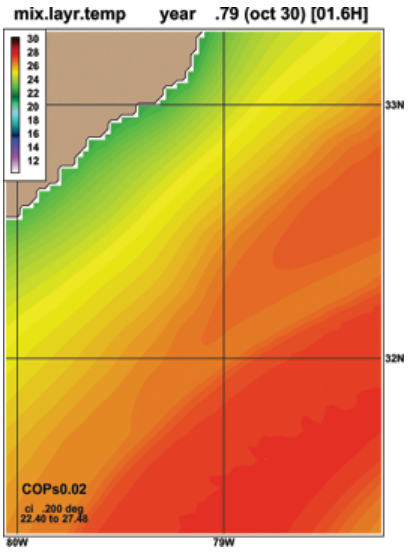
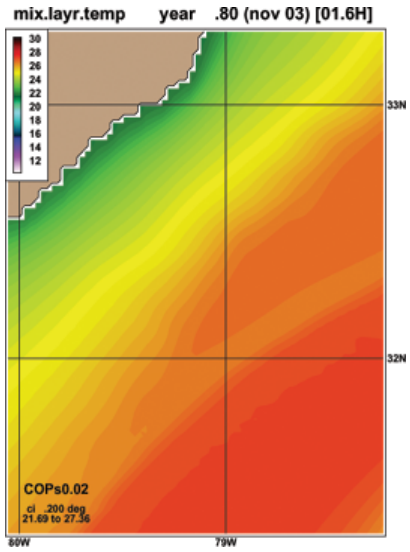


Figure 8 mixed-layer SST in the 0.027 degree simulation on Nov. 11

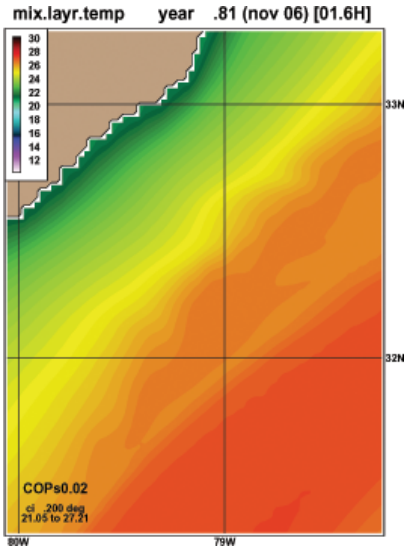
Figure 9 SST of 0.027º simulation from Oct. 30 to Nov. 15


mix.layr.temp year .79 (oct 30) [01.6H]
30
28
26
24
22
20
18
16
14
12
33N
32N
COPs0.02
ci .200 deg
22.40 to 27.48
80W
79W

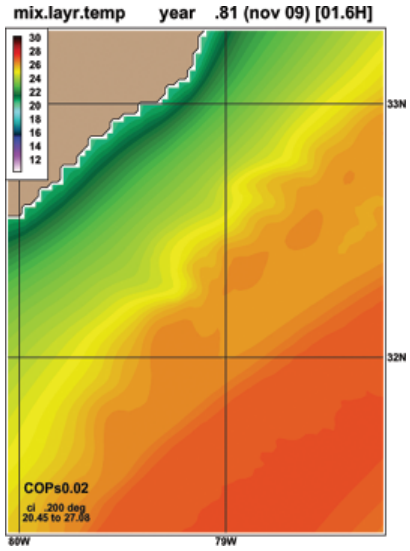
(a)


mix.layr.temp year .80 (nov 03) [01.6H]
30
28
26
24
22
20
18
16
14
12
33N
32N
COPs0.02
ci .200 deg
21.69 to 27.36
80W
79W

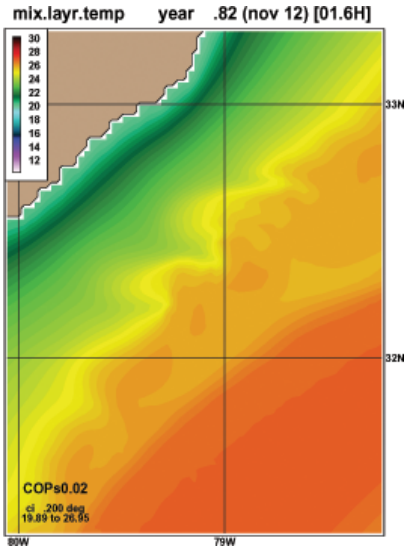
(b)


mix.layr.temp year .81 (nov 06) [01.6H]
30
28
26
24
22
20
18
16
14
12
33N
32N
COPs0.02
ci .200 deg
21.05 to 27.21
80W
79W

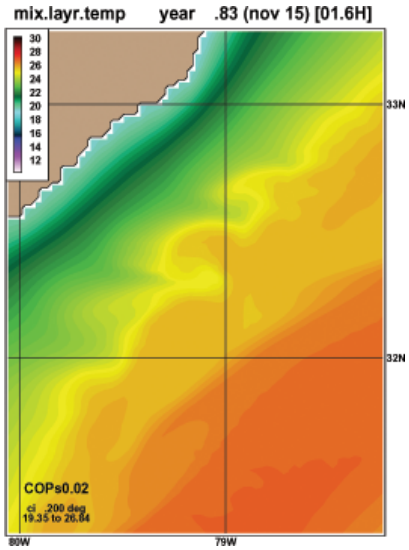
(c)


mix.layr.temp year .81 (nov 09) [01.6H]
30
28
26
24
22
20
18
16
14
12
33N
32N
COPs0.02
ci .200 deg
20.45 to 27.08
80W
79W

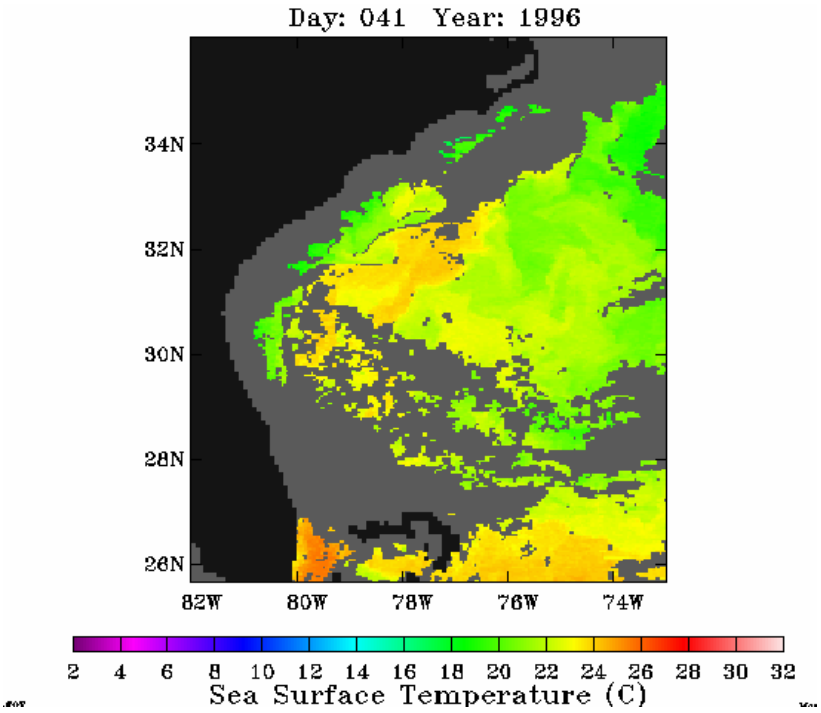
(d)


mix.layr.temp year .82 (nov 12) [01.6H]
30
28
26
24
22
20
18
16
14
12
33N
32N
COPs0.02
ci .200 deg
19.89 to 26.95
80W
79W

(e)


mix.layr.temp year .83 (nov 15) [01.6H]
30
28
26
24
22
20
18
16
14
12
33N
32N
COPs0.02
ci .200 deg
19.35 to 26.84
80W
79W

(f)



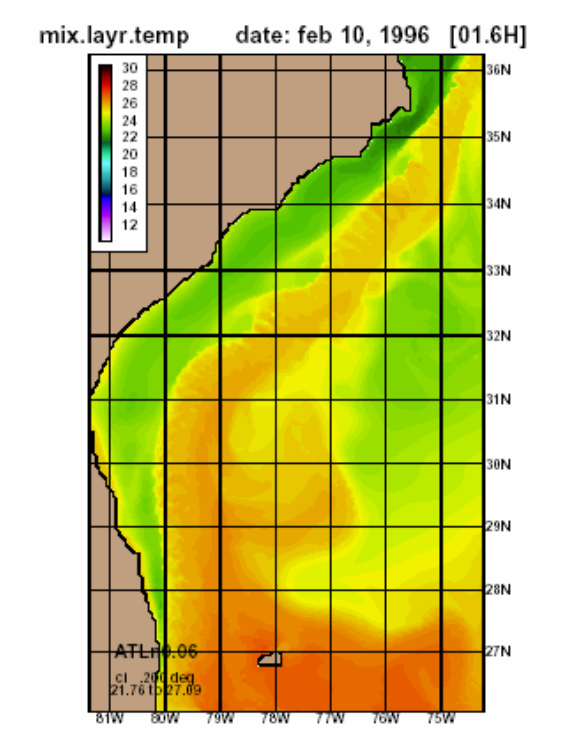


Figure 10 Comparison of satellite SST image and simulated mixed layer SST on Feb. 10, 1996

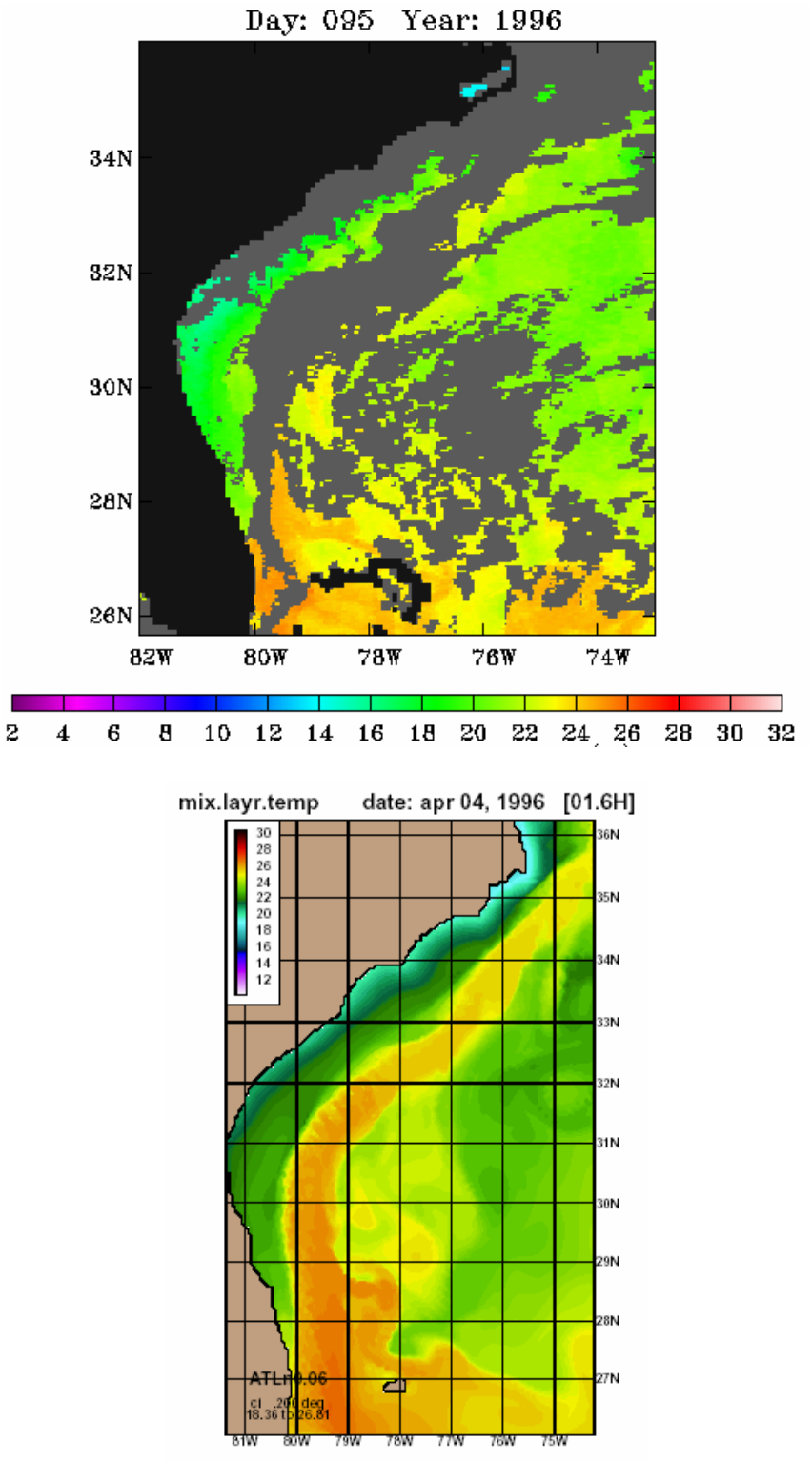


Figure 11 Comparison of satellite SST image and simulated mixed layer SST on April 4, 1996

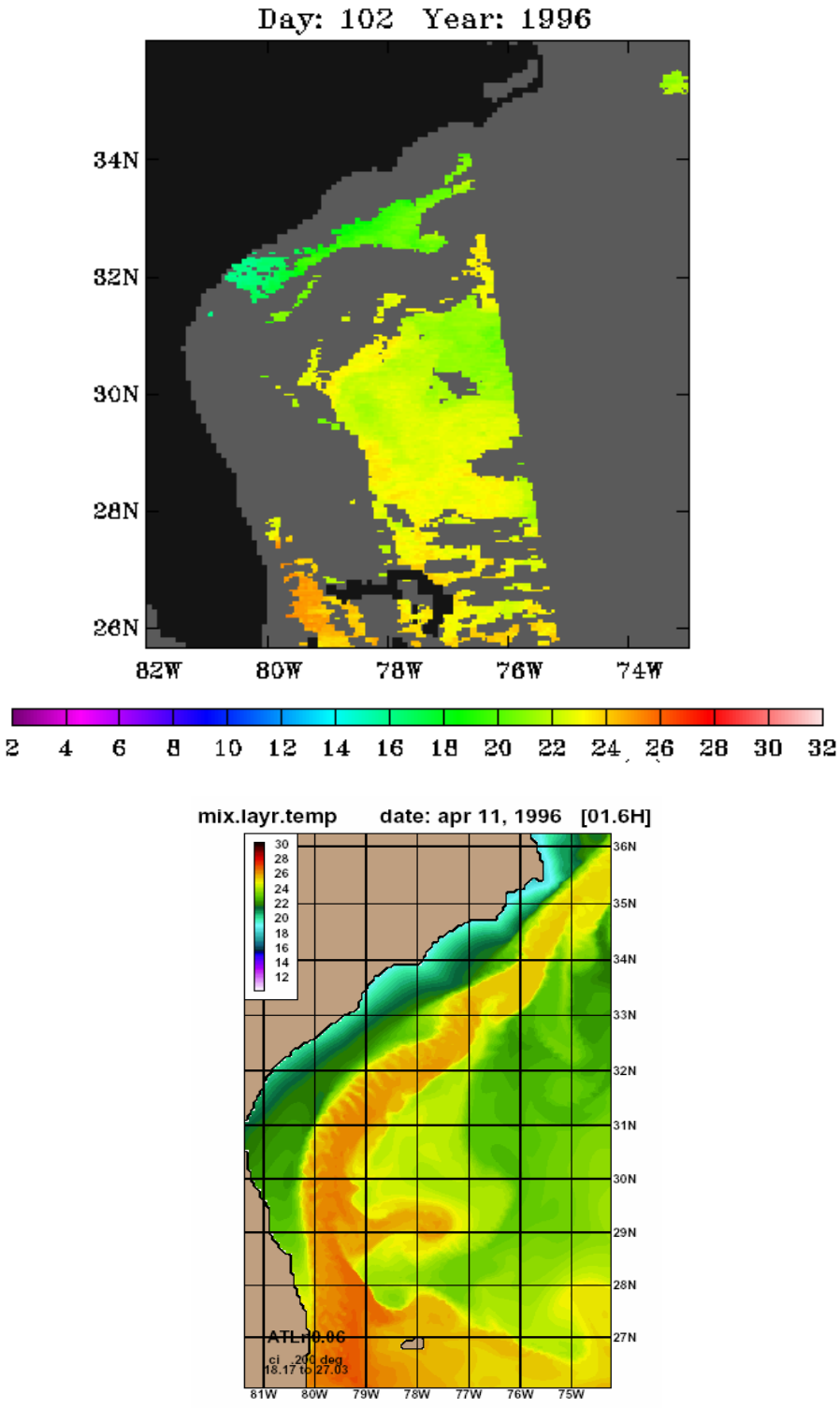


Figure 12 Comparison of satellite SST image and simulated mixed layer SST on April 11, 1996

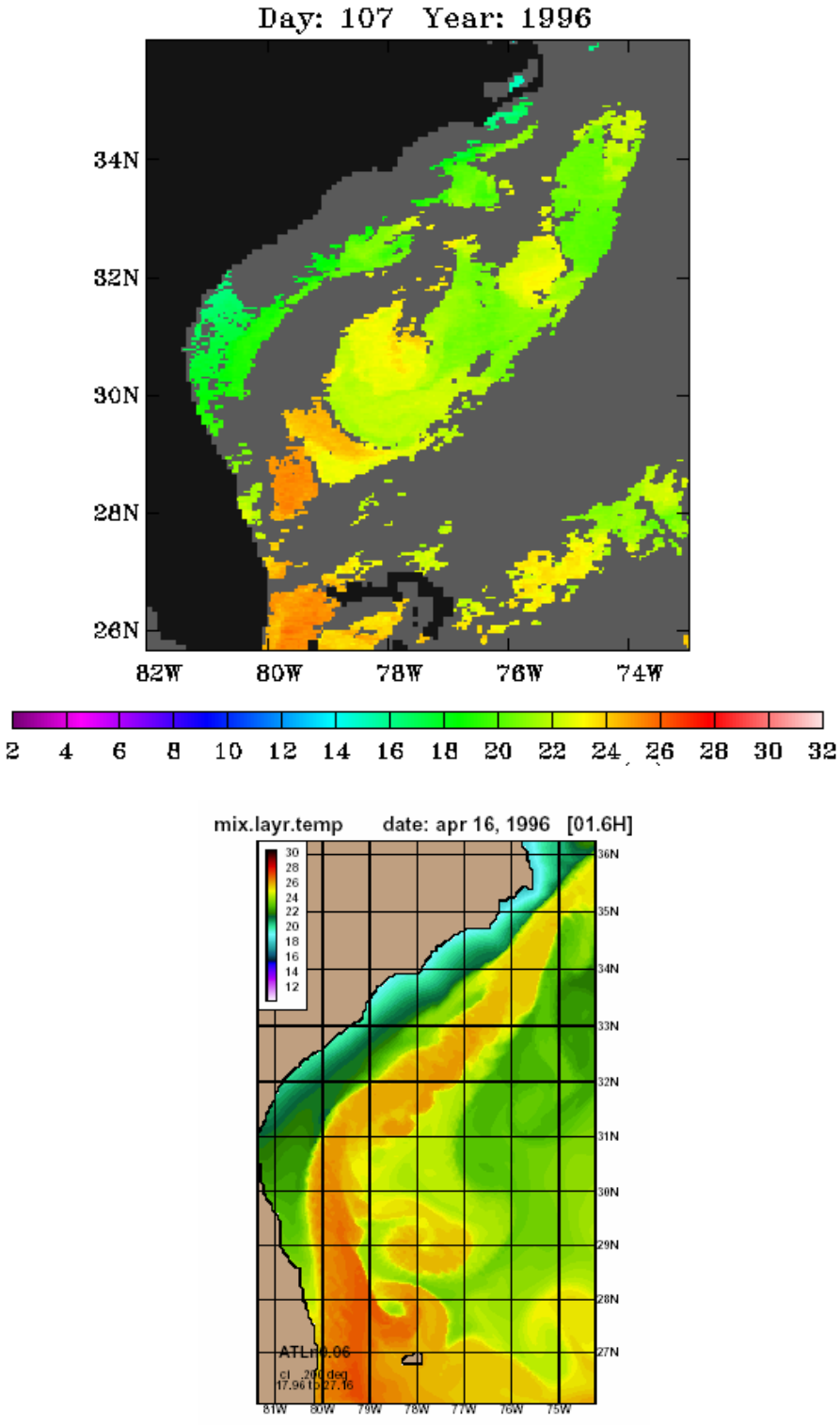


Figure 13 Comparison of satellite SST image and simulated mixed layer SST on April 16, 1996

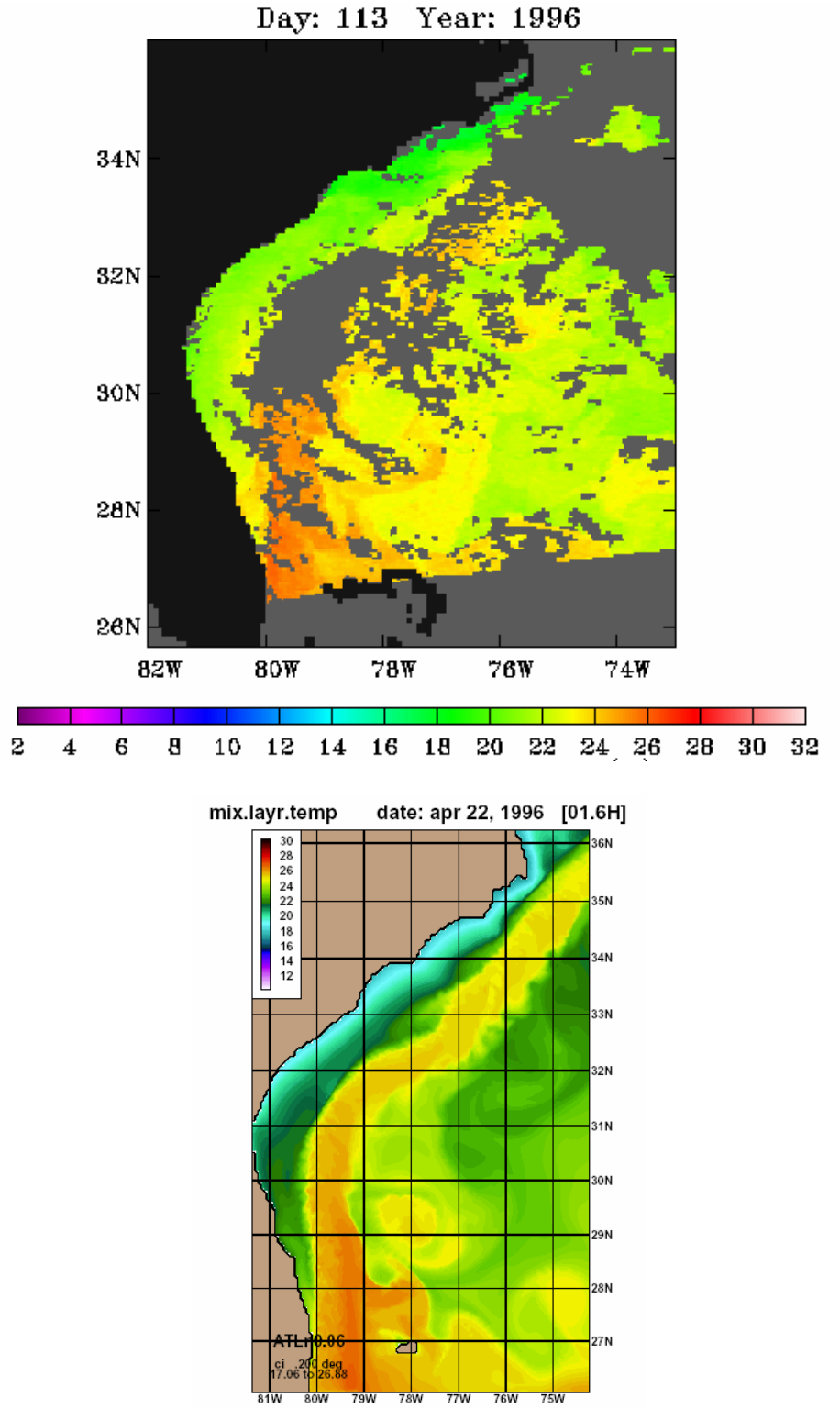


Figure 14 Comparison of satellite SST image and simulated mixed layer SST on April 22, 1996

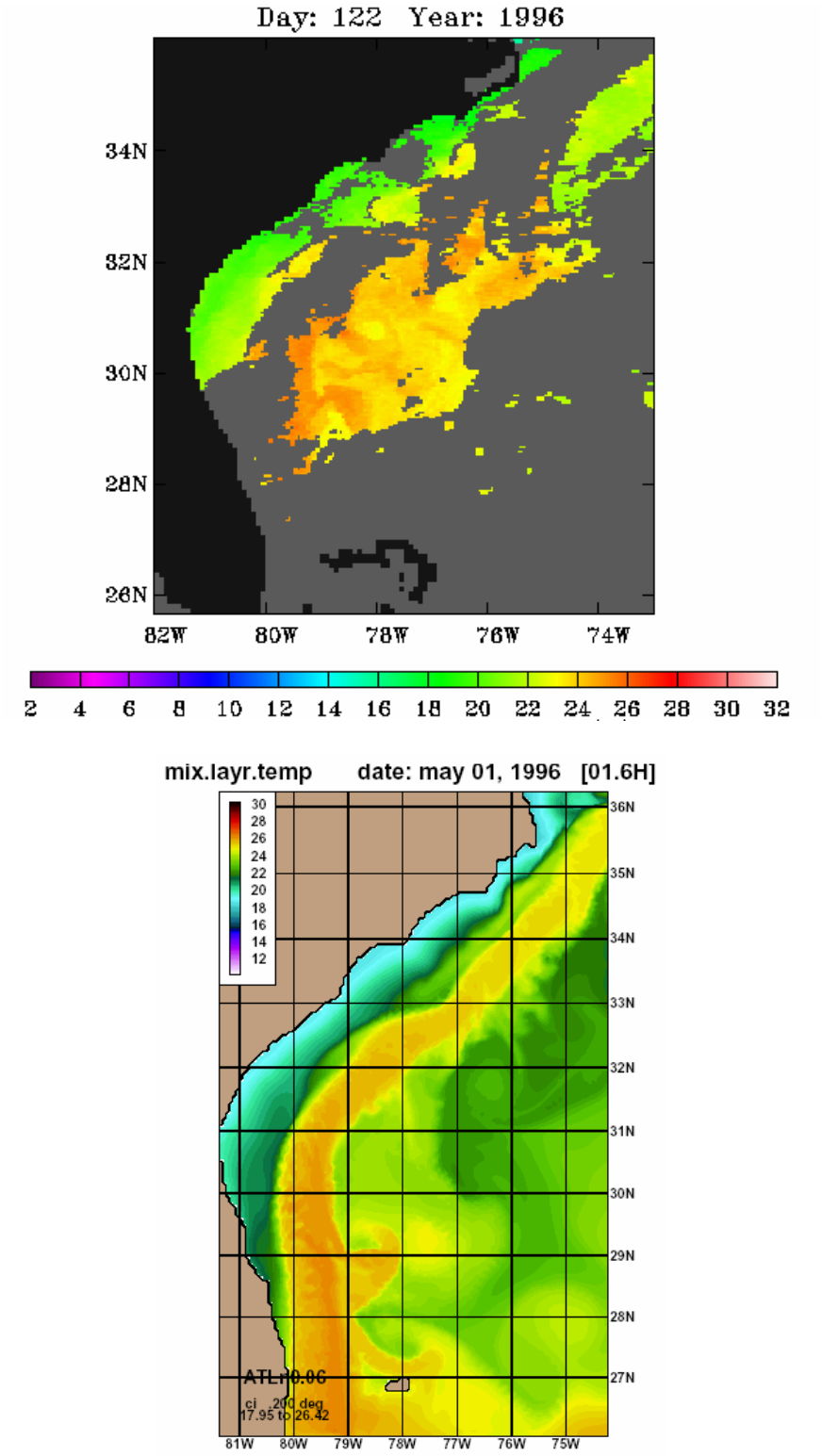


Figure 15 Comparison of satellite SST image and simulated mixed layer SST on May 01, 1996

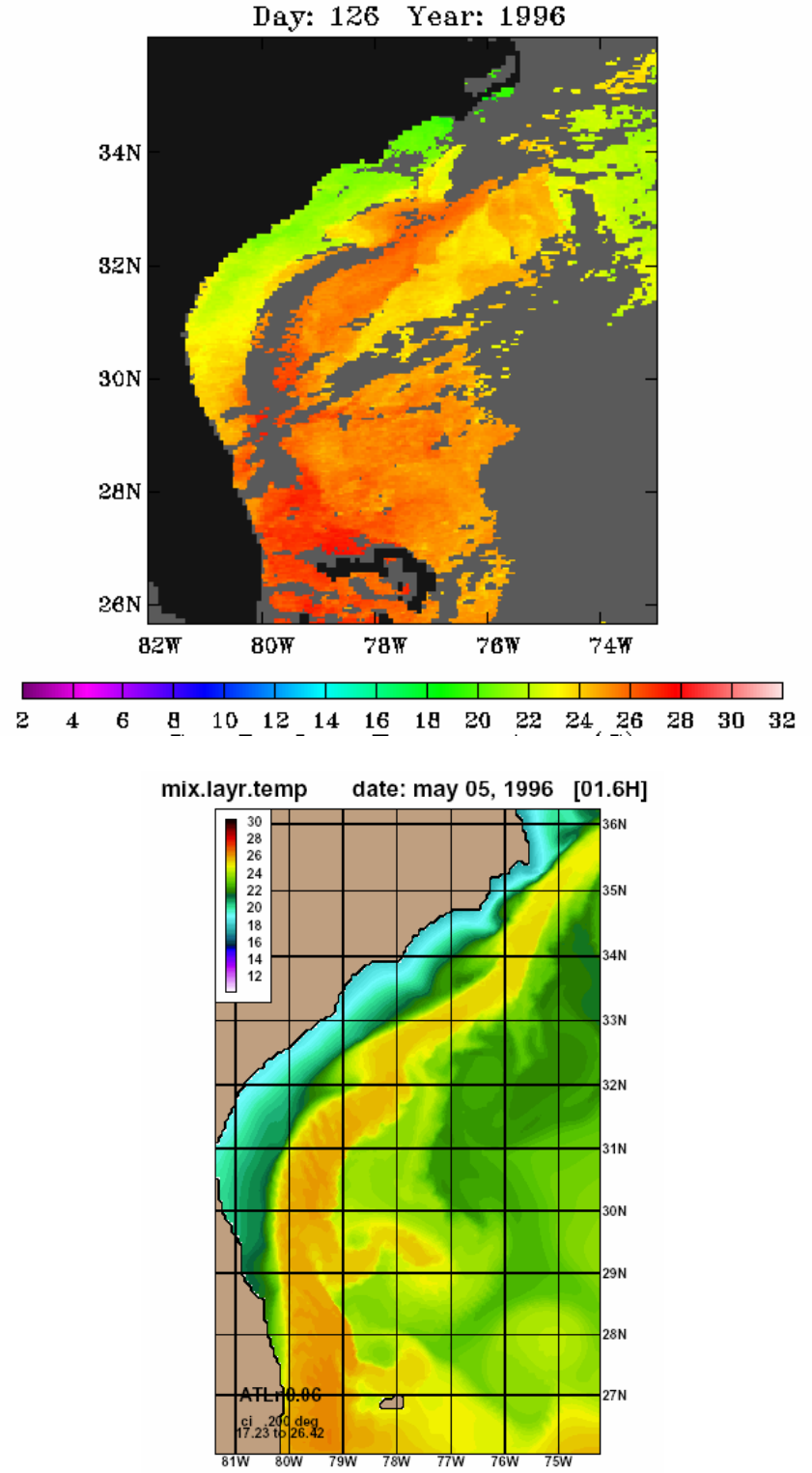


Figure 16 Comparison of satellite SST image and simulated mixed layer SST on May 05, 1996

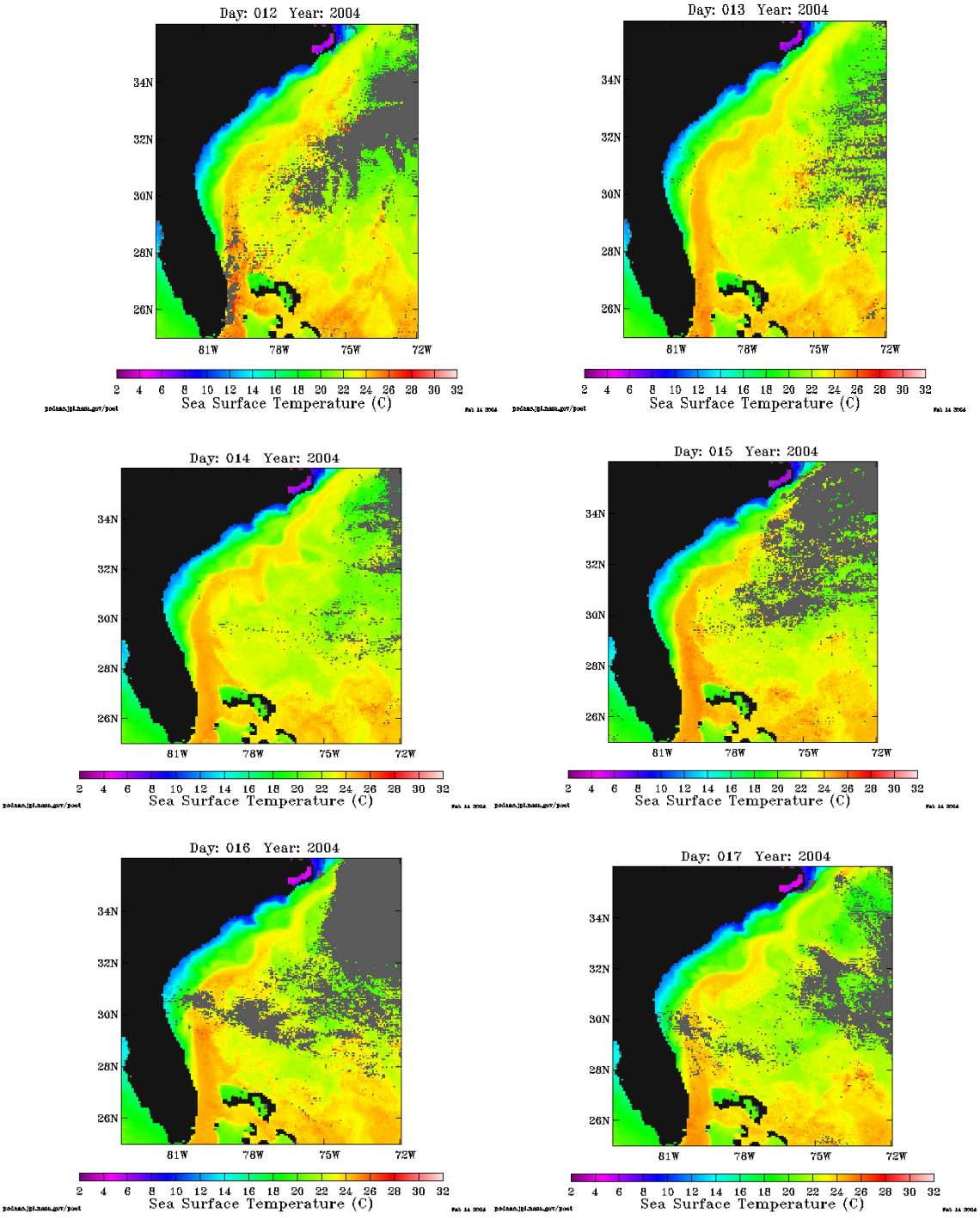
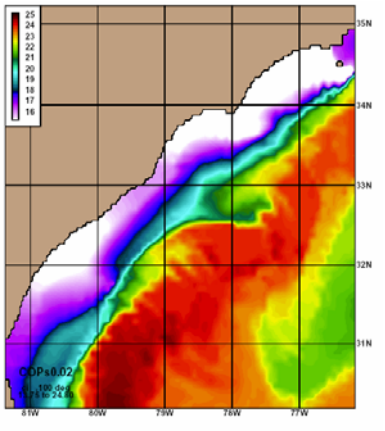
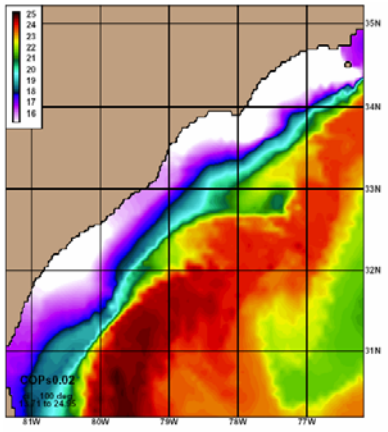


Figure 17. MODIS SST of SAB from Jan. 12 to Jan. 17, 2004

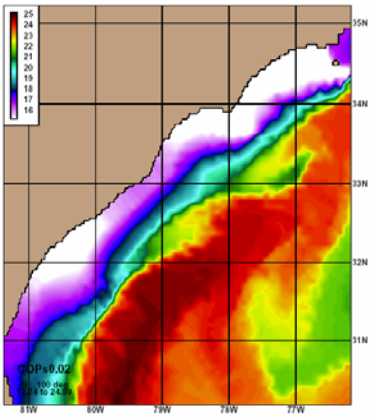
Jan. 12



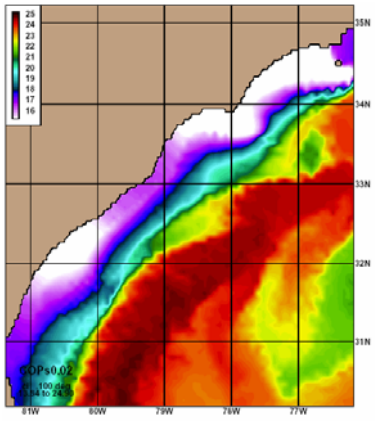
Jan.13



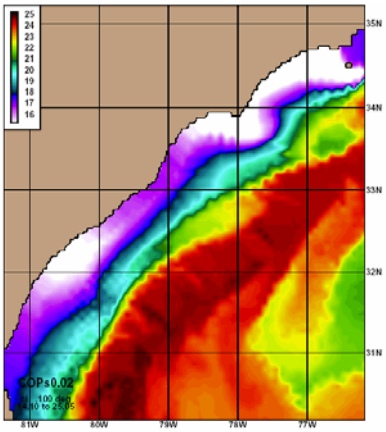
Jan. 14



Jan. 15



Jan. 16



Jan. 17

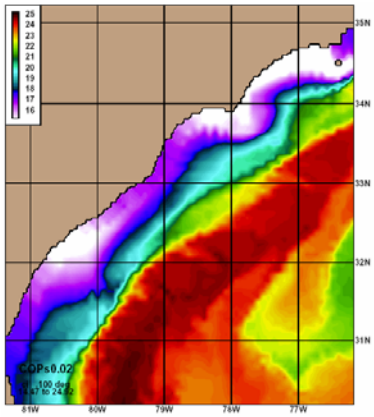
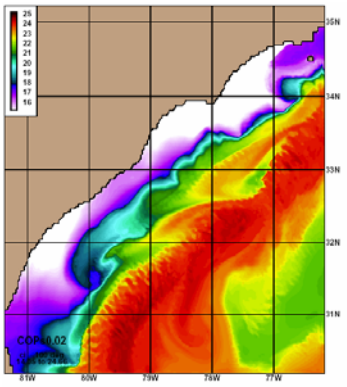
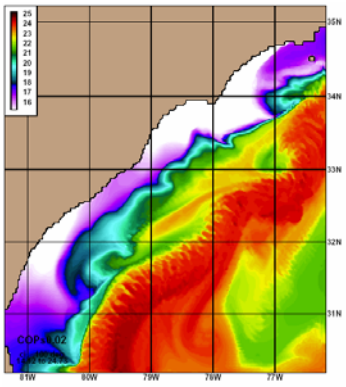


Figure 18 SST of NAOPS without nesting

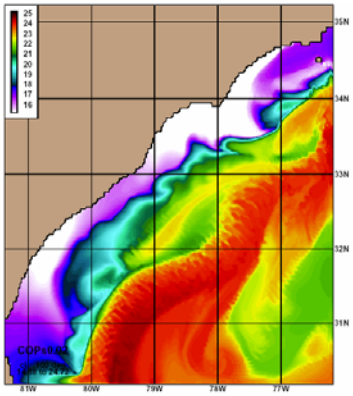
Jan. 12



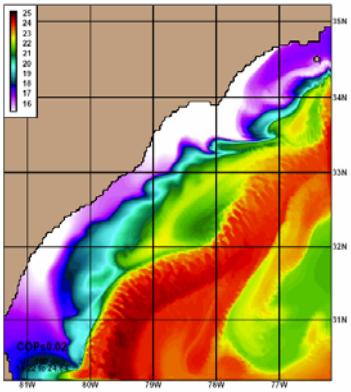
Jan. 13



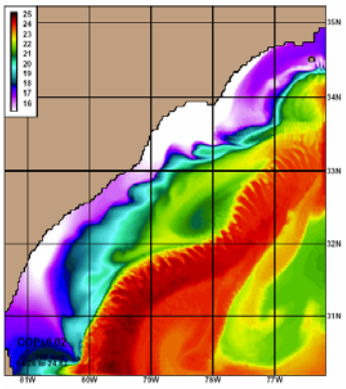
Jan. 14



Jan. 15



Jan. 16



Jan. 17

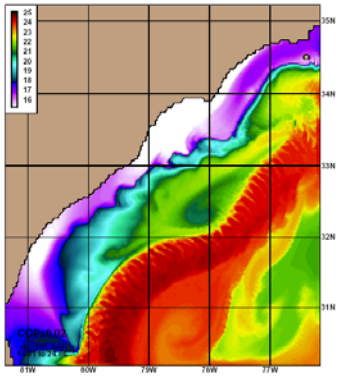


Figure 19 SST of 0.027-degree nested NAOPS simulation

Chapter 4

EFFECT OF BATHYMETRIC CURVATURE ON THE GULF STREAM INSTABILITY IN THE VICINITY OF THE CHARLESTON BUMP

1. **Introduction**

It was revealed by early sea surface temperature (SST) satellite radiometer data and derived images that wavelike perturbations traveled northward along the western edge of the Gulf Stream front at a speed of about 30 km/day (Legeckis, 1975, 1979) in the South Atlantic Bight (SAB, Figure 1). Northward propagation of similar wavelike patterns was also evident in Lee and Mayer's (1977) current measurements in the Florida Strait, off Onslow Bay, North Carolina (Pietrafesa and Janowitz, 1980; Bane et al., 1981) and in the GABEX I moored array (Lee and Atkinson, 1983). These wavelike perturbations were believed to be manifestations of Gulf Stream lateral meanders and eddies. In fact, Pietrafesa and Janowitz (1980) provided phase speed, 25-75 cm/s and wavelength, 100-300km, estimates of the frontal waves as they passed by mooring current meters in Onslow Bay.

At proximately 32°N, a submarine ridge called the Charleston Bump (referred to as CB here after) extends seaward from the continental slope offshore of Charleston, South Carolina (Figure 1). This topographic feature produces an eastward deflection in the Gulf Stream (Pietrafesa et al., 1978; Rooney, et al, 1978; Brooks and Bane, 1978), forming a quasi-permanent 10 to 150 km meander. It has also been reported that the lateral meanderings of the Gulf Stream undergo a dramatic 'amplification' (Knauss, 1969; Maul

et al., 1978; Bane and Brooks, 1979; Bane, 1983; Hood and Bane, 1983; Olson et al., 1983) downstream from the CB. Accumulating evidence has suggested a regional difference in spatial scale of Gulf Stream meanders: south of the latitude of the CB, cold-core frontal eddies tend to occur as smaller, elongated filaments (Lee and Mayer, 1977; Lee at al., 1981; Lee and Atkinson, 1983); north of CB, frontal eddies tend to be considerably larger (Pietrafesa and Janowitz, 1979, 1980; Bane and Brooks, 1979; Pietrafesa and Janowitz, 1980; Bane et al., 1981; Brooks and Bane, 1981, 1983). A recent example consistent with these prior observations is presented in Figure 2 which shows the MODIS SST distribution throughout the SAB from 12 to 17 January, 2004. A perturbation on January 12, 2004 at 32°N was amplified after passing over the CB.

The triggering mechanism for the larger meanders and filaments downstream of the CB is presumably the topographic effect of the CB (Pietrafesa et al, 1978; Rooney et al, 1978; Brooks and Bane, 1978; Chao and Janowitz, 1979; Legeckis, 1979; Pietrafesa, 1983; Dewar and Bane, 1985). Since Gulf Stream flow has both horizontal and vertical shear, many studies surmise that the large meanders result from local barotropic and baroclinic instabilities. In a two-layer model of the Gulf Stream, Orlanski (1969) demonstrated that topographical slope is a stabilizing factor, while the height of the topography is a destabilizing factor. Sun and Pietrafesa (1992) extended the Orlanski model by including both laterally and vertically sheared horizontal currents in a two-layer Gulf Stream model and showed that the energy are transferred between the eddy and the mean flow in both barotropic and baroclinic processes. Xue and Mellor (1992) solved the eigenvalue problem for the instability study of the Gulf Stream using two analytical cross sections representing the mean conditions of the Gulf Stream upstream and downstream

of the CB, and found that the most unstable solution in the region downstream of the CB has a slightly longer wavelength and slower phase speed than those in the region upstream of the Bump. Dewar and Bane (1985) computed the energy budgets of the eddies and the mean flow in the Gulf Stream near the CB using observations from DAMEX current meter mooring deployments, hydrographic surveys, and AXBT surveys, and found that immediately north of the CB, the flow appears to be both barotropically and baroclinically unstable. Miller and Lee (1995a) provided a thorough review on the stability of Gulf Stream meanders in the South Atlantic Bight (SAB). They conducted a series of numerical simulations of the Gulf Stream meanders in the SAB using the Princeton Ocean Model and analyzed the energetics of the simulated circulation. They showed that a hybrid baroclinic-barotropic instability of the Gulf Stream flow was responsible for the growth of meanders. Miller and Lee (1995b) further examined the dynamics of a particular Gulf Stream meander event produced in the SAB, and conclude that geostrophic balance dominated the along-isobath flow, and the nonlinear advection terms in the horizontal momentum equation played an important role in the spatial-temporal development of the Gulf Stream meander.

Another characteristic of the bathymetry in the SAB is the curvature of the isobaths (Figure 1). The isobaths are north-south oriented south of 30ºN, and turn sharply to northeast-southwest oriented around 31ºN. The CB is located in the region of large curve where the Gulf Stream turns from northward to northeast-ward. So, the question is, could the curvature of the isobaths have an effect on development of Gulf Stream meanders and eddies? The radius of the curvature can be as small as 200-300 km, and the centrifugal force required for a current of approximately 2 m/s is of magnitude 10^{-5} N which is the

same order of magnitude of the local Coriolis force. The vorticity created by the curvature is of the order of 10^{-5} s^{-1} which is of same order of magnitude of the planetary vorticity. Thus, two hypotheses to be tested are: isobathic curvature has a significant effect on the stability of the Gulf Stream; and the combined effects of isobaths curvature and the influence of the CB are responsible for the development of the CB.

The significance of understanding the amplification of Gulf Stream meanders and eddies in the vicinity of the CB is three fold. First, large meanders and eddies propagating downstream of the CB have great influence on coastal circulation and cross-shelf transport. Lee et al. (1989) studied the response of South Carolina shelf waters to wind and Gulf Stream forcing with the aid of a comprehensive set of atmospheric and oceanic observations collected during the GALE (Genesis of Atlantic Lows Experiment). They showed that the Gulf Stream appears to have two preferred modes, either on-shore or off-shore, and the sub-tidal variability in the outer shelf is dominated by synoptic frontal eddies and meanders when the stream is in an on-shore mode. Savidge et al. (1992) found that the offshore position of the Gulf Stream front appears to have facilitated the influence of the Gulf Stream on the shelf waters all across the continental shelf. Second, Gulf Stream frontal waves have a significant influence on the productivity of the southeast U.S. continental shelf as demonstrated by Atkinson et al (1982) and Hoffmann et al. (1980). These pioneering works demonstrated that without the onshore flux of nutrient laden Gulf Stream frontal wave waters, the North Carolina continental shelf would be a biological desert. Lee et al. (1991) stated that the onshore transport of the new nitrogen from the nutrient-baring strata beneath the Gulf Stream indicates that frontal eddies serve as a “nutrient pump” for the shelf. New nitrogen flux to the shelf due to Gulf

Stream input could support new production of 7.4 x 10^{12} gC/yr, and the continental shelf area upstream from the CB was identified as a high carbon production area, while there is net nutrient loss downstream from CB. Finally, the warm filament associated with the large eddies downstream of the Bump can transport *Karenia brevis* cells from the Gulf Stream to the inshore area. Pietrafesa et al (1988), Tester et al. (1991) and Tester and Steidinger (1997) found that red tide bloom which occurred in the Fall of 1987 in the Onslow Bay was caused by the across shelf transport of red tide laden Gulf Stream frontal filament waters that were driven across the continental shelf by persistent northeasterly winds. Clearly these frontal waves and their interactions with bottom topography and atmospheric winds are biologically important throughout the SAB. To better understand the dynamics of these frontal waves in the vicinity of the CB, we now attempt to numerically simulate the processes associated with their formation and amplification.

In the present study, a series of numerical experiments were carried out to study the effect of bathymetry on the development and evolution of the Gulf Stream meanders and eddies downstream from the CB in terms of both the bottom bump feature and the curvature of the isobaths. The numerical model used in this study and the set of experiments conducted are described in Section 2. Results are presented in Section 3. Section 4 presents the diagnostic results of the energetics of the simulated Gulf Stream, followed by a conclusion section.

2. Brief Description of the Numerical Model and Numerical Experiments

2.1 Description of the numerical model and data

The Hybrid-Coordinate Ocean Model (HYCOM) (Bleck, 2002) is used in this study. HYCOM is a primitive equation ocean general circulation model that evolved from the Miami Isopycnic-Coordinate Ocean Model (MICOM) (Bleck et al, 1992). HYCOM was developed to address known shortcomings of the MICOM vertical coordinate scheme. Vertical coordinates in HYCOM remain isopycnic in the open, stratified ocean. However, they smoothly transition to z coordinates in the weakly-stratified upper-ocean mixed layer, to terrain-following sigma coordinates in shallow water regions, and back to level coordinates in very shallow water. The latter transition prevents layers from becoming too thin where the water is very shallow. HYCOM has been widely used to study the North Atlantic circulation and Gulf Stream variability (Chassignet et al., 2003 and references therein) and the Gulf of Mexico Loop Current and its eddy shedding processes (Romanou et al., 2004).

In this study, the HYCOM model will be driven by the following atmospheric forcing fields at the ocean surface: wind, air-temperature, relative humidity, short-wave radiation and long-wave radiation. To resolve small-scale perturbations of the Gulf Stream front, a nested grid covering the North Atlantic, then scaled down to the SAB will be implemented. The outer domain covers the North Atlantic (98°W – 14°E, 17°S – 52°N) while the inner domain covers the SAB (82°W – 71°W, 26°N – 36°N). The horizontal resolutions for the outer and inner domains are 0.18 and 0.06 degrees, respectively, and

the vertical resolution will be 22 layers that stretch or shrink vertically as a function of total depth. The bathymetry is derived from the ETOP2 database. The outer domain North Atlantic model will be spun up for 1 year with an initial condition constructed from the Levitus Data Set (Levitus, 1982) and forced by Comprehensive Ocean Atmosphere Data Set (COADS) monthly climatology atmospheric forcing, and the result will be used as the initial and boundary conditions of the inner domain simulations.

2.2 Numerical experiments

The purpose of the study is to investigate the topographic effect of the CB and the curvature of the isobaths in the vicinity of the CB on the amplification of smaller perturbation on the shoreward edge of the Gulf Stream front. To study the effect of the curvature of the isobaths, two sets of bathymetries, one with isobathic curvature that is less than what actually occurs (Figure 3a, b) and the other with isobathic curvature similar to the realistic bathymetry (Figure 3c,d), will be used in the simulations and the results will be compared. In each of the two sets of bathymetries, two bathymetries, one without a bump (Figure 3a,c) and the other with a bump (Figure 3b,d), will be used in the simulations and the results will be compared to assess the effect of the bump in different isobathic curvature settings. A summary of the simulations are listed in Table 1.

3. Results

In this section, the results from the four inner-domain simulations will be presented and compared. SST and temperature anomaly at 125 meter depth will be shown in sections 3.1 and 3.2 respectively.

3.1 Manifestation of Gulf Stream meanders depicted by SST

The evolution of the SST of Case I from January 17 to Feb. 3 is shown in Figure 4 (Ia-c). In this simulation, isobathic curvature is smaller than that of the actual isobaths, and the horizontal isotherms approximately follow the isobaths. Disturbances on the shoreward edge or west wall of the Gulf Stream are barely noticeable in this simulation, suggesting that the Gulf Stream is stable.

The SST of Case II from January 17 to Feb. 3 is shown in Figure 4 (IIa-c). In this simulation, the curvature is the same as in Case I, but a bump is added to the bathymetry. A significant Gulf Stream meander occurred downstream of the bump near 32 ºN from January 21 to January 25, and a warm filament appeared on the shore-ward edge of a Gulf Stream eddy. It intensified after passing over the bump.

The SST of Case III from January 17 to Feb. 3 is shown in Figure 4 (IIIa-c). The bathymetry in this case contains no CB as in Case I, but the isobathic curvature is larger than that in Case I. Gulf Stream frontal perturbations traveling northeastward on the west edge of the Gulf Stream front can be clearly seen in these figures. Since there is no bump in the bathymetry and the Gulf Stream is initialized the same way as in Case I, the difference between Figure 4 (Ia-c) and Figure 4 (IIIa-c) indicates the effect of the

curvature of the isobaths on the instability of the Gulf Stream. Clearly, the increase in isobathic curvature in the region near 30-32ºN in Case III resulted in well-defined meanders that were not present in Case I.

The SST of Case IV from January 17 to Feb. 3 is shown in Figure 4 (IVa-c). In this simulation, a large meander/eddy pair occurred downstream of the CB near 32° N from January 25 to Feb. 03, and the scale of the meander/eddy is much larger than the one in Cases II and III. Both the scale and the shape are comparable to the satellite observations shown in Figure 2. The frontal feature is also traveling northeastward, but at a slower speed than that in Cases II and III. Comparing the results among Cases I-IV, it becomes evident that realistic Gulf Stream meanders are reproduced only when both realistic isobathic curvature and the CB are considered.

3.2 Temperature anomaly at 125 meter depth

The propagation and amplification of the Gulf Stream meanders and eddies can be seen more clearly in the temperature anomaly field below the mixed layer than at the sea surface. The temperature anomaly field at 125 meter depth from January 17 to Feb. 3 of Cases I, II, III and IV is shown in Figures 5 (Ia-c) to (IVa-c), respectively. In Case I, there were only very weak cold and warm anomalies ($-1\ ^\circ C < T < 1\ ^\circ C$) on the shore-ward edge of the Gulf Stream [Figures 5 (Ia-c)]. They travel northeastward along the isobaths, but are not amplified during this propagation. In Case II, a cold anomaly originally located at 32.2 N on January 17 was amplified after passing over the CB. Because of the bump, the cold anomaly was deflected sea-ward. The warm anomaly that followed this cold anomaly also increased, the range of the cold and warm anomaly was

–2 to 2 °C, which is about twice as large as that in Case I. The difference between Case I and Case II depicts the effect of the CB.

In Case III, there were cold and warm anomalies propagating northeastward along the Gulf Stream front at 125 m depth, and they were amplified even though there is no bump in the bathymetry of this simulation. The range of the cold/warm anomaly was –3 to 3°C, which was larger than that in both Cases I and II. This suggests that isobathic curvature played a significant role in the development of Gulf Stream meanders.

In Case IV, a cold anomaly developed near 31.2 N on January 23, and was significantly amplified after passing over the CB. The minimum of the cold anomaly reached –4°C. The difference between Case IV and Case III was the bump effect. The difference between Case IV and Case I was the combined effect of the bump and the isobathic curvature. It is evident that the combined effect of isobathic curvature and the CB produced the largest temperature anomalies below the mixed layer among all four cases. The Gulf Stream meanders depicted at 125 m depth is consistent with the results depicted by SST.

The question then is: how does isobathic topography affect either the attenuation or amplification of Gulf Stream meanders and eddies? The assumption is that the topography affects baroclinic and barotropic process. According to Pedlosky (1979), perturbation flow can extract energy from the mean flow via the $\overline{u'v'}$ (barotropic) and $\overline{u'\rho'}$, $\overline{v'\rho'}$ (baroclinic) processes. Further, Janowitz and Pietrafesa (1982) showed that bottom topography can kinematically induce onshore (offshore) motions when the isobaths spread, i.e the cross-shelf slope decreases or the topography deepens (converge,

i.e. the cross shelf slope increases or the topography shallows) in the direction of flow of both barorotropic and baroclinic boundary currents. Figures 6a and b show the density fluxes ($\overline{u'\rho'}$, $\overline{v'\rho'}$) at 125 meter depth. It can be seen clearly that in a large area around the cold anomaly, the ($\overline{u'\rho'}$, $\overline{v'\rho'}$) terms were positive, so that there was release of potential energy from the mean flow to the eddy, which indicates the presence of a baroclinic instability. Figures 7a-c show the momentum flux ($\overline{u'v'}$) superimposed on the mean flow. The positive value of $\overline{u'v'}$ indicates that energy was transferred from the mean flow to the perturbation through barotropic process.

Since the cold anomaly is associated with cyclonic vorticity and the warm anomaly is associated with anti-cyclonic vorticity, both the topography and the curvature of the isobaths tend to affect the cold and warm anomalies due to the conservation of potential vorticity. From SST and the temperature anomaly at 125 m depth, we can see that both the CB and the curvature tend to amplify the cold/warm anomaly. The combination of the CB and the curvature produced the largest impact on the amplification of the cold/warm anomalies as shown in Case IV. Thus, it seems that both isobathic curvature and the CB played a significant role in inducing the baroclinic and barotropic stability of the Gulf Stream. In the next section, more indepth energy analysis will be carried out to identify barotropic and baroclinic processes.

4. Diagnostics of Energy Conversion

In this section, an energy analysis will be applied to Case IV using two methods. The first method is based on traditional eddy kinetic and potential energy equations. This

medthod was used for analyzing the energetics of the Florida Current (Brooks and Niiler, 1977) and of the Gulf Stream after it has passed Cape Hatteras (Rossby, 1987). The second method is based on a Multi-scale Energy and Vorticity Analysis (MS-EVA) (Liang and Robinson, 2003a, b). The result of the first method is discussed in section 4.1 and the second method in section 4.2. MS-EVA will also be applied to Cases II and III, and the results will be discussed in Section 4.3.

4.1 Energy Analysis using Brooks and Niiler (1977) Energy Equation for Case IV

Consider, first, the energy balance in the simulated circulation using the energy balance equation of Brooks and Niiler (1977) and Rossby (1987), as shown in Equation 1a-f.

$$\frac{d}{dt}\left\{\frac{1}{2}\left(\overline{u'^2}+\overline{v'^2}\right)+\frac{1}{2}g\overline{\rho'^2}\Big/\left|\frac{\partial\bar{\rho}}{\partial z}\right|\rho_0\right\}= \tag{1a}$$

$$-\left\{\frac{\partial}{\partial x}\left(\overline{u'p'}/\rho_0\right)+\frac{\partial}{\partial y}\left(\overline{v'p'}/\rho_0\right)+\frac{\partial}{\partial z}\left(\overline{\omega'p'}/\rho_0\right)\right\} \tag{1b}$$

$$-\left\{\overline{u'^2}\frac{\partial\bar{u}}{\partial x}+\overline{v'^2}\frac{\partial\bar{v}}{\partial y}+\overline{u'v'}\left(\frac{\partial\bar{v}}{\partial x}+\frac{\partial\bar{u}}{\partial y}\right)\right\} \tag{1c}$$

$$-\left\{g\overline{u'\rho'}\frac{\partial\bar{\rho}}{\partial x}\Big/\left|\frac{\partial\bar{\rho}}{\partial z}\right|\rho_0+g\overline{v'\rho'}\frac{\partial\bar{\rho}}{\partial y}\Big/\left|\frac{\partial\bar{\rho}}{\partial z}\right|\rho_0\right\} \tag{1d}$$

$$-\left\{\overline{u'w'}\frac{\partial\bar{u}}{\partial z}+\overline{v'w'}\frac{\partial\bar{v}}{\partial z}\right\} \tag{1e}$$

$$-\left\{\frac{1}{2}u'\left(u'^2+v'^2+g\rho'^2\Big/\left|\frac{\partial\bar{\rho}}{\partial z}\right|\rho_0\right)_x+\frac{1}{2}v'\left(u'^2+v'^2+g\rho'^2\Big/\left|\frac{\partial\bar{\rho}}{\partial z}\right|\rho_0\right)_y\right\} \tag{1f}$$

The first term on the right-hand side (1b) represents the pressure-work term; the second term (1c) the conversion of perturbation kinetic energy; the third term (1d) the

conversion of perturbation potential energy from the mean kinetic and potential energy, respectively. The fourth term (1e) represents the energy transfer due to small-scale shear instabilities (Brooks and Niiler, 1977), and the fifth term (1f) represents the conversion of perturbation kinetic and potential energy by the perturbation field. Dewar and Bane (1985) analyzed the eddy energy in the CB region based on observations from the DAMEX project. In the analysis, energy balance terms were nearly identical to terms 1b, 1c, and 1d, with only two slight differences. First, (1) includes both eddy kinetic energy and eddy potential energy, so that the total eddy energy decay and growth can be estimated, whereas Dewar and Bane (1985) considered eddy kinetic and potential energies separately. Second, terms 1b, 1c and 1d equal to the corresponding terms in Dewar and Bane (1985) divided by water density. Note that Dewar and Bane (1985) estimated each term in cm-gram-second (CGS) units (i.e. ergs $cm^{-3}s^{-1}$), whereas m-kg-second (MKS) units are used in our calculations. Therefore, the energy unit used in our calculation differs from Dewar and Bane's by a factor of 10^4 (assuming water density is approximately 1000 $kg \cdot m^{-3}$). The values of the four terms (1a), (1b), (1c) and (1d) which are the major terms of (1) are presented below.

Figure 8 shows the baroclinic transfer rate term (term 1d in eq. 1) of Case IV at depth of 7.5, 25, 47.5, 80, 125, 190, 305, 495, and 760 meters. In this figure, it can be seen that the largest transfer rate is located at 80 and 125 m depth. The location of the largest transfer rate is at approximately (78.5ºW, 32°N), which is immediately north of the CB. The maximum value of the baroclinic transfer rate is 5×10^{-7} m^2s^{-3} which is consistent with the calculations of Dewar and Bane (1985). The baroclinic transfer rate further

downstream of the CB around (77.5ºW, 32.7°N) is negative, indicating that potential energy is transferred back to the mean flow in that region.

Figure 9 shows the barotropic transfer rate (term 1c in eq. 1) of Case IV at depth of 7.5, 25, 47.5, 80, 125, 190, 305, 495, and 760 meters. Unlike the baroclinic transfer rate, the barotropic transfer rates from the surface down to the 125 m depth are about the same magnitude, and begin to decrease with depth below 125 m. The highest transfer rate occurs near (78º W, 31.8° N), which is immediately north of the bump. The magnitude of the barotropic transfer rate is 3×10^{-7} m^2s^{-3} which is also in agreement with the Dewar and Bane (1985) calculation based on the observational data (0.12×10^{-2} ergs cm^{-3} s^{-1}).

Since the barotropic and baroclinic energy transfer processes occur mainly above 125 m depth, in the following we will analyze the energy balance at 25 and 125 m depth. The terms (1a) and (1b) in eq. 1 are calculated at 25 and 125 m depth, and the results are shown in Figures 10 and 11, respectively. The results indicate that barotropic transfer is the major contributor to the energy change at the 25 m depth, whereas baroclinic transfer is the major contributor to the energy change at the 125 m depth. It is worth noting that in Figure 11a, the region south of the CB is a weak energy loss region (-1.0×10^{-7} m^2s^{-3}), while the region immediately north of the bump is a region of strong energy growth region (8.0×10^{-7} m^2s^{-3}), and the region further north is a region of strong energy decay region (-5.0×10^{-7} m^2s^{-3}). Lee et al (1991), after analyzing the cross-front momentum and heat fluxes based on historical observation data, concluded that two stable regions in the SAB are from 30° to 32°N and from 33° to Cape Hatteras, and eddies grow rapidly after the Gulf Stream impinges upon the CB and turns offshore. The modeling results presented above are in agreement with the conclusion of Lee et al. (1991). The model

results also show the presence of large differences between the cyclonic and anti-cyclonic flanks of the Gulf Stream. According to Dewar and Bane (1985), for the most part of the Gulf Stream, eddies on the cyclonic side of the flow perform net work on the mean flow, while those on the anti-cyclonic side are energized by the mean flow. This feature is consistent with the model results as shown in Figures 10 and 11.

4.2 Analysis with MS-EVA for Case IV

The multiscale energy and vorticity analysis (MS-EVA) is a new methodology for the investigation of multiscale interactive oceanic processes that are intermittent in space and time (Liang and Robinson, 2003a, b). Through exploring pattern generation and energy transfers, transports, and conversions, the intricate relationships between events on varying scales and locations in phase space and physical space can be sorted out. The basic idea for this has been delineated and the formulation developed, by Liang and Robinson (2003a), and an avenue to application is established in Liang and Robinson (2003b). The latter study also established a generalization of the concept of stability on a localized basis, which allows one to build an easy-to-use criterion for the identification of baroclinic and barotropic instability processes utilizing actual or modeled ocean and atmosphere datasets. Since our hypothesis is that the combined effect of the CB and the isobathic curvature in the region let to the generation and amplification of the Charleston Trough through baroclinic and barotropic instability processes, we will use MS-EVA to analyze the dataset obtained from Case IV.

In the MS-EVA, processes are represented on scale windows. A scale window implies a subspace of the space to which the field under consideration belongs, with a

certain range of the scales involved. A scale level j is a dimensionless index such that 2^{-j} measures the passage of the events since the beginning for a time series scaled by its duration. We need three scale levels, j_0, j_1, and j_2, $j_0 \le j_1 \le j_2$, that demarcate three mutually exclusive windows: 1) large-scale ($j \le j_0$); 2) meso-scale ($j_0 < j \le j_1$); and 3) submesoscale ($j_1 < j \le j_2$). For simplicity, a window may be referenced as $\hat{w}$, with $\hat{w} = 0, 1, 2$ standing for largescale, mesoscale and submesoscale, respectively. MS-EVA provides a way to study the interactions between these windows.

In a symbolic form, the growths of kinetic energy $K^{\hat{w}}{}_n$ and available potential energy $A^{\hat{w}}{}_n$ on window $\hat{w}$ ($\hat{w} = 0, 1, 2$) and at time step n for a frictionless fluid flow are governed by

$$\bar{K_n^w} = \Delta Q_{K_n^w} + \Delta Q_{P_n^w} + T_{K_n^w} - \bar{b_n^w} \tag{2}$$

$$\bar{A_n^w} = \Delta Q_{A_n^w} + T_{A_n^w} + \bar{b_n^w} \tag{3}$$

In the equations, the ΔQ-terms represent the multi-scale transport process on the specified scale window, 'b-terms' represent buoyancy conversion terms, and the "T-terms" are perfect transfers among scale windows in the sense that they vanish when averaged over windows $\hat{w}$ and time step n. Perfect transfer is a key concept in the MS-EVA formulation (Liang and Robinson, 2003a). It allows one to separate transport processes from the nonlinear energetic terms based on a firm physical ground and, hence, to tell whether the energy growth for a window at a particular location and time is due to the local energy transfer or transport from surrounding regions.

A natural generalization of these stability theories to handle real world problems is fulfilled with these terms. In the simple case with only two windows (window 0 and window 1), let

$$BC = T_{A_n^1}^{0\to 1} = T_{A_n^1,h}^{0\to 1} + T_{A_n^1,z}^{0\to 1} + TS_{A_n^1}^{0\to 1} \quad (4)$$

$$BT = T_{K_n^1}^{0\to 1} = T_{K_n^1,h}^{0\to 1} + T_{K_n^1,z}^{0\to 1} \quad (5)$$

where the superscript 0->1 denotes the energy transfer from window 0 (large scale) to window 1 (meso scale), and T_A terms represent potential energy transfer and T_K terms represent kinetic energy transfer. The subscripts, 'h' and 'z' denote the energy transfer in the vertical and horizontal direction respectively. A criterion was derived in Liang and Robinson (2003a) for instability identification:

1) a flow system is locally unstable if BT + BC > 0, and vice versa;

2) for an unstable system, if BT > 0 and BC < 0, the instability the system undergoes is barotropic;

3) for an unstable system, if BC is positive but BT is not, then the instability is baroclinic; and

4) if both BT and BC are positive, the system must be undergoing a mixed instability.

For convenience, BC and BT may be referred to as, respectively, the baroclinic instability indicator and the barotropic instability indicator, though neither of them per se is enough for instability identification. All the above terms are local in time and space, and hence the criterion is applicable to problems on a generic basis. The traditional energy analysis method uses an energy equation of either a time average or a space average. However, with MS-EVA, we can get the energy balance localized in time and space.

The first step is to determine the scale windows to start the MS-EVA process. From moored or Eulerian current meter observations, Pietrafesa and Janowitz (1980) determined the periods of meanders and eddies in the SAB to be 2-14 days. As we have

previously found, a perturbation in the flow field occurred from January 23 to Feb. 03 in Case IV. For the MS-EVA process, we extracted a time series of 256 time steps with a time interval $\Delta t = 7200\ s$, therefore, the total length of study is 21.33 days from January 12 to February 02. We choose $j_0 = 0$, $j_1 = 4$, and $j_2 = 8$ for the scale window limitations. With this setting: the large-scale window covers variations with a time scale greater than 21.33 days ($j_0 = 0$); the mesoscale window covers variations from 1.33 days ($j_1 = 4$) to 21.33 days ($j_0 = 0$); and the submesoscale window covers variations from 0.083 days ($j_2 = 8$) to 1.33 days ($j_1 = 4$).

The MS-EVA setup also includes a preparation of the background density profile and projection of data onto the model grid. We first interpolate linearly all the field variables defined on the density coordinates onto nine z levels: 7.5, 25, 47.5, 80, 125, 190, 305, 495, and 780 m. The stationary background density profile $\rho(z)$ is then calculated by averaging all the interpolated density data, and its vertical gradient $(\partial\rho/\partial z)$ is used to compute the Brunt–Vaisala frequency which is needed for computing available potential energy.

Figures 12 (a1-6) show the MS-EVA baroclinic transfer rate of Case IV on January 27 at 25, 47.5, 80, 125, 190, 305, 495 m depth, respectively. We can see that the highest baroclinic transfer rate occurs at 125 m depth, and maximum transfer rate reaches 10^{-6} m^2s^{-3} at (78°W, 32ºN). The baroclinic transfer rate is small on the surface levels and bottom levels. Both the value and the location of the baroclinic transfer are in agreement with the traditional analysis shown in Section 3.1. Figures 12 (b1-6) show the corresponding barotropic transfer rate, and it is large from the surface level to 125 m

depth and small below 125 m depth. This is also in agreement with the traditional analysis described in the previous section (4.1).

Since both baroclinic and barotropic transfer rates are large at the 125 m depth, we will look at the interaction between the perturbation and mean flow at this depth for the meander event which occurred between January 23 to 31. Figure 13 shows the evolution of the baroclinic transfer rate from January 23 to 31. It shows that the baroclinic transfer rate north of the CB increased from January 23 to January 26 and decreased from January 27 to 31. Figure 14 shows the evolution of the barotropic transfer rate from January 23 to 31. During the event, the barotropic transfer rate downstream of the CB near 32ºN was positive, and large values occurred on January 26 and 29. These indicate that mixed instability is involved in this eddy amplification process.

Local energy balance: Figures 15a,b depict the time series of eddy Available Potential Energy (APE) and its budget at (77.9°W, 32.2°N), respectively. Large eddy APE occurred on January 25 and 29, and a relative minimum occurred on January 27 (Figure 15a). This is mainly because of the northward propagation of the cold and warm anomalies and the associated energy transfer. As shown in Figure 15b, the local change of APE is mainly due to along-stream advection processes associated with the northward propagation of the temperature anomalies. The baroclinic transfer rate (solid line) is the largest, but it is largely balanced buoyancy convection (dash line). As a result, the local change of APE (dash-dot line) is in close agreement with the advection of APE (dot line). The fact that the baroclinic transfer is mainly balanced by buoyancy convection suggests that most of the APE transferred from mean flow to the eddy by the baroclinic process is converted into eddy kinetic energy through the buoyancy conversion process. Comparing

Figure 15a with Figure 15b, it should be noted that the baroclinic process transfers energy into eddy APE, but the local eddy APE is decreasing because of advection between January 25 and 27. This is further illustrated by Figure 16. Figure 16a shows the times series of the eddy kinetic energy (KE) at the same location as in Figure 15. It shows that the eddy KE increased significantly from January 19 to 29. A relative peak occurred on January 25, and a minimum on January 27, coinciding with the corresponding peak and minimum of eddy APE (Figure 15a), suggesting that mean flow supplied both APE and KE into the eddy. Some of the eddy KE was transferred from the eddy APE. A closer examination of the KE transfer processes (Figure 16b), one can find that both the barotropic and buoyancy processes increased the KE, whereas the advection and pressure work processes led to a decrease in the KE. The sum of these terms (local change of KE, dash-dot line) was mostly positive from January 19 to 28, so that the total energy at the study location increased with time during this period.

4.3 MS-EVA analysis for Cases II and III

As discussed in the last section, amplification of meanders and perturbations in Case IV are due to mixed baroclinic and barotropic energy transfers that occurred in regions with large isobathic curvature and downstream of the CB. To further quantify the contribution from the CB and the isobathic curvature, in this section, we present the results of MS-EVA analysis in Cases II and III, and the results will be compared with that of Case IV. MS-EVA is applied to Cases II and III with the same settings as in Case IV. Since barotropic and baroclinic transfer terms (Equations 4 and 5) are the indicators of the Gulf Stream instability, we will mainly compare the results of these two terms with

those of Case IV. Because the stratification is the same as in Case IV, we will only look at the barotropic and baroclinic transfer rates at the 125 m depth.

The baroclinic and barotropic transfer rates at the 125 m depth on January 25 of Cases II and III are shown in Figure 17. In Case II, there are both baroclinic and barotropic energy transfers from the mean flow to the eddy (Figure 17c and d). However, the magnitude of the transfer rate is 3×10^{-8} m^2s^{-3}, which is much smaller compared with that in Case IV. In Case II, although there is a bump in the bathymetry, isobathic curvature is small compared with that in Case IV. Therefore, the curvature of the isobaths seems to play a very important role in both baroclinic and barotropic processes. In Case III, the bump is removed from the bathymetry, but the isobathic curvature is the same as in Case IV. From Figure 17a,b, we can see that there are barotropic and baroclinic energy transfers from the mean flow to the eddy in Case III, and the magnitude of the energy transfer rate is about 3×10^{-7} m^2s^{-3} (Figure 17a and b). Although this energy transfer rate is smaller than that in Case IV, it is much larger than that of Case II, which indicates that isobathic curvature alone can contribute more to the baroclinic and barotropic energy transfer processes than does the bump effect.

However, the amplification of the Gulf Stream meander/eddy in Case IV is due to the combined effect of isobathic curvature and the bump. Neither isobathic curvature nor the bump alone will cause large amplification enough to produce the Charleston Trough as seen in Case IV. Intuitively, a frontal perturbation behaves differently when passing over a bump on a large curve than from passing over a bump on a small curve. The stability analyses presented in previous sections consistently indicate that the combined effects of

isobathic curvature and the CB on baroclinic and barotropic instability processes are what are needed to explain the meander/eddy growth previously reported in the literature.

5. Discussions and Conclusions

The effect of the isobathic curvature on the development and evolution of Gulf Stream frontal waves (meanders and eddies) in the vicinity of the CB is studied using HYCOM. Baroclinic and barotropic energy transfers from the Gulf Stream to its meanders and eddies are computed using the traditional energy balance equation as well as the MS-EVA method for four different cases. In Case I, the curvature of the isobaths is artificially reduced and the CB is removed from the bathymetry. In this simulation, the simulated Gulf Stream meanders are barely noticeable in the study region. Energy transfer from the Gulf Stream to meanders and eddies is negligible. In Case II, the curvature of the isobaths is kept the same as in Case I, but a topographic rise of the scale of the CB is added to the bathymetry. In this simulation, Gulf Stream meanders that appear as cold and warm anomalies are amplified after passing over the bump. The total baroclinic and barotropic energy transfer rate in the CB region is on the order of 3×10^{-8} m^2s^{-3}. In Case III, the bathymetry contained realistic isobathic curvature similar to that of the actual bathymetry in the region, which is larger than that of Cases I and II. However, the CB is removed from the bathymetry as in Case I. In this simulation, large meanders are simulated, but the development of these meanders was not confined to the region of the downstream region of the CB. The total baroclinic and barotropic energy transfer rate in this case (approximately 3×10^{-7} m^2s^{-3}) is an order of magnitude greater than in Case II, suggesting that isobathic curvature can generate Gulf Stream meanders and eddies even

without the presence of the CB. In Case IV, actual bathymetry data which contains both the "CB" and the isobathic curvature was used. In this case, large-amplitude Gulf Stream meanders were simulated and there was also a tendency for the amplification of the meanders to be anchored downstream of the CB. For Case IV, the simulated amplitude as well as the location of the simulated Gulf Stream meander in the CB region is consistent with observations.

Case III, which has a larger isobathic curvature but no bump, produced larger amplitudes in the Gulf Stream meanders than those seen in Cases I and II. A question that needs to be answered is whether the smaller amplitude of the Gulf Stream meanders seen in Cases I and II as compared to that in Case III is indeed due to the smaller isobathic curvature in Cases I and II or caused by the difference of the stabilization effect associated with the isobathic slope among the cases. Might the larger isobathic curvature in Case III keep the Gulf Stream in deeper water and thus further away from the large continental slope than in Cases I and II? If so, the Gulf Stream in Case III may be more unstable than in Cases I and II simply due to the smaller bottom topographic slope. A careful diagnosis of the model results indicates that this is not the case. The Gulf Stream position is self-adjusted to the bathymetry in all cases. In Cases I and III, the Gulf Stream axis followed the 550m-isobath closely. As a result, the stabilization effect of the isobath slope remains more or less the same in both Cases I and III.

To further quantify the stabilization effect in Cases I and III, the potential vorticity balance is analyzed using the method suggested by Pickart and Watts (1993). Figures 18a,b shows the bottom layer potential vorticity balance among local time rate of change, along-stream advection and cross-stream advection in Cases I and III at the 550m-isobath

at 31° N. In both cases, the local time rate of change is mainly balanced by the along-stream advection term. This is different from the case studied by Pickart and Watts (1993) where the local time rate of change term is mainly balanced by the cross-stream advection term since the Gulf Stream meanders were over steep topography in their case. In both Cases I and III, the cross-stream advection terms are small compared with the other terms in the balance. This is because the slope of the isobaths and isopycnic slope are inclined at the same angle, so that cross-stream movement of the bottom layer does not cause much squeezing or stretching of the water column. The magnitude of the cross-stream advection term in Cases I and III are about the same (0.2×10^{-11} $s^{-2}m^{-1}$), which indicates that the stabilization effect of the slope of the isobaths are about the same in the two cases. Therefore, the larger meander in Case III is not the result of the lateral drift of the Gulf Stream, but rather, the isobathic curvature.

The results from this study suggest that the formation of the Charleston Trough, a Gulf Stream meander that appears as a low pressure or depressed water surface region downstream of the bump, is the result of the combined effect of the CB and the isobathic curvature in the region. The isobathic curvature plays a major role in enhancing the baroclinic and barotropic energy transfer rates, whereas the bump provided a localized mechanism to maximize the energy transfer rate over the CB. In our simulations, the maximum baroclinic transfer rate occurred at the 125 m depth. However, the barotropic transfer rate was large and uniform above the 125 m depth, but was relatively small below.

5. References

Atkinson, L. P., L. J. Pietrafesa, and E. E. Hofmann, 1982: An evaluation of nutrient sources to Onslow Bay, North Carolina, J. Mar. Res., 40, 679-699.

Bane, J. M., Jr., and D. A. Brooks, 1979: Gulf Stream meanders along the continental margin from the Florida Straits to Cape Hatteras, Geophys. Res. Lett., 6, 280-282.

Bane, J. M., Jr., D. A. Brooks, and K. R. Lorenson, 1981: Synoptic observations of the three-dimensional structure and propagation of Gulf Stream meanders along the Carolina continental margin, J. Geophys. Res., 86(C7), 6411-6425, 1981.

Bane, J. M., Jr., 1983: Initial observation of the subsurface structure and short-term variability of the sea-ward deflection of the Gulf Stream off Charleston, South Carolina, J. Geophys. Res., 88(C8), 4673-4684.

Bleck, R., 2002: An oceanic general circulation model framed in hybrid isopycnic-Cartesian coordinate, Ocean Modeling, 4, 55-88, 2002

Bleck, R., C. Rooth, D. Hu and L. T. Smith, 1992: Salinity-driven thermocline transients in a wind and thermohaline-forced isopycnic coordinate model of the North Atlantic, J. Phys. Oceanogr., 22, 1486-1505

Brooks, D. A. and J. M. Bane, Jr., 1978: Gulf Stream deflection by a bottom feature off Charleston, SC, Science, 201, 1225-1226.

Brooks, D. A. and J. M. Bane, Jr., 1981: Gulf Stream fluctuations and meanders over the Onslow Bay upper continental slope, J. Physical Oceanogr., 11, 247-256.

Brooks, D. A. and J. M. Bane, Jr., 1983: Gulf Stream meander off North Carolina during winter and summer, 1979, J. Geophys. Res., 88(C8), 4633-4650.

Brooks, I. H., and P. P. Niiler, 1977: Energetics of Florida Current, J. of Marine Research, 35, 163-191.

Chao, S. Y. and G. S. Janowitz, 1979; The effect of a localized topographic irregularity on the flow of a boundary current along the continental margin, J. Physical Oceanogr., 9, 900-910.

Chassignet, E, L. Smith, G. Halliwell, and R. Bleck, 2003: North Atlantic simulations with the hybrid Coordinate Ocean Model (HYCOM): Impact of coordinate choice, reference pressure, and thermobaricity, J. Phys. Oceanogr., 33, 2504-2526.

Dewar, W. K., and J. M. Bane Jr., 1985: Subsurface energetics of the Gulf Stream near the CB. J. Physical Oceanogr., 15, 1771-1789.

Hoffmann, E. E., L. J. Pietrafesa, J. M. Klinck, and L. P. Atkinson, A time-dependent model of nutrient distribution in continental shelf waters, Ecol. Modell., 10, 193-214.

Hood, C. A. and J. M. Bane, Jr., 1983; Subsurface energetics of the Gulf Stream cyclonic frontal zone off Onslow Bay, North Carolina, J. Geophys. Res., 88(C8), 4651-4662

Janowitz, G. S. and L. J. Pietrafesa, 1982: The effect of alongshore variation in bottom topography on a boundary current, Continental Shelf Res., Vol. 1, No. 2, 123-141

Knauss, J. A., 1969: A note on the transport of the Gulf Stream. Deep Sea Res., 16(Suppl.), 117-123.

Lee, T. N., et al, 1991: Gulf Stream Frontal eddy Influence on Productivity of the Southeastern U.S. continental shelf, J. Geophys. Res., 96, 22,191-22,105

Lee, T. N., E. Williams, J. Wang, R. Evans, and L. Atkinson, 1989: Response of South Carolina continental shelf waters to wind and gulf stream forcing during winter of 1986. J. Geophys. Res., 94, 10,715–10,754

Lee, T. N. and L. P. Atkinson, 1983: Low frequency current and temperature variability from Gulf Stream frontal eddies and atmospheric forcing along the Southeast U.S. outer continental shelf. J. Geophys. Res., 88(C8), 4541-4567

Lee, T. N., L. P. Atkinson, and R. Legeckis, 1981: Observations of a Gulf Stream frontal eddy on the Georgia continental shelf, April 1977, Deep Sea Research, Part A, 28(4), 347-378.

Lee, T. N. and D. A. Mayer, 1977: Low frequency current variability and spin-off eddies along the shelf off the Southeast Florida. J. Marine Res., 35, 193-220.

Legeckis, R. V., 1975: Application of synchronous meteorological data to the study of time-dependent sea surface temperature changes along the boundary of the Gulf Stream. Geophys. Res. Lett., 24, 435-438.

Legeckis, R.V., 1979: Satellite observation of the influence of bottom topography on the seaward deflection of the Gulf Stream off Charleston, South Carolina. J. Phys. Oceanogr., 9, 483-497

Levitus, S.,1982: Climatological atlas of the world ocean, NOAA Prof. Pap. 13, U.S. Govt. Print. Off., Washington, D. C.

Liang and Robinson, 2003a: Localized multiscale energy and vorticity analysis. Part I: Fundamentals. Dyn. Atmos. Oceans, in press.

Liang and Robinson, 2003b: Localized multiscale energy and vorticity analysis. Part II: Instability theory and validation. Dyn. Atmos. Oceans, in press.

Liang, X. S., and A. R. Robinson, 2004: A study of the Iceland–Faeroe Frontal Variability Using the Multiscale Energy and Vorticity Analysis, J. of Physical Oceanor., 34, 2571-2591.

Maul, G. A., P. W. deWitt, A. Yanaway, and S. R. Baig, 1978: Geostationary satellite observations of Gulf Stream Meanders: Infrared measurements and time series analysis, J. Geophys. Res., 83, 6123-6135.

Miller, J. L. and T. N. Lee, 1995a: Gulf Stream meanders in the South Atlantic Bight. 1. Scaling and energetics, J. Geophys. Res., 100(C4), 6687–6704.

Miller, J. L. and T. N. Lee, 1995b: Gulf Stream meanders in the South Atlantic Bight. 2. Momentum balances, J. of Geophysical Research, 100(C4), 6705-6724

Olson, D. B., O. B. Brown, and S. R. Emmerson, 1983: Gulf Stream frontal statistics from Florida Straits to Cape Hatteras derived from satellite and historical data, J. Geophys. Res., 88(C8), 4569-4577

Orlanski, I., 1969: The influence of bottom topography on the stability of jets in a baroclinic fluid. J. Atmos. Sci., 45, 3253-3267.

Pedlosky, J., 1979: Geophysical Fluid Dynamics. Springer-Verlag.

Pietrafesa, L. J., J. O. Blanton, and L. P. Atkinson, 1978: Evidence for deflection of the Gulf Stream at the Charleston Rise, Gulf Stream, 4(9), 3 and 6-7

Pietrafesa, L. J., and G. S. Janowitz, 1979: A note on the identification of a Gulf Stream spin-off eddy from Eulerian data, Geophys. Res. Lett., 6, 549-552, 1979.

Pietrafesa, L. J., and G. S. Janowitz, 1980: On the dynamics of the Gulf Stream front in the Carolina Capes, in Proceedings of the Second International Symposium on Stratified Flows, pp. 184-197, Tapir Publications, Trondheim, Norway.

Pietrafesa, L. J., 1983; Survey of a Gulf Stream frontal filament, Geophys. Res. Lett., 10, 203-206.

Pietrafesa, L. J., G. S. Janowitz, K. S. Brown, F. Askari, C. Gabriel, and L. A. Salzillo, 1988: The invasion of the Red Tide In North Carolina Coastal Waters, UNC Sea Grant Publication UNC-SG-WP-88-1, August 1988.

Romanou, A, E. P. Chassignet, W. Sturges, 2004: Gulf of Mexico circulation within a high-resolution numerical simulation of the North Atlantic Ocean, J. Geophys. Res., 109, C01003, doi:10.1029/2003JC001770, 2004

Rooney, D. M., G. S. Janowitz and L. J. Pietrafesa, 1978: A simple model of deflection of the Gulf Stream by the Charleston rise, Gulf-stream, 4(11), 3-7

Rossby, 1987: Gulf Stream energetics, J. of Marine Research, 45, 61-94

Savidge, D. K., J. O. Blanton, T. N. Lee and R. H. Evans, 1992: Influence of an offshore shift in the Gulf Stream on water of the South Carolina continental shelf, J. Phys. Ocean., 22, 1085-1094.

Sun, L. C. and L. J. Pietrafesa, 1992: Baroclinic-barotropic instabilities and energy transfers in the Gulf Stream, Proceedings of the First World Congress of Nonlinear Analysts, Tampa, Florida, August 19-26, 1992

Tester, P. A. and K. A. Steidinger, 1997:Gymnodinium breve Red Tide Blooms: Initiation, Transport, and Consequences of Surface Circulation, Limnology and Oceanography, 42, 1039-1051.

Tester, P. A., R. P. Stumpf, F M. Vukovich, P. K. Flower, J. T. Turner, 1991: An expatriate Red Tide Bloom: Transport, Distribution, and Persistence, Limnology and Oceanography, 36, 1053-1061.

Xue, H., and G. Mellor, 1992: Instability of the Gulf Stream Front in the South Atlantic Bight, J. of Physical Oceanogr., 23, 2326-2350

Table 1. List of Numerical Simulations

Simulation	Curvature	Bump	Bathymetry	Description
I	small	no	Figure 3a	Small curvature without bump
II	small	yes	Figure 3b	Effect of bump alone
III	large	no	Figure 3c	Effect of curvature alone
IV	large	yes	Figure 3d	Combined effect of bump and curvature

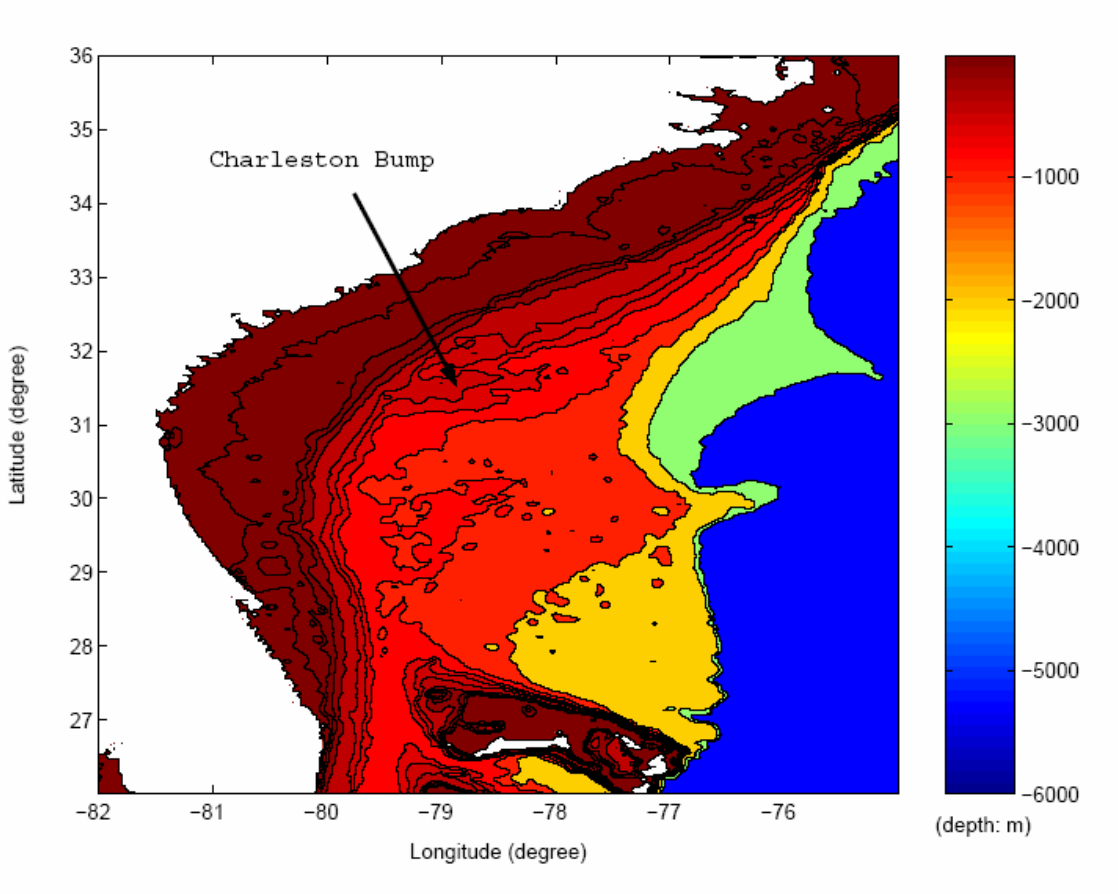


Figure 1. Bathymetry of South Atlantic Bight from ETOPO2

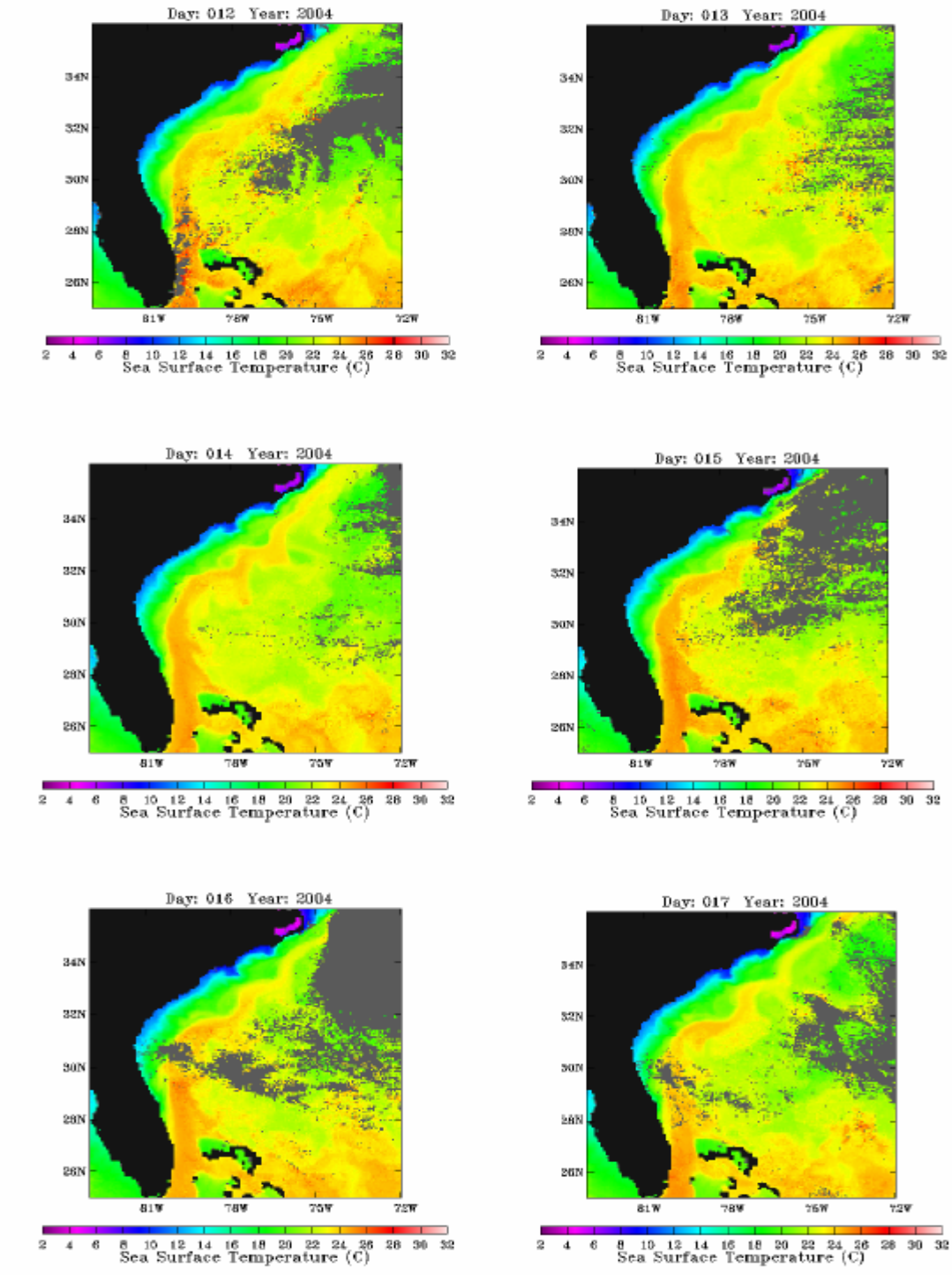


Figure 2. MODIS SST of SAB from January 12 to January 17, 2004. An eddy on the west edge of the Gulf Stream at 32°N is amplified

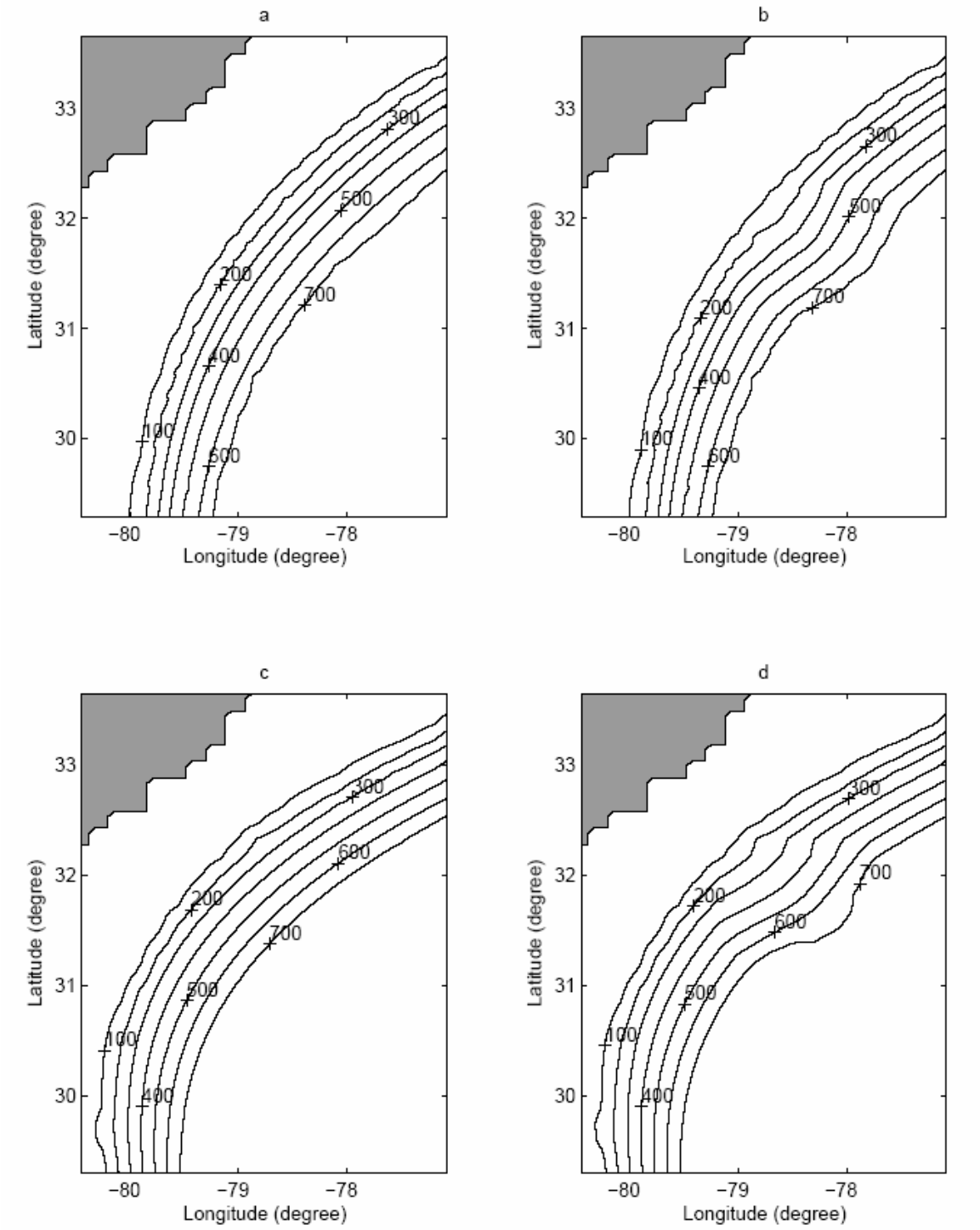


Figure 3. Bathymetry contour: a) small curvature without a bump; b) small curvature with a bump; c) large curvature without a bump; d. large curvature with a bump (units: m)

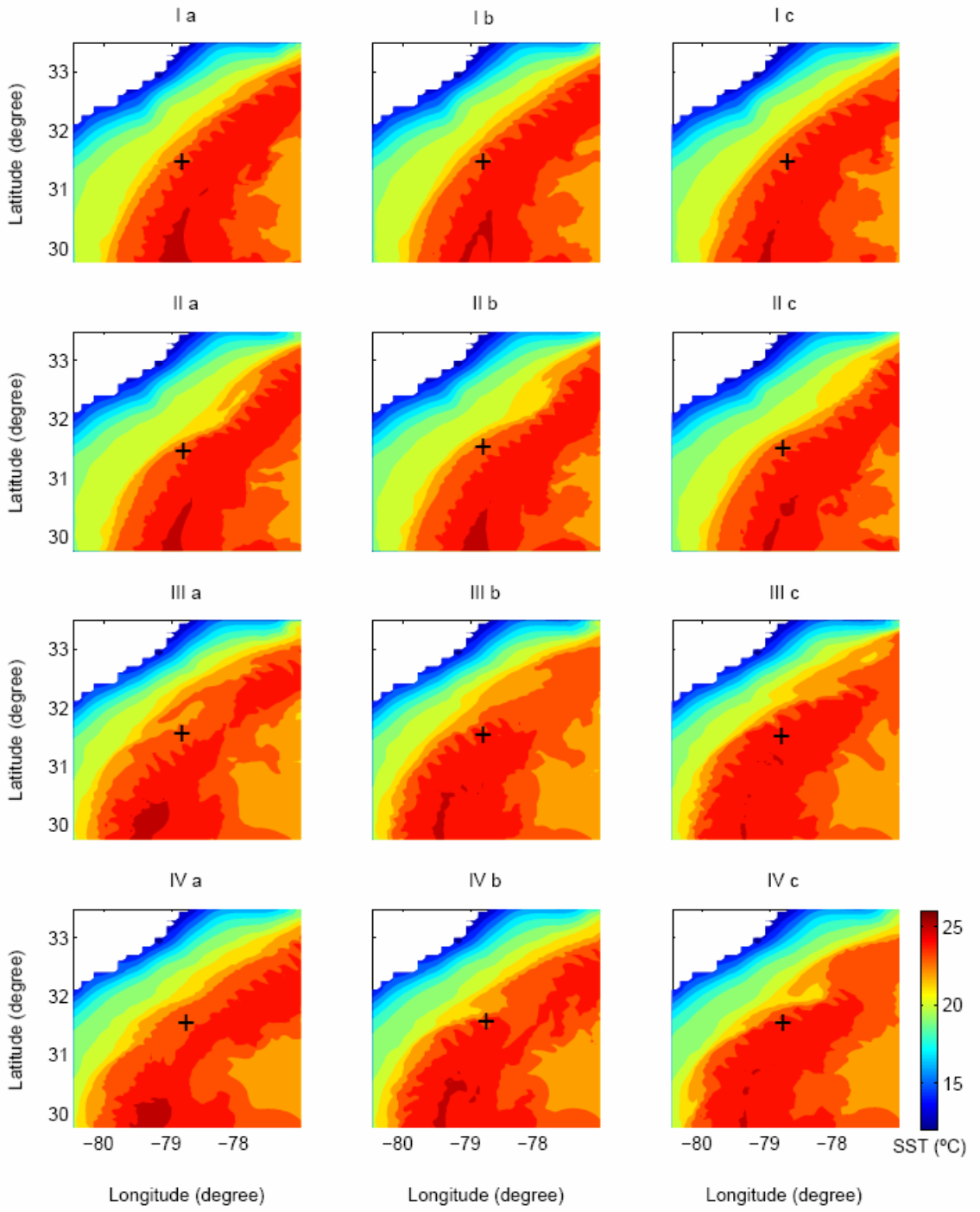


Figure 4. SST (7.5 m depth) of January 23, 25 and 27 for Case I (panel I a-c), Case II (panel II a-c), Case III (panel III a-c) and Case IV (panel IV a-c).

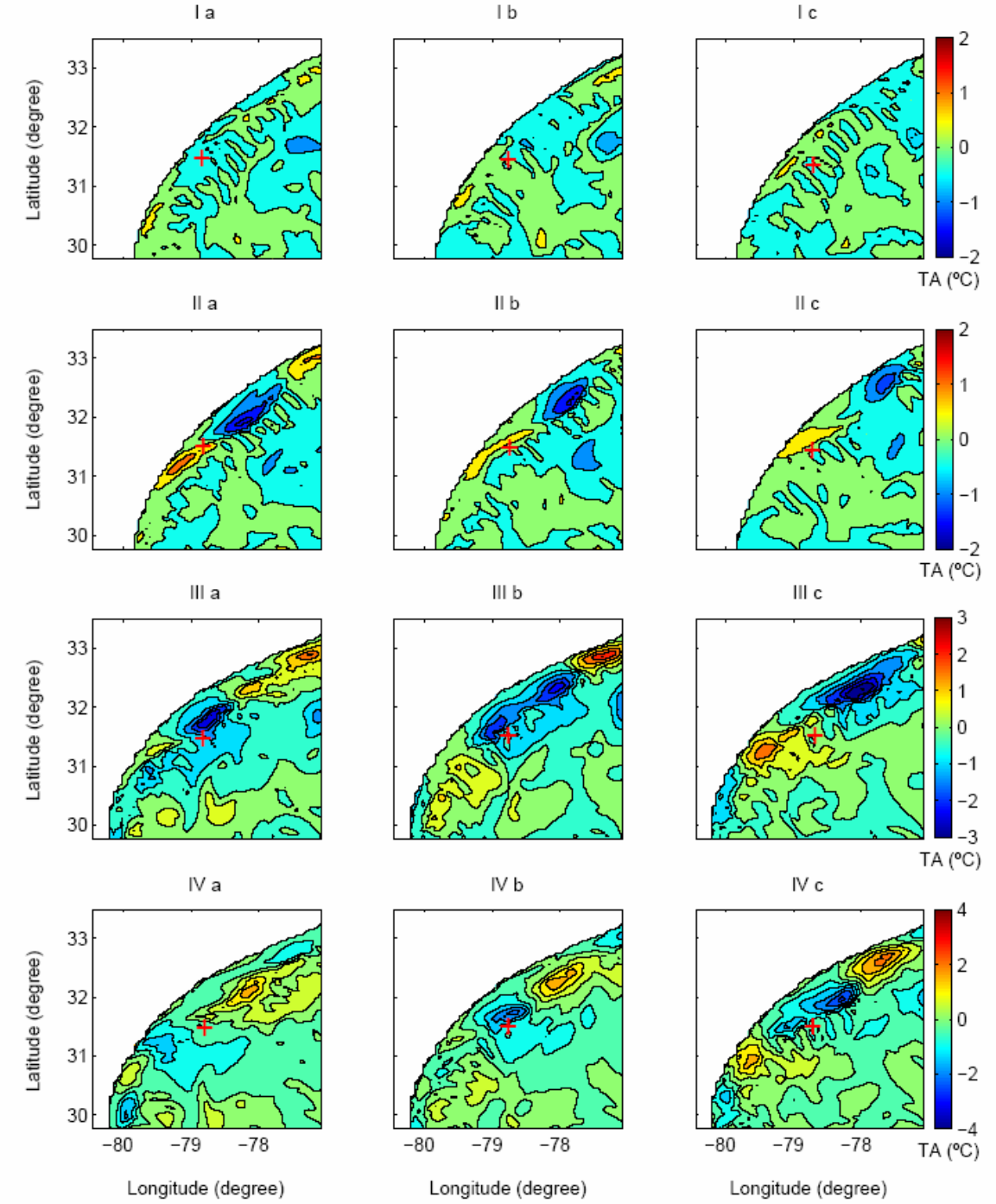


Figure 5. Water temperature anomaly (TA) at 125 meter depth of January 23, 25 and 27 for Case I (panel I a-c), Case II (panel II a-c), Case III (panel III a-c) and Case IV (panel IV a-c).

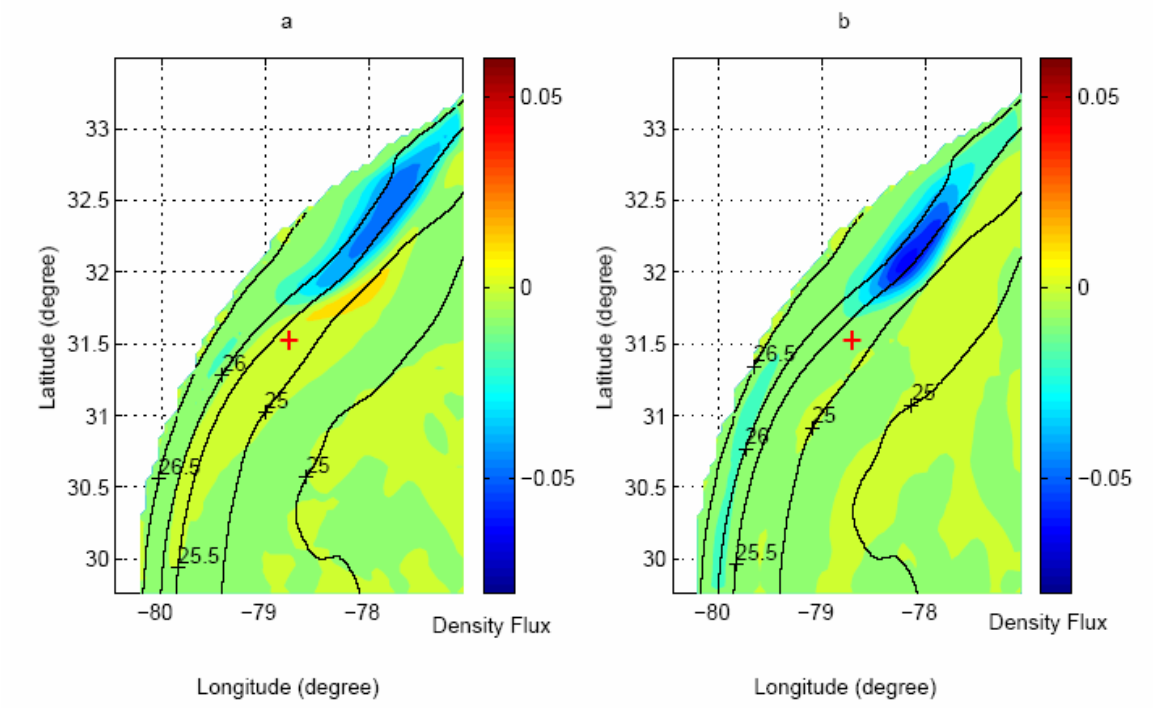


Figure 6. a) x-component of density flux $\overline{\rho' u'}$; b) y-component of density flux $\overline{\rho' v'}$ of Case IV at 125 meter depth (units: Kg $m^{-2}s^{-1}$)

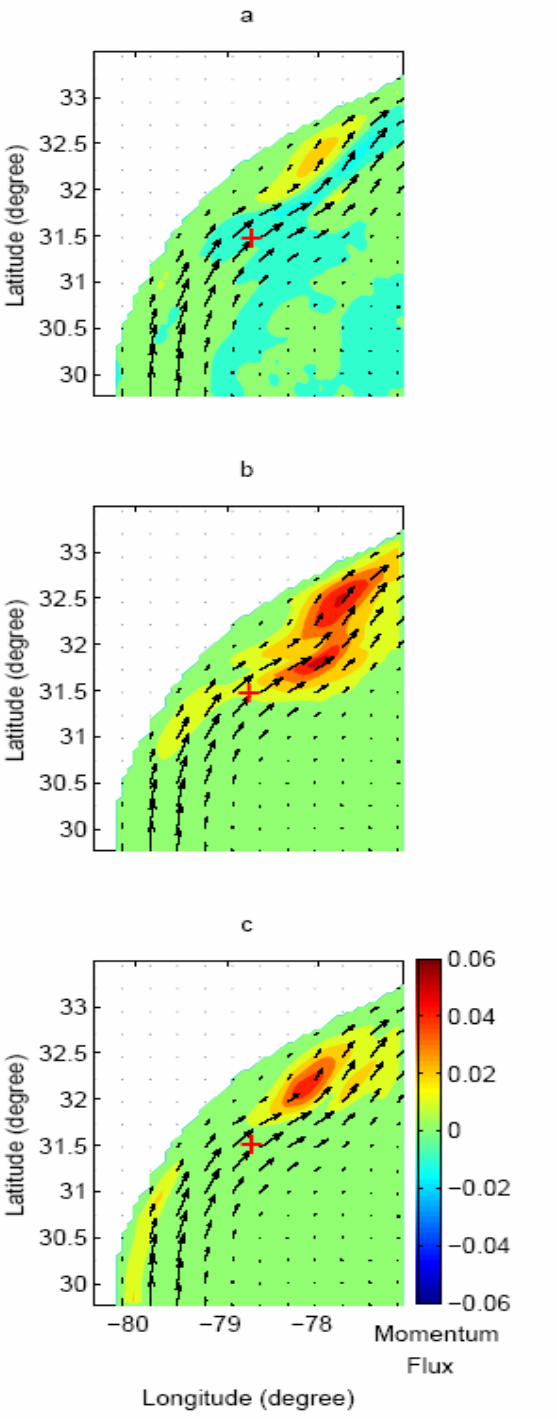


Figure 7. Momentum fluxes: a) $\overline{u'v'}$; b) $\overline{u'u'}$; and c) $\overline{v'v'}$ of Case IV at 125 meter depth (units: m^2s^{-2})

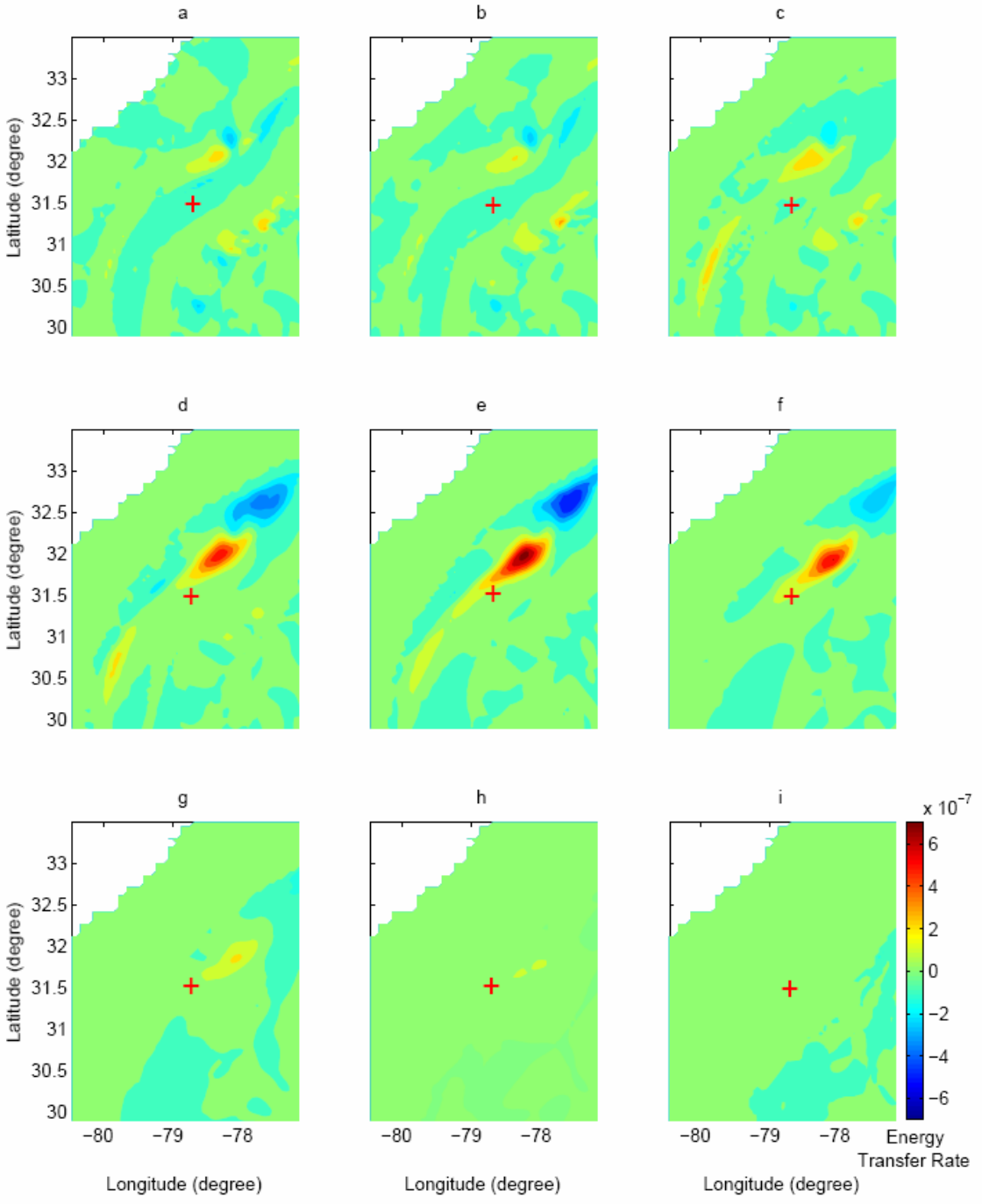


Figure 8. Baroclinic transfer rate of Case IV at 7.5, 25, 47.5, 80, 125, 190, 305, 495, and 760 meter depth. (units: m^2s^{-3}).

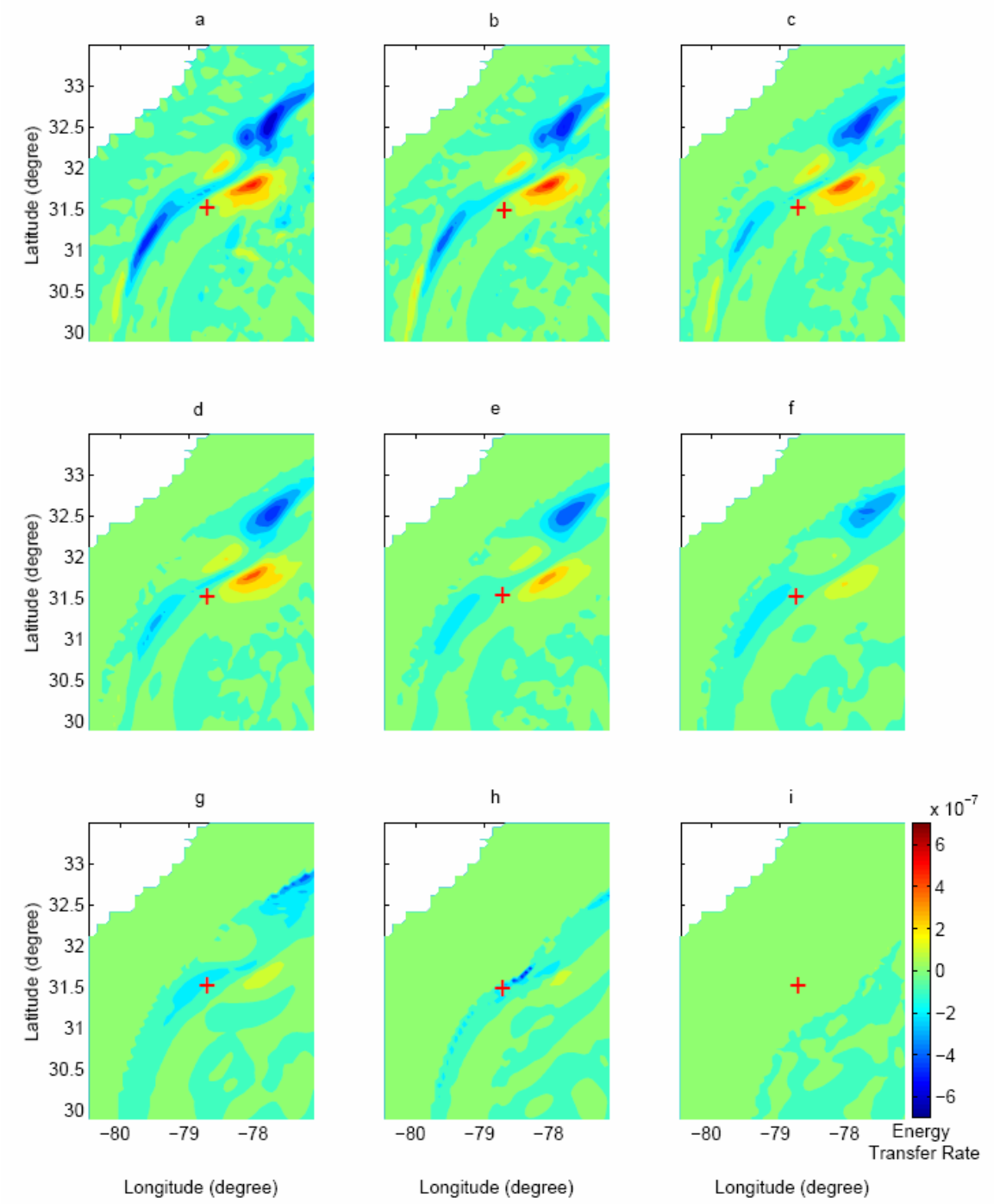


Figure 9. Barotropic transfer rate of simualtion IV at 7.5, 25, 47.5, 80, 125, 190, 305, 495, and 760 meter depth. (units: m^2s^{-3}).

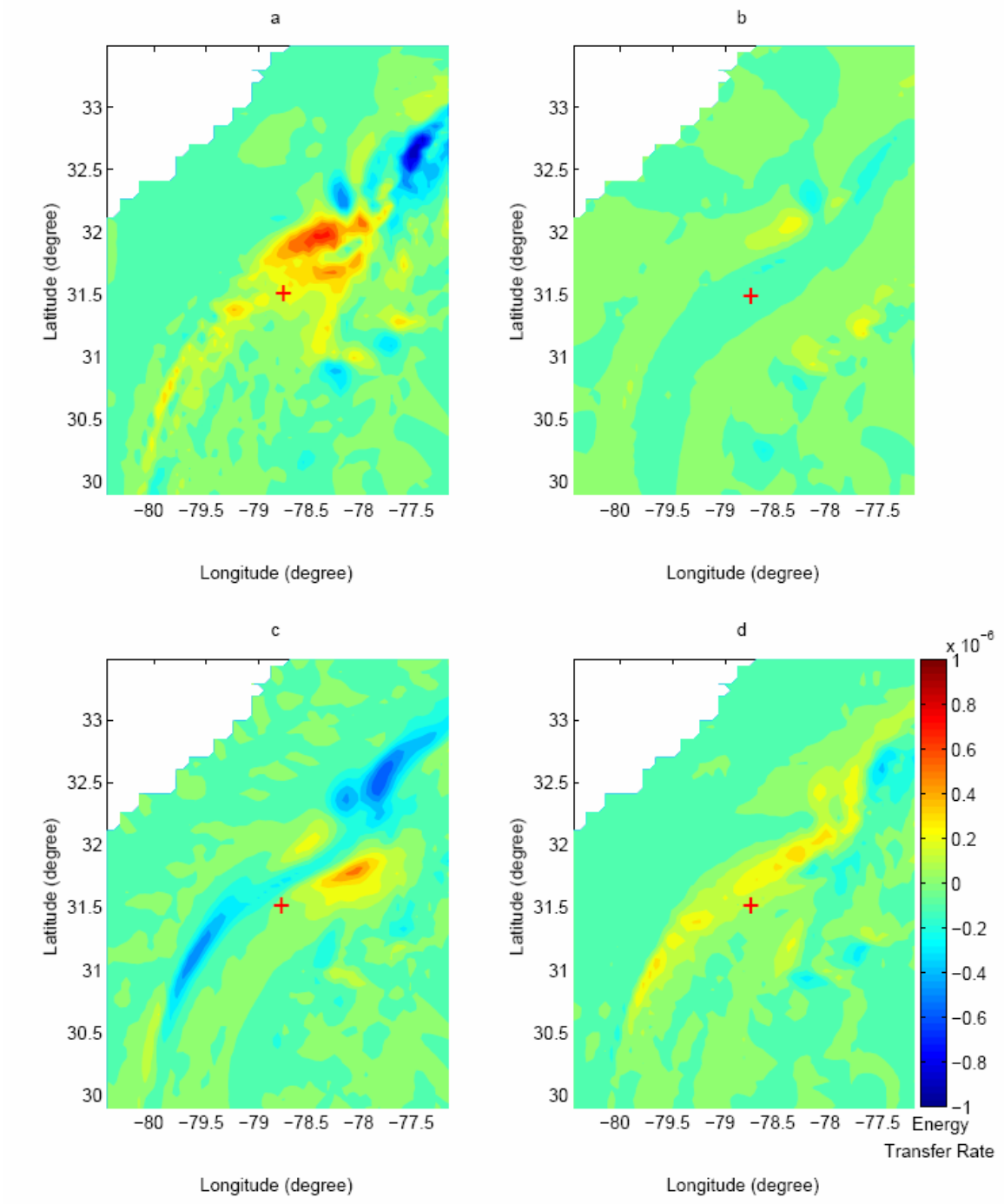


Figure 10. Eddy energy budget of Case IV at 25 m depth: a) total rate change of energy; b) baroclinic transfer rate; c) barotropic transfer rate; d) pressure work. (units: m^2s^{-3}).

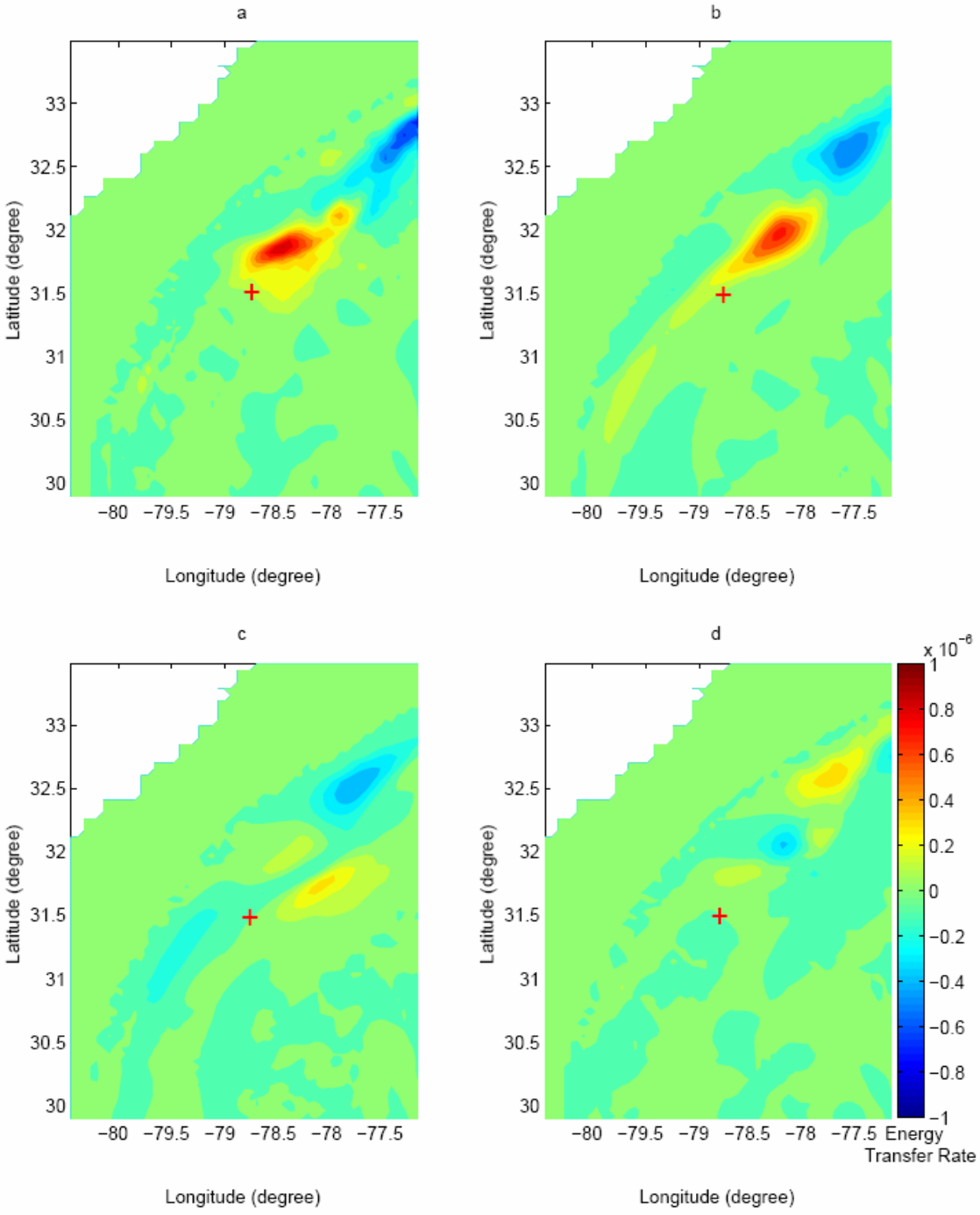


Figure 11. Eddy energy budget of Case IV at 125 m depth: a) total rate change of energy; b) baroclinic transfer rate; c) barotropic transfer rate; d) pressure work. (units: m^2s^{-3}).

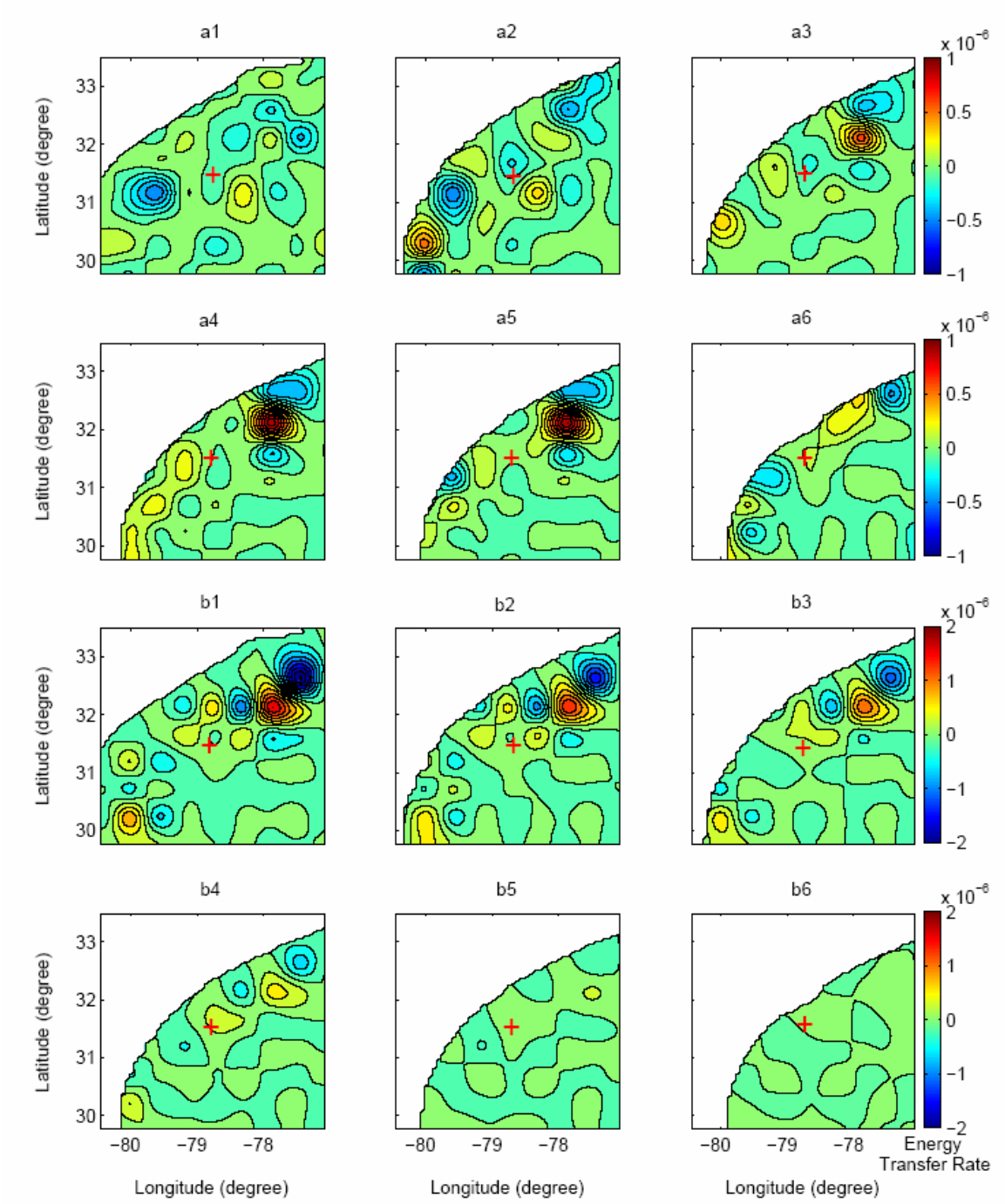


Figure 12. MS-EVA baroclinic transfer rate of Case IV on January 27 at 25, 47.5, 80, 125, 190, 305 m depth (panel a 1-6 respectively) and barotropic transfer rate of Case IV on January 27 at 25, 47.5, 80, 125, 190, 305 m depth (panel b 1-6 respectively)

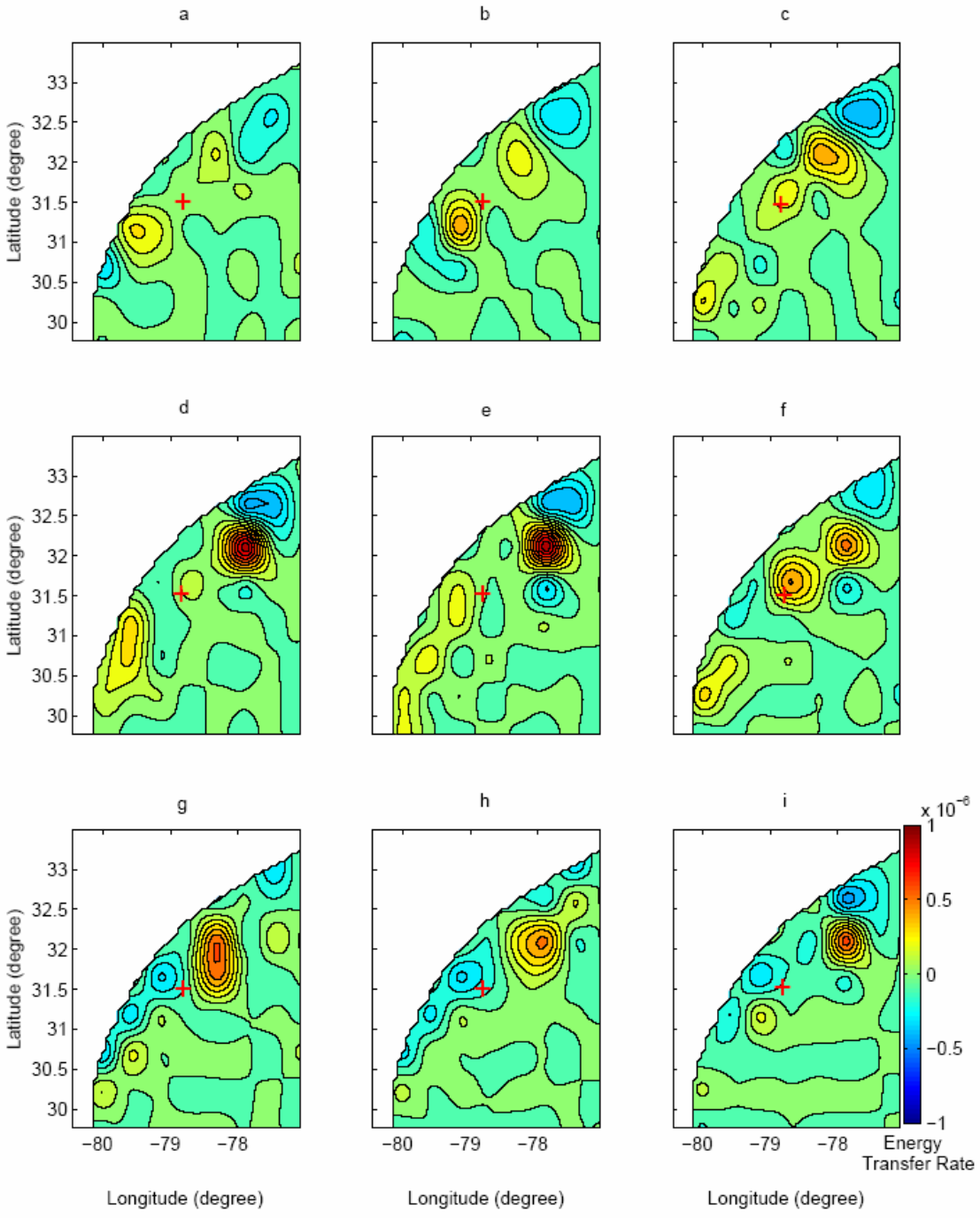


Figure 13. Baroclinic transfer rate of Case IV at 125 m depth from January 23 to 31 (units: m^2s^{-3}). Panels a) through h) correspond to January 23 through 31, respectively.

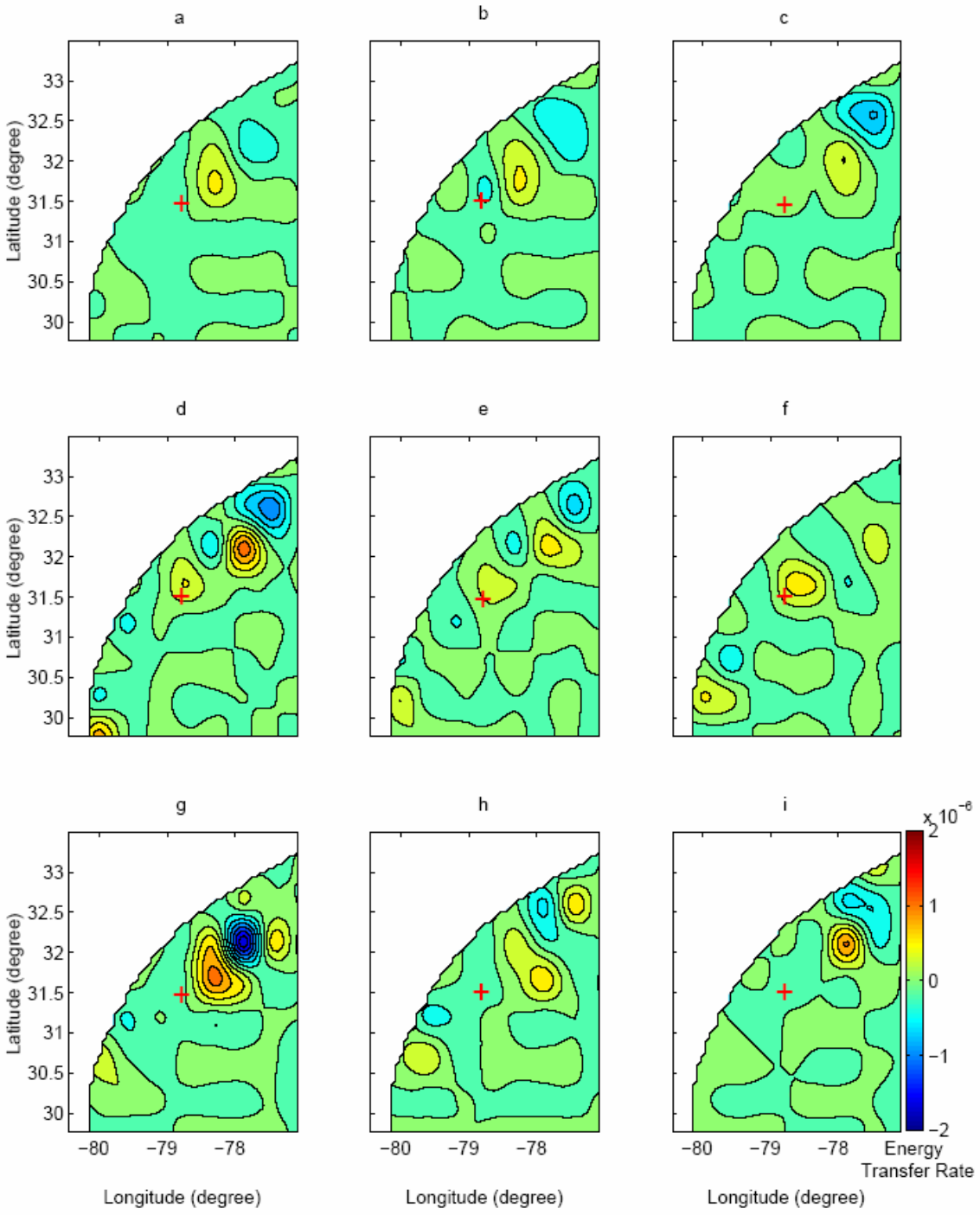


Figure 14. Barotropic transfer rate of Case IV at 125 m depth from January 23 to 31 (units: m^2s^{-3}). Panels a) through h) correspond to January 23 through 31, respectively.

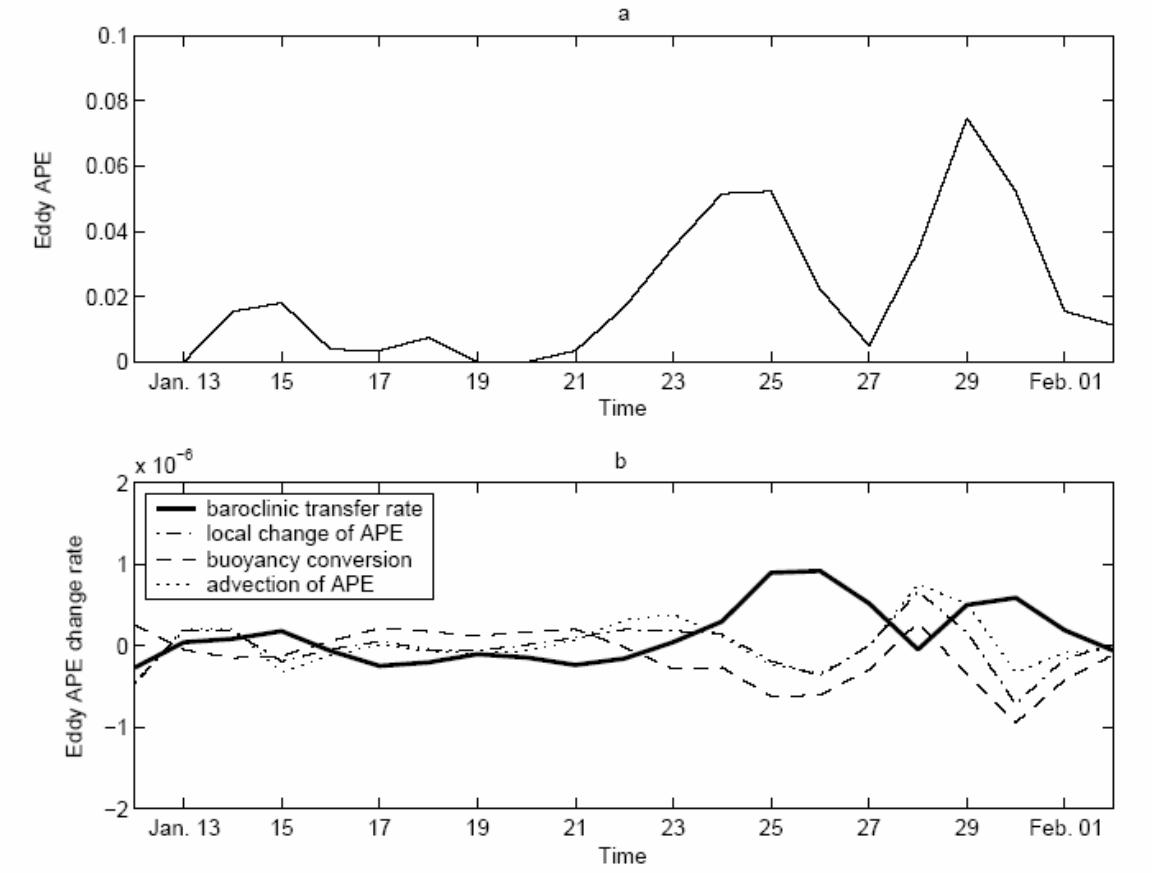


Figure 15. a) Eddy available potential energy (APE, units: m^2s^{-2}); b) APE budget (units: m^2s^{-3}) at (77.9ºW, 32.2ºN).

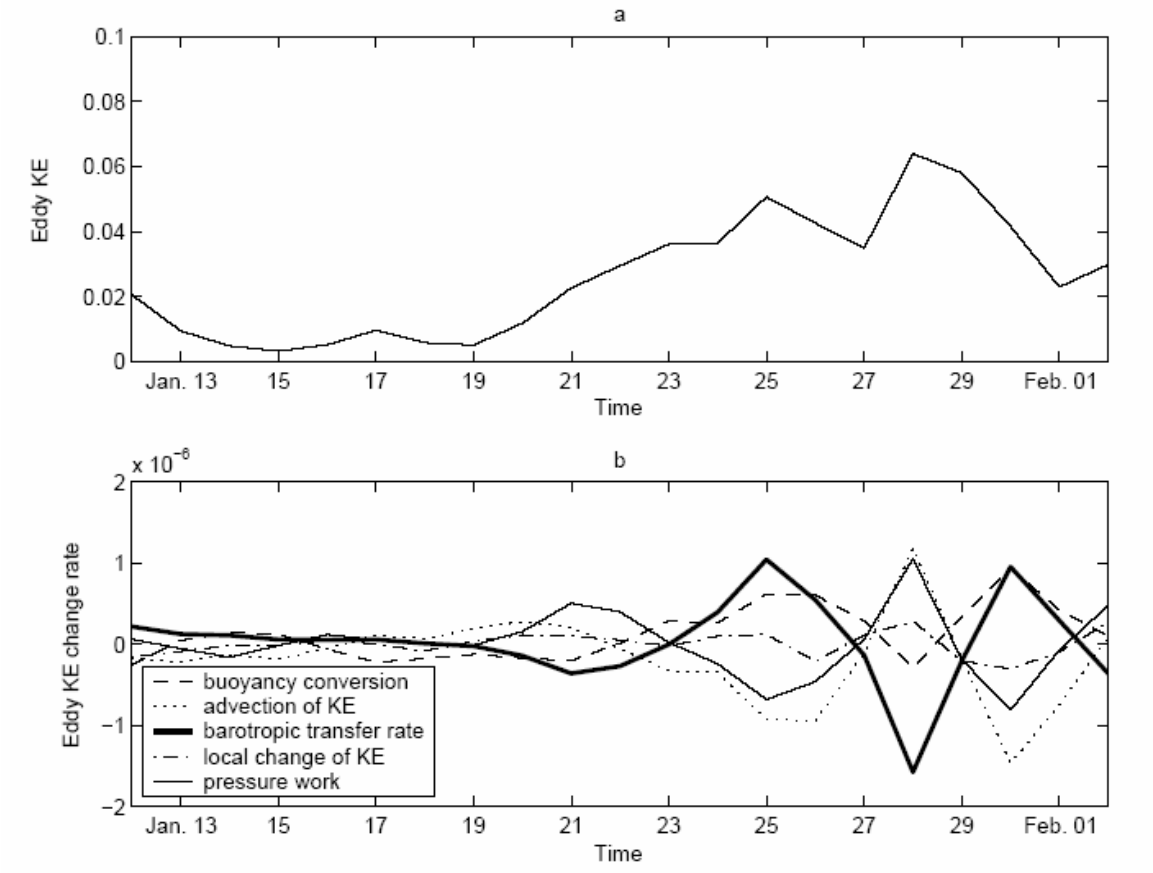


Figure 16. a) Eddy kinetic energy (KE, units: m^2s^{-2}); b) Eddy kinetic energy budget (units: m^2s^{-3}) at (77.9ºW, 32.2ºN).

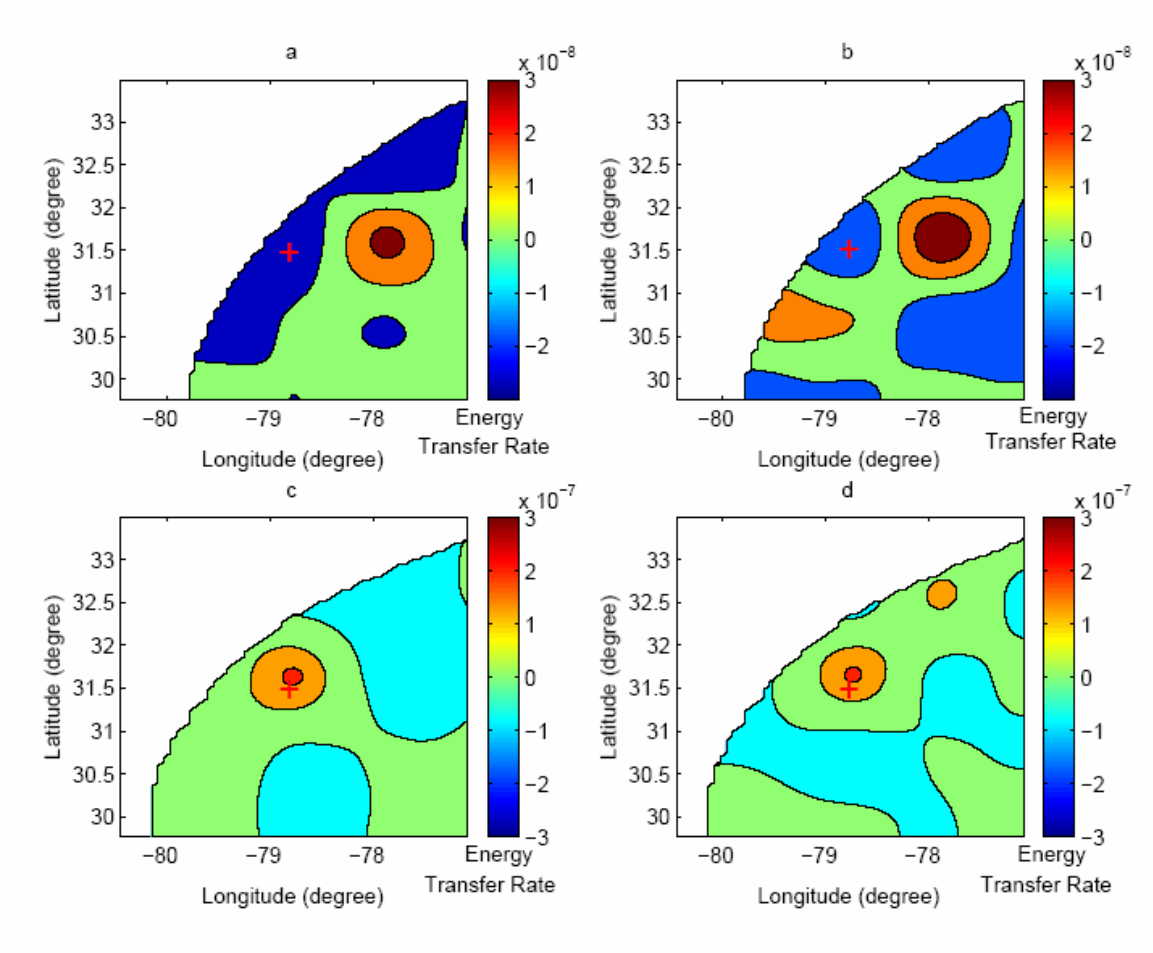


Figure 17. Baroclinic and barotropic transfer rates at the 125 m depth on January 25 of Cases II and III: (a) barotropic transfer rate of Case II; (b) baroclinic transfer rate of Case II; (c) barotropic transfer rate of Case III; (d) baroclinic transfer rate of Case III. (Units: m^2s^{-2})

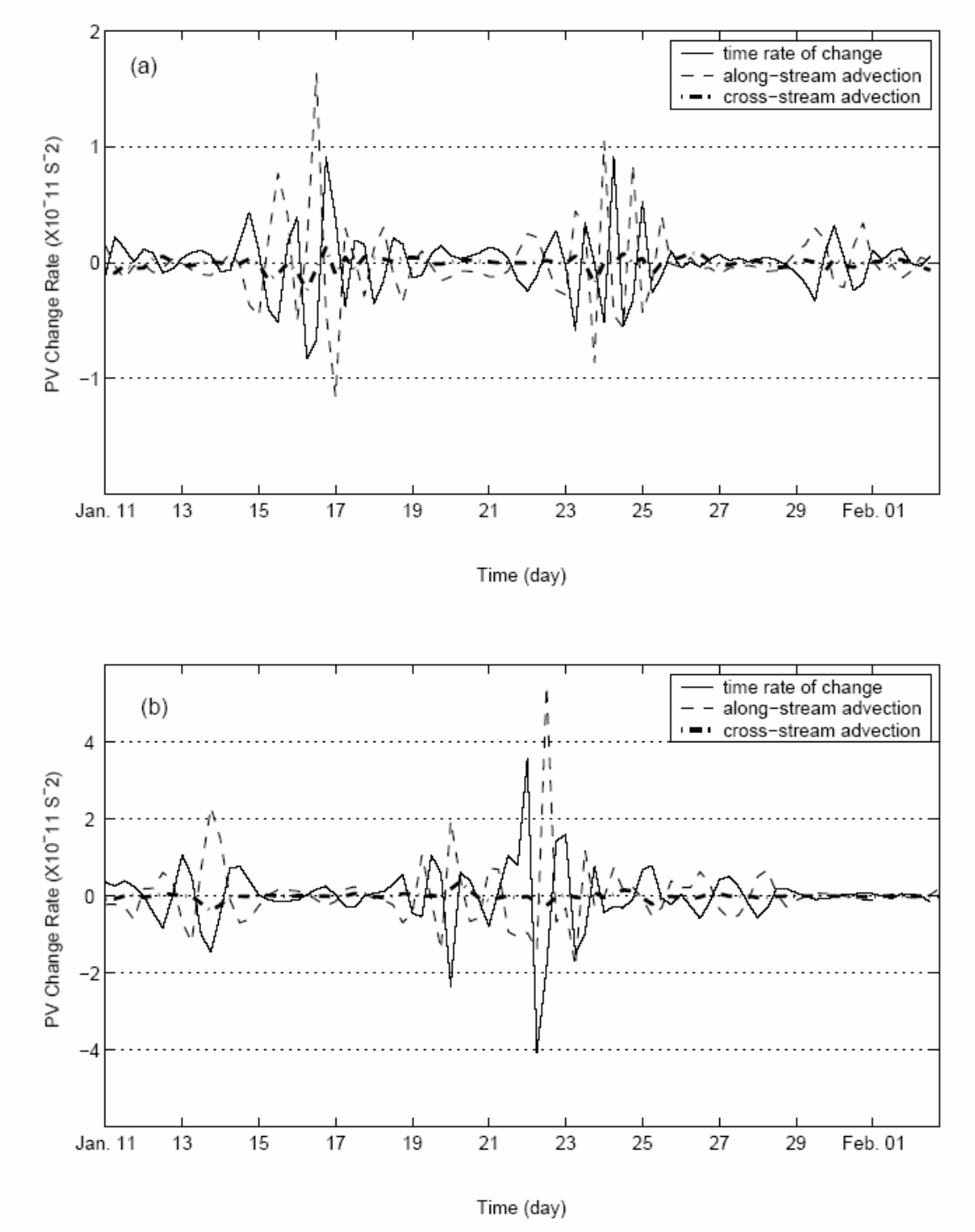


Figure 18. Potential vorticity balance in Case I (panel a) and Case III (panel b).

Chapter 5

Numerical Simulation of the Transport Process of *Karenia Brevis* Cells from Gulf of Mexico to North Carolina Coast using Passive Tracer

1. Introduction

Karenia brevis is a one-celled red tide dinoflagellate. K. brevis blooms can cause fish kills and shellfish poisoning, and this red tide organism contains a neurotoxin that affects the nervous system and causes respiratory irritation in humans. It occurs very often along the west coast of Florida (Steidinger 1983), and there have been some documented occurrences of this species along the Atlantic coast of Florida (Murphy et al. 1975; Roberts 1979; Steidinger and Haddad 1981).

On October 31, 1987, shelf waters in the Onslow Bay, North Carolina became infested with red tide bloom, which continued for 4-5 months. Shellfish such as clams, scallops and oysters became infected and were rendered inedible. Shellfishing was banned from Avon to Long Beach. Beachcombers felt burning eyes and lungs, and became nauseous and dizzy. This bloom resulted in 48 documented cases of neurotoxic shellfish poisoning, closure of up to 1480 km^2 of North Carolina waters to shellfish harvesting, and economic losses exceeding $24 million (Tester and Fowler 1990). This red tide bloom occurred at Onslow Bay, North Carolina is the first record of K. Brevis north of Jacksonville, Florida (Tester et. al, 1991). Scientists have speculated that the K.

Brevis cells were transported from the Gulf of Mexico to the North Carolina coast via the Loop Current – Florida Current – Gulf Stream system.

Pietrafesa et al. (1988) reported that the dinoflagelate found off the coast of North Carolina was accompanied by a marine blue-green algae indigenous to subtropical waters. So it became suspicious that the dinoflagelate was transported to the North Carolina from the south. They analyzed the National Weather Service atmospheric pressure map, and found that the winds associated with the weather system on the west Florida shelf were affecting an offshore transport of surface waters from the shelf into the Loop Current during a red tide breakout event off the coast of Naples, Florida. Pietrafesa et al (1988) also analyzed the sea surface temperature imagery off the North Carolina coast collected via the NOAA-9 Advanced Very High Resolution Radiometer (AVHRR) sensor, and found that there were frontal warm filaments associated with Gulf Stream meanders and eddies off the North Carolina coast. The wind field as observed at the Cape Hatteras Lighthouse station was then further analyzed and it was found that from Oct. 9 through Nov. 9, the wind velocity is directed towards the southwest to south sector. The observed wind fields were then applied to Ekman transport theory to estimate the Ekman transport and concluded that the wind is strong enough to transport the K. Brevis cells out of the filaments and across the shelf in Onslow Bay.

Tester et al (1991) analyzed the cell count sampling during the red tide bloom event, along with satellite SST images and observed wind. It is found that the transport of cells onto the inner continental shelf may have resulted from the large meanders of the Gulf Stream. The warm filament associated with this meander persisted on the continental shelf for at least 19 days, and inshore surface waters of both Onslow and Raleigh Bays

were warmed. Both windspeed and direction are important in determining its distribution. It is concluded that the persistence of the filament in the inshore area for nearly 3 weeks in October-November 1987 is the key factor that could have provided ample time for cell division and bloom development. Tester and Steidinger (1997) reviewed the process of initiation, transport and consequences of surface circulation of the red tide bloom event from Gulf of Mexico to U.S. South Atlantic Bight.

In this study, an ocean numerical model will be used to simulate the process of transportation of K. Brevis cell from the West Florida Shelf in Gulf of Mexico to the inshore area of the North Carolina coast. The numerical model used is the Hybrid Coordinate Ocean Model (HYCOM) with highest resolution of 0.02 degrees. Since the process covers a large area, it is very time-consuming to run the simulation in the whole area of interest. Therefore, a triple-nested approach was taken to achieve the high resolution: the outer domain covers the whole north and equatorial Atlantic, the intermediate domain covers the south east U.S. continental shelf, and the inner domain covers the North and South Carolina continental shelf.

The purpose of this research is to testify the hypothesis that the red tide bloom in the North Carolina coast was originated and transported from the West Florida Shelf. The individual and combined effect of the wind and Gulf Stream meander and eddy on transportation of the K. Brevis cell from the Gulf Stream to North Carolina inshore area will also be investigated. In section 2, the background of physical oceanography in the West Florida Shelf and the Southeast U.S. continental shelf will be reviewed. In section 3, the ocean model and atmospheric forcing will be briefly described and the cases of

simulation will also be discussed. The simulation results will be discussed in section 4, and finally, summary and conclusions in section 5.

2. Background of Physical Oceanography of Study Area

Although the continental shelf of the southeastern United States and the West Florida Shelf (WFS) are separated by the Florida Peninsula, they are linked by a very important aspect: the entire contiguous 5000 km of shelf is never far from the dynamic of the Gulf Stream system. The Gulf Stream and its associated eddies can profoundly affect the shelf waters. However, the ocean circulations and their interactions with the Gulf Stream on the two continental shelves have their own characteristics. The general physical oceanography involved in the South Atlantic Bight will be briefly reviewed in section 2.1, and that of West Florida Shelf in section 2.2.

2.1 South Atlantic Bight

It was revealed by early sea surface temperature satellite radiometer data and derived images that wavelike perturbations traveled northward along the western edge of the Gulf Stream front at a speed of about 30 km/day (Legeckis, 1975, 1979) in the South Atlantic Bight. Northward propagation of similar wavelike patterns was also evident in Lee and Mayer's (1977) current measurements in the Florida Strait, off Onslow Bay, North Carolina (Pietrafesa and Janowitz, 1980; Bane et al., 1981) and in the GABEX I moored array (Lee and Atkinson, 1983). These wavelike perturbations were believed to be manifestations of Gulf Stream lateral meanders and eddies. In fact, Pietrafesa and

Janowitz (1980) provided phase speed, 25-75 cm/s and wavelength, 100-300km, estimates of the frontal waves as they passed by mooring current meters in Onslow Bay.

At proximately 32°N, a submarine ridge called the Charleston Bump extends seaward from the continental slope offshore of Charleston, South Carolina. This topographic feature produces an eastward deflection in the Gulf Stream (Pietrafesa et al., 1978; Rooney, et al, 1978; Brooks and Bane, 1978), forming a quasi-permanent 10 to 150 km meander. It has also been reported that the lateral meanderings of the Gulf Stream undergo a dramatic 'amplification' (Knauss, 1969; Maul et al., 1978; Bane and Brooks, 1979; Bane, 1983; Hood and Bane, 1983; Olson et al., 1983) downstream from the Charleston Bump. Accumulating evidence has suggested a regional difference in spatial scale of Gulf Stream meanders: south of the latitude of the Charleston Bump, cold-core frontal eddies tend to occur as smaller, elongated filaments (Lee and Mayer, 1977; Lee at al., 1981; Lee and Atkinson, 1983); north of Charleston Bump, frontal eddies tend to be considerably larger (Pietrafesa and Janowitz, 1979, 1980; Bane and Brooks, 1979; Pietrafesa and Janowitz, 1980; Bane et al., 1981; Brooks and Bane, 1981, 1983).

The triggering mechanism for the larger meanders and filaments downstream of the Charleston Bump is presumably the topographic effect of the Charleston Bump (Pietrafesa et al, 1978; Rooney et al, 1978; Brooks and Bane, 1978; Chao and Janowitz, 1979; Legeckis, 1979; Pietrafesa, 1983; Dewar and Bane, 1985). Since Gulf Stream flow has both horizontal and vertical shear, many studies surmise that the large meanders result from local barotropic and baroclinic instabilities. In a two-layer model of the Gulf Stream, Orlanski (1969) demonstrated that topographical slope is a stabilizing factor, while the height of the topography is a destabilizing factor. Sun and Pietrafesa (1992)

extended the Orlanski model by including both laterally and vertically sheared horizontal currents in a two-layer Gulf Stream model and showed that the energy are transferred between the eddy and the mean flow in both barotropic and baroclinic processes. Xue and Mellor (1992) solved the eigenvalue problem for the instability study of the Gulf Stream using two analytical cross sections representing the mean conditions of the Gulf Stream upstream and downstream of the Charleston Bump, and found that the most unstable solution in the region downstream of the Charleston Bump has a slightly longer wavelength and slower phase speed than those in the region upstream of the Bump. Dewar and Bane (1985) computed the energy budgets of the eddies and the mean flow in the Gulf Stream near the Charleston Bump using observations from DAMEX current meter mooring deployments, hydrographic surveys, and AXBT surveys, and found that immediately north of the Charleston Bump, the flow appears to be both barotropically and baroclinically unstable. Miller and Lee (1995a) provided a thorough review on the stability of Gulf Stream meanders in the South Atlantic Bight (SAB). They conducted a series of numerical simulations of the Gulf Stream meanders in the SAB using the Princeton Ocean Model and analyzed the energetics of the simulated circulation. They showed that a hybrid baroclinic-barotropic instability of the Gulf Stream flow was responsible for the growth of meanders. Miller and Lee (1995b) further examined the dynamics of a particular Gulf Stream meander event produced in the SAB, and conclude that geostrophic balance dominated the along-isobath flow, and the nonlinear advection terms in the horizontal momentum equation played an important role in the spatial-temporal development of the Gulf Stream meander.

Xie et al (2006) studied the effect of the curvature of the isobaths on the Gulf Stream meanders and eddies near the Charleston Bump. The isobaths are north-south oriented south of 30ºN, and turn sharply to northeast-southwest oriented around 31ºN. The Charleston Bump is located in the region of large curve where the Gulf Stream turns from northward to northeast-ward. It is found that isobathic curvature has a significant effect on the stability of the Gulf Stream; and the combined effects of isobaths curvature and the influence of the Charleston Bump are responsible for the development of the Gulf Stream meanders and eddies near Charleston Bump.

2.2 West Florida Shelf

The width of continental shelf of the eastern Gulf of Mexico increases from less than 50 km off Pensacola, Florida to the broad 200-km-wide expanses of the West Florida Shelf. The inner shelf connects to a system of bays and sounds through gaps in barrier islands. The eastern Gulf of Mexico receives little fresh water from rivers, being outside of the normal influence of the Mississippi River system's discharge. With this low-buoyancy forcing and the insulation from offshore eddies, the middle and inner regions of the WFS are driven primarily by the wind (Marmorino, 1982, 1983; Allen et al, 1983; Cragg et al, 1983; Mitchum and Clarke, 1986). Over the outer shelf, the influence of the Loop Current can be felt from entrainment, meandering, upwelling and detached eddies. Occasional, large intrusions of Loop Current water can penetrate to the inner shelf, dominating the local circulation over time interval of two to three weeks.

The lack of strong buoyancy forcing and the variability inherent in both the predominant wind forcing and occasional Loop Current interaction has prevented

definitive characterization of a mean, or seasonally flow on the WFS. The primary variability in the circulation arises from wind stress fluctuations and variations in Loop Current forcing. Marmorino (1982) analyzed coastal sea level and meteorological forcing during winter on the WFS and found significant coherence in the 6-day band over the entire shelf. Mitchum and Sturges (1982) found that currents on the middle and inner WFS were highly coherent with local wind, with primary momentum balance being between wind stress and bottom stress. Marmorino's (1983) analysis of coastal sea level and currents for the WFS in winter indicates that the flow response to wind stress varies with along-shelf position. Weisberg et al. (1996) suggest a seasonal baroclinic flow, northwest-ward in the late summer and early fall and southeast-ward in winter, exists near the latitude of Tampa.

Niiler (1976) and Koblinskya and Niiler (1980) present evidence that the prevailing eastward and southward flow over the outer shelf is driven by the Loop Current. The eight-month mean flow at 39 m depth on the 105-m isobath of the WFS was southward at 8.6 cm/s. Niiler found that the current fluctuations over the outer shelf were not coherent with the wind stress fluctuations. Hurlbert and Thompson's (1980, 1982) model of Loop Current produces eddy shedding of a scale similar to that observed along the outer shelf. Niiler (1976) and Sturges and Evans (1983) proposed that wind stress could affect the Loop Current forcing. Niiler (1976) suggest that atmospheric forcing on the Loop Current might increase the shedding of eddies and waves onto the WFS. Sturges and Evans (1983) found significant coherence between the Loop Current positions and the north-south component of the wind at periods of 24 months and longer.

Most recently, using in situ currents and hydrographic data along with satellite SST and SSH analyses, He and Weisberg (2002) described an LC intrusion event that occurred on the WFS in June 2000 and explore the relative roles of LC-induced and local wind-induced currents in accounting for the observations through idealized numerical model experiments. It is found that the shelfbreak currents are largely LC-controlled, whereas the inner-shelf currents are largely controlled by the local winds. A barotropic LC impact on the shelf slope is confined seaward of the shelf break, setting up a shelf-slope current to the north (in the cyclonic direction of continental shelf wave propagation). Adding either upwelling- or downwelling-favorable winds demonstrates that the wind-driven responses greatly exceed the LC responses over the inner shelf.

Loop Current intrusions onto the WFS in reality have both barotropic and baroclinic parts. The isopycnals associated with the shelf-slope current to the north of the impact region therefore tilt upward toward the shelf causing relatively deep water to upwell at the shelf break. If the shelf break either shoals or the shelf narrows in the cyclonic direction, then water upwelled in the shelf-slope current may reach isobaths that are shallower than those that can be attained locally where the LC impacts the shelf. The WFS geometry provides both of these factors. The shelf break at the impact region is about 80 m deep, whereas in DeSoto Canyon it is about 40 m deep. The shelf also narrows appreciably between Cape San Blas and DeSoto Canyon. The addition of wind-driven upwelling over the narrower portions of the shelf can further facilitate upwelling onto the shelf. Note that for the period 3–8 June, at the beginning of this LC intrusion event, the winds were upwelling favorable. Thus, the ingredients (an LC-induced shelf-slope jet with currents of magnitude 0.4 m s21, upstream topography changes, and

upwelling-favorable wind forcing) existed to account for the observed deepwater properties being upwelled and transported from the north.

3. Numerical Model, Wind Forcing and Simulations

3.1 Numerical Model

The Hybrid-Coordinate Ocean Model (HYCOM) (Bleck, 2002) is used in this study. HYCOM is a primitive equation ocean general circulation model that evolved from the Miami Isopycnic-Coordinate Ocean Model (MICOM) (Bleck et al, 1992). HYCOM was developed to address known shortcomings of the MICOM vertical coordinate scheme. Vertical coordinates in HYCOM remain isopycnic in the open, stratified ocean. However, they smoothly transition to z coordinates in the weakly-stratified upper-ocean mixed layer, to terrain-following sigma coordinates in shallow water regions, and back to level coordinates in very shallow water. The latter transition prevents layers from becoming too thin where the water is very shallow. HYCOM has been widely used to study the North Atlantic circulation and Gulf Stream variability (Chassignet et al., 2003 and references therein) and the Gulf of Mexico Loop Current and its eddy shedding processes (Romanou et al., 2004).

3.2 Wind Forcing

Two sets of atmospheric forcing data of year 1987 will be used in the case study: North America Regional Reanalysis (NARR) data and ECMWF reanalysis data. Horizontally, the NARR data has 32 km resolution, while the ECMWF data has 1.125 degree resolution. In this study, the HYCOM model will be driven by the following

atmospheric forcing fields at the ocean surface: wind, air-temperature, relative humidity, short-wave radiation and long-wave radiation. The outer domain North Atlantic model will be spun up for 1 year with an initial condition constructed from the Levitus Data Set (Levitus, 1982) and forced by Comprehensive Ocean Atmosphere Data Set (COADS) monthly climatology atmospheric forcing, and the result will be used as the initial and boundary conditions of the inner domain simulations.

3.3 Simulations

To resolve small-scale perturbations of the Gulf Stream front, a triple-nested grid covering the North Atlantic, then scaled down to the SAB and Carolinas coast is implemented. The outer domain covers the North Atlantic (98°W – 14°E, 17°S – 52°N), the intermediate domain covers the SAB (82°W – 71°W, 26°N – 36°N), and the inner domain covers the Carolinas coast (81.36°W-76.16°W, 30.18°N-35.23°N). The horizontal resolutions for the outer, intermediate, and inner domains are 0.18, 0.06 and 0.02 degrees, respectively, and the vertical resolution will be 22 layers that stretch or shrink vertically as a function of total depth. The bathymetry is derived from the ETOP02 dataset.

The purpose of the study is to testify the hypothesis that the red tide bloom in the North Carolina coast was originated and transported from the West Florida Shelf. The effect of the wind and Gulf Stream meander and eddy on transportation of the K. Brevis cell from the Gulf Stream to North Carolina inshore area will be investigated. The following simulations will be conducted:

Simulation I and II: These simulations cover the outer domain, North Atlantic (98°W – 14°E, 17°S – 52°N). Simulation I will be driven by NARR wind, while Simulation II will be driven by ECMWF wind. This simulation will be compared to Simulation I to see the effect of different atmospheric forcing data. The simulation I will be down scale to simulation III, which covers the intermediate SAB.

Simulation III: This simulation covers the intermediate domain, SAB (82°W – 71°W, 26°N – 36°N), and will be nested in Simulation I.

Simulation IV-VII: These four inner-domain simulations will all be nested in Simulation III. In Simulation IV and V, the realistic bathymetry will be used, so that the amplitude of the eddy are comparable to the real observed eddies. Simulation IV is driven by NARR wind, while in Simulation V the wind forcing is set to zero. In Simulation VI and VII, the bump near the Charleston, South Carolina, is artificially decreased in the bathymetry, so that the amplitude of the eddy are smaller than the real observed eddies. Simulation VI is driven by NARR wind, while in Simulation VII the wind forcing is set to zero.

A summary of the simulations are listed in Table 1.

Table 1. List of Numerical Simulations

Simulation #	Domain	Resolution	Wind Forcing	Eddy
I	17.4S – 51.6N 97.0W - 14.5E	0.18	NARR	N/A
II	17.4S – 51.6N 97.0W - 14.5E	0.18	ECMWF	N/A
III	26.1-41.7N 81.3-70.2W	0.06	NARR	N/A
IV	31.1-36.5N 81.3-73.8W	0.02	NARR	large
V	31.1-36.5N 81.3-73.8W	0.02	Zero wind	large
VI	31.1-36.5N 81.3-73.8W	0.02	NARR	small
VII	31.1-36.5N 81.3-73.8W	0.02	Zero wind	small

4. Results

4.1 Results of simulations in the outer domain

The outer domain simulations were driven by two sets of atmospheric forcing: NARR and ECMWF. The wind data in the two datasets show similarity in general atmospheric circulation on the ocean surface. From September 15 To 26, the wind on the West Florida Shelf is basically southward, which is in favor of transporting the K. Brevis cells from the Florida coast to the Loop Current – Florida Current – Gulf Stream system. According to Tester et al. (1991), there was a red tide bloom event near Charlotte Harbor – Sarasota on the southeast coast of Florida beginning from September 10, 1987. The NARR wind from 15 to 26 of September on the West Florida Shelf is in favor of transporting the K. Brevis cell from the shelf to the Loop Current – Gulf Stream system.

Now, let's look at the result from Simulation I, which was started on September 11, 1987. The Sea Surface Height (SSH) on September 11 is shown in Figure 1a. In Figure 1a, we can see that the flow on the WFS is basically northward, therefore, initially, it is not in favor of transporting the K. Brevis cells out from the continental shelf. The Loop Current is at the location of 84ºW – 25ºN, and there is a warm-core ring further west which was shredded from the Loop-Current at an earlier time. Beginning from September 15, the wind starts blowing southward, and the current on the WFS starts flowing southward, as it can be seen from Figure 1b (the SSH on September 15). This southward wind is in favor of the offshore transport of the K. Brevis cells on the WFS, and the southward flow can transport these cells from the WFS to the Gulf Stream system. Since

southward wind continued till September 26, the wind-driven current on the WFS is southward during this time period as we can see in Figure 1 c and d.

The response of the ocean circulation to local wind forcing on the WFS in April 1998 was studied by Weisberg et al. (2001). Using in situ data and a numerical model simulation, the authors studied how well the currents over the inner shelf are accounted for by local wind forcing alone. In doing this they describe the boundary layer effects that account for the transports across the inner shelf, provide a dynamical definition of the inner shelf, and describe an asymmetry in the inner shelf responses to upwelling versus downwelling favorable wind. It was found that during an upwelling favorable wind event, with respect to momentum the sea level response to downwelling winds results in an offshore-directed pressure gradient force, and the current is flowing southward along-shore; while during a downwelling favorable wind event, the sea level response to upwelling winds results in an onshoredirected pressure gradient force, and the current is flowing northward along-shore. It is concluded that local winds are a major driver of the inner shelf circulation. Our simulation is in agreement with Weisberg et al. (2001).

Passive tracer is added to the surface water near Charlotte Harbor – Sarasota (82.5°W, 27°N) on the southeast coast of Florida on September 11 (Figure 2). The initial value is 10,000 cells/litter. Figure 3 shows the simulated transportation process of passive tracer. On September 17, the passive tracer moves southward reaching 25°N. Since the water depth near Florida keys is shallow, the tracers are transported around them. On September 23, the tracer reaches Key West and starts moving eastward with the Florida Current. Between September 29 and October 5, the tracer reaches the east coast of Florida, and starts moving northward. On October 17, the tracer reaches the Carolina

coast area. This simulated speed of transportation process is in agreement with Pietrafesa et. al. (1988), and Tester et. al. (1993).

While keeping all other settings identical to simulation I, ECMWF wind data is used to replace the NARR wind data and drive the ocean model in simulation II. In general, the ECMWF wind circulation pattern is similar to that of NARR; however, they do show significant differences on the West Florida Shelf. For example, Figure 4 show (a) the NARR wind and (b) the ECMWF wind on September 16. In Figure 4(a), the southward wind of NARR data on the West Florida Shelf near Sarasota (82.5°W, 28°N) is strong (>8 m/s); but wind of ECMWF at the same location is very weak (<3 m/s). This is very significant difference, since the wind forcing is the major factor that affecting the ocean circulation on the WFS. Figure 5 shows the simulation results of the passive tracer transport of (a) simulation I and (b) simulation II on October 29. For simulation I, the tracer reach the Carolina's coast by the end of October, but not in simulation II. Since the 1987 red tide bloom event started (or first reported on Oct. 30), the results of Simulation I are more reasonable compared with the observations. The main reason of the large difference between the NARR wind and the ECMWF wind may come from the horizontal resolution of dataset. NARR has horizontal resolution of 32 km, while ECMWF has the resolution of 1.25°, which is about three-times coarser than that of the NARR data. So it can be concluded that the horizontal resolution of the wind data is very important in simulation of the continental shelf circulation and the transportation process of the passive tracers on the WFS.

4.2 Results of the intermediate domain simulation

Although the 0.18-degree simulations can simulate Gulf Stream and the along stream transport process very well, the finer structure of the coastal ocean circulation such as Gulf Stream meanders and eddies and their associated warm filament can not be resolved. A triple-nested approach is used to achieve the finer resolution in this study. In this section, the intermediate domain simulation will be discussed. In Simulation III, the computation domain covers the area of southeast U.S. continental shelf from Florida coast to North Carolina coast, and the horizontal resolution is 0.06 degree. The output of Simulation I is used as the initial and boundary conditions. Since the passive tracers are transported to the southeast U.S. continental shelf in October, the intermediate-domain integration started on October 1.

The simulation is driven by the NARR wind. Figure 6 shows the monthly-averaged wind of October 1987. From Figure 6 we can see that the along-shelf northeast wind dominated on the South Atlantic Bight in the time period of simulation. According to the Ekman transport theory, this type of wind is exactly in favor of transporting the passive tracers from the Gulf Stream to the Carolina inshore area (onshore transport).

Figure 7 shows the simulated SSH in simulation III on October 7, 12, 18 and 23 respectively. It can be seen clearly that there are two eddies in the simulations. The first eddy is at the location of 32.5N – 78.5W on October 7 and moving northward during the simulation. By October 23, it moves to the location of 33.5N – 76.5W. The second eddy is at the location of 32.3N – 78.7W on October 23, and it is also moving northward. The two eddies are very important in the simulation of the cross- and along-shelf transport process as we will see later in Section 4.3. However, they cannot be resolved well in the

Simulation I and II, therefore, the resolution higher than 0.18-degree is needed, and 0.06-degree resolution is sufficient to resolve the Gulf Stream eddies and meanders.

Figure 8 shows the simulated SST in simulation III on October 7, 12, 18 and 23 respectively. The two eddies discussed above can also be seen clearly in the SST field. In addition, the warm filament associated with the Gulf Stream eddies can also be resolved in simulation III. On October 23, the warm filament of the two eddies are simulated very well. However, they is not transported to the inshore area on the North Carolina coast, so that their effect on the SST at near-shore area is not very significant. The reason of the deference may due to coarse resolution of the simulation of the circulation of in the mid- and inner-shelf areas. Since in the inner- and mid-shelf area, the wind effect is also very important than the Gulf Stream forcing, and higher resolution is required for simulation of the wind-induced cross-shelf and along-shelf transport process. The combined effect of the wind and Gulf Stream forcing using higher resolution simulations will be discussed in Section 4.3.

Figure 9 shows the simulated passive tracer concentration in simulation III on October 7, 12, 18 and 23 respectively. We can see that the tracers are transported both along-stream and cross-stream. Beginning from October 7, the tracers started reaching the Carolina continental shelf, and in the meantime, were transported to the inshore area. However, since the cross-shelf transport process is under the influence of both the wind and the Gulf Stream forcing, it cannot be told which is more important in transporting the passive tracers to the North Carolina inshore area. In the next section, four simulations are designed to analyze the separate and combined effects of the wind and Gulf Stream meanders and eddies on the cross-shelf transport.

4.3 Results of the inner domain simulations

There are two factors that affect the ocean circulations on the continental shelf off the North and South Carolina coast: wind and the Gulf Stream meanders and eddies. Basically, wind factor is more important in the inner shelf, the Gulf Stream meanders and eddies are more important in the outer shelf, and the combined effect of the two factors are important in the mid-shelf. However, in cases of very strong wind or very large Gulf Stream meanders and eddies such as in October 1987 during the red tide bloom event, their effects on the ocean circulation and transport process become more complicated. In this section, four simulations (IV-VII) as described in section 3 are designed to study the effect of wind and Gulf Stream meanders, and the results of these four simulations are discussed as follows.

Simulation IV is driven by NARR wind and with large Gulf Stream meanders and eddies. The large Gulf Stream meanders and eddies are produced from ETOP02 from realistic bathymetry and curvature near the Charleston Bump. Figure 10 shows the simulated SSH on October 21, 23, 25, 27, 29 and 31 respectively in Simulation IV. On October 21, since the SSH is high on the east side and gradually decreased towards west, the ocean currents on the continental shelf are northeastward. Beginning from October 23, the strong northeast wind started to blow, which transport the sea water onshore and cause the SSH near the coast increased gradually. The change of the SSH, in turn, causes strong southwest-ward flow near shore as we can see in the SSH plot of October 27, 29 and 31. The ocean circulation during this time periods has direct impact on both the SST and passive tracer distributions on the continental shelf. Figure 11 shows the SST field on October 21, 23, 25, 27, 29 and 31 respectively in simulation IV. The SST in the near-

shore off the North Carolina coast are increased during this time period. There are two reasons that are responsible for the SST increment:1. cross-shelf transport of Gulf Stream water into the near shore area; and 2. Gulf Stream filament intrusion into the near shore area. Figure 12 shows the simulated passive tracer concentration off the North Carolina coast on October 21, 23, 25, 27, 29 and 31 respectively in simulation IV. We can see that the passive tracers are transported to the near-shore area by the end of October, which is in agreement with observations.

Simulation V has the same settings with simulation IV, but with the wind forcing shut off. Figure 13 shows the simulated SSH in simulation V on October 21, 23, 25, 27, 29 and 31 respectively, which has very large difference from that of simulation IV. In simulation V, the ocean circulation on the continental shelf is under the influence of the Gulf Stream only, and the wind factor is eliminated from the simulations. Therefore, because of lacking the Ekman transport, the SSH in the near-shore area are not increasing, but remains low during this time periods, and the ocean current are northeast-ward. Figure 14 show the simulated SST in simulation V on October 21, 23, 25, 27, 29 and 31 respectively. From Figure 14, we can see that near-shore warming in simulation V is not as significant as in simulation IV. Figure 15 shows the passive tracer concentration of simulation V on October 21, 23, 25, 27, 29 and 31 respectively. In Figure 15, we can see that the passive tracers cannot reach the near-shore area of the North Carolina coast without wind. Therefore, we can conclude that wind factor plays a critical role in the 1987 red tide bloom event. This is in agreement with Pietrafesa et al. (1988).

To investigate the contribution of the Gulf Stream meanders and eddies to the continental shelf circulation and the cross-shelf transport process, simulation VI and VII

are designed for this purpose. In simulation VI and VII, the water depth near the Charleston Bump is increased artificially, so that the bump is partially removed from the bathymetry, and the bump effect will be greatly reduced. In simulation VI, the NARR wind is used to drive the ocean model; while the wind forcing is shut off in Simulation VII. Figure 16 shows the simulated SSH on October 21, 23, 25, 27, 29 and 31 respectively in simulation VI. We can see that the SSH in the near-shore area increases as a result of the wind forcing. However, because of the bump effect are greatly reduced in this simulation, the amplitude of the Gulf Stream meanders/eddies and their associated warm filament are small. Figure 17 shows the simulated SST on October 21, 23, 25, 27, 29 and 31 respectively in simulation VI. From Figure 17, we can see that the SST in the near-shore area of the North Carolina are not increased during this time period. From the passive tracer concentration as shown in Figure 18, we can see that the passive tracer can not reach in the Onslow Bay. However, it can reach in the Raleigh Bay, which means the passive tracer is transported further inshore in simulation VI than in simulation V. Therefore, we can conclude that the wind itself without the large meanders and eddies can not transport the passive tracer to the North Carolina near-shore area in the 1987 red tide bloom event. The combination effect of the wind and the large meanders and eddies are very important to cause the happening of the events. Furthermore, the wind alone seems to have more effect on the cross-shelf transport than the Gulf Stream meander/eddy alone.

Figure 19 shows the simulated SSH on October 21, 23, 25, 27, 29 and 31 respectively in simulation VII. As in Simulation V, SSH in the near-shore area doesn't increase, since there is on-shore Ekman transport of sea water. The ocean current is mainly

northeastward under the influence of the Gulf Stream. The SST warming is less significant than in simulation V (Figure 20), and the transportation of the passive tracer is also less significant than in simulation V (Figure 21). Therefore, the Gulf Stream the amplitude of meander and eddies does affect the ocean circulation and the cross-shelf transport near the North Carolina continental shelf, however, its effect is not as significant as the wind.

In summary, we have concluded that the combination of the wind effect and the effect of the Gulf Stream meanders and eddies caused the red tide bloom event in the North Carolina near shore waters in October 1987. Neither wind alone nor the Gulf Stream meander/eddy alone is sufficient to transport the passive tracer to the near-shore area. However, the wind alone does have more significant effect than the Gulf Stream meander alone in transporting the passive tracer to the North Carolina near shore area. There is no doubt that the wind plays a critical role in transporting the passive tracer from the Gulf Stream to the near-shore area. However, the mechanism by which the wind transports the passive tracer from the Gulf Stream to the near-shore area needs to be addressed in more detail.

It is well known that the wind-induced Ekman transport can cause the cross-shelf transport of passive tracers. On the North Carolina coast, northeast wind may cause on-shore transport, while southwest wind may cause off-shore transport. In our simulations, we find that the along-shelf transport can also bring the passive tracers from the Gulf Stream to the near-shore area, and the mechanism is explained as follows. The width of the continental shelf in the SAB increases from the Florida to Charleston, South Carolina, and then decreases from South Carolina to Cape Hatteras, North Carolina. The Gulf

Stream in Raleigh Bay, North Carolina is very close to the coast due to very narrow continental shelf, especially when there are warm filaments associated with Gulf Stream meanders and eddies. In case of the northeast wind, the ocean current in the inshore area is southward in Raleigh Bay and Onslow Bay, which could brings the Gulf Stream water southward near-shore. In fact, this is the case in our simulation IV. Figure 22 shows the surface velocity vector on October 29. From Figure 22, we can see there is very strong wind-induced southward along-shore current in Raleigh Bay and Onslow Bay. Because of large meanders and eddies in Simulation IV, the passive-tracer-led Gulf Stream water is very close to the coast in Raleigh Bay, so that the along-shore current can bring the passive tracers from the Raleigh Bay to Onslow bay, and cause the red ride bloom. The distance from the Gulf Stream near Cape Hatteras is critical in this mechanism. If the Gulf Stream is too far way from the coast, the waters from the Mid-Atlantic Bight can come through Cape Hatteras with the along-shore current, and become a barrier preventing the passive-tracer-led Gulf Stream water reaching the near-shore area in Raleigh Bay and Onslow Bay. In the case of large meanders and eddies, the warm filament can become very close to the near shore. Therefore, our conclusion that the combination of the wind and large meander and eddies are important seems to be reasonable.

5. Summary and conclusions

In this study, HYCOM is used to simulate the process of transportation of K. Brevis cell from the West Florida Shelf in Gulf of Mexico to the inshore area of the North Carolina coast. Since the process covers a large area, it is very time-consuming to run the simulation in the whole area of interest. Therefore, a triple-nested approach was taken to achieve the high resolution: the outer domain covers the whole north and equatorial Atlantic, the intermediate domain covers the south east U.S. continental shelf, and the inner domain covers the North and South Carolina continental shelf. From September 15 to 26, the wind on the West Florida Shelf is basically southward, which is in favor of transporting the K. Brevis cells from the Florida coast to the Loop Current – Florida Current – Gulf Stream system. In the outer-domain simulation, the ocean current on the WFS is originally flowing northward. Beginning from September 15, the wind starts blowing southward, and the current on the WFS starts flowing southward. This southward wind is in favor of the offshore transport of the K. Brevis cells on the WFS, and the southward flow can transport these cells from the WFS to the Gulf Stream system. The simulated response of the ocean current to wind is in agreement with Weisberg et al. (2001). The tracer reaches North Carolina coast at the end of October, which is in agreement with observations.

The process of transportation of passive tracer from the Gulf Stream to the North Carolina coast area is also simulated in the inner domain runs. There are two factors that affect the ocean circulations on the continental shelf off the North and South Carolina coast: wind and the Gulf Stream meanders and eddies. Four simulations (IV-VII) are

designed to study the effect of wind and Gulf Stream meanders. In simulation IV, the model is driven by NARR wind and the meander and eddies are large, the passive tracers are transported to the near-shore area by the end of October. Simulation V is identical to simulation IV, except that the wind is shut off. The passive tracer cannot reach the North Carolina coast area. In simulation VI, the NARR wind is used to drive the ocean model, but the bump effect is artificially reduced. The passive tracer cannot reach the North Carolina coast either. Simulation VII is the same as in Simulation VI, but the wind is shut down. It is concluded that the combination of the wind effect and the effect of the Gulf Stream meanders and eddies caused the red tide bloom event in the North Carolina near shore waters in October 1987. Neither wind alone nor the Gulf Stream meander/eddy alone is sufficient to transport the passive tracer to the near-shore area. However, the wind alone does have more significant effect than the Gulf Stream meander alone in transporting the passive tracer to the North Carolina near shore area. There is no doubt that the wind plays a critical role in transporting the passive tracer from the Gulf Stream to the near-shore area. However, the mechanism by which the wind transports the passive tracer from the Gulf Stream to the near-shore area needs to be addressed in more detail.

6. References

Allen et al, 1983: Physical Oceanography of continental shelves. Rev. Geophys. Space Phys., 21, 1149-1181.

Bane, J. M., Jr., and D. A. Brooks, 1979: Gulf Stream meanders along the continental margin from the Florida Straits to Cape Hatteras, Geophys. Res. Lett., 6, 280-282.

Bane, J. M., Jr., D. A. Brooks, and K. R. Lorenson, 1981: Synoptic observations of the three-dimensional structure and propagation of Gulf Stream meanders along the Carolina continental margin, J. Geophys. Res., 86(C7), 6411-6425, 1981.

Bane, J. M., Jr., 1983: Initial observation of the subsurface structure and short-term variability of the sea-ward deflection of the Gulf Stream off Charleston, South Carolina, J. Geophys. Res., 88(C8), 4673-4684.

Bleck, R., 2002: An oceanic general circulation model framed in hybrid isopycnic-Cartesian coordinate, Ocean Modeling, 4, 55-88, 2002

Bleck, R., C. Rooth, D. Hu and L. T. Smith, 1992: Salinity-driven thermocline transients in a wind and thermohaline-forced isopycnic coordinate model of the North Atlantic, J. Phys. Oceanogr., 22, 1486-1505

Brooks, D. A. and J. M. Bane, Jr., 1978: Gulf Stream deflection by a bottom feature off Charleston, SC, Science, 201, 1225-1226.

Brooks, D. A. and J. M. Bane, Jr., 1981: Gulf Stream fluctuations and meanders over the Onslow Bay upper continental slope, J. Physical Oceanogr., 11, 247-256.

Brooks, D. A. and J. M. Bane, Jr., 1983: Gulf Stream meander off North Carolina during winter and summer, 1979, J. Geophys. Res., 88(C8), 4633-4650.

Brooks, I. H., and P. P. Niiler, 1977: Energetics of Florida Current, J. of Marine Research, 35, 163-191.

Chao, S. Y. and G. S. Janowitz, 1979; The effect of a localized topographic irregularity on the flow of a boundary current along the continental margin, J. Physical Oceanogr., 9, 900-910.

Chassignet, E, L. Smith, G. Halliwell, and R. Bleck, 2003: North Atlantic simulations with the hybrid Coordinate Ocean Model (HYCOM): Impact of coordinate choice, reference pressure, and thermobaricity, J. Phys. Oceanogr., 33, 2504-2526.

Cragg et al, 1983: Wind-induced sea-surface slopes on the West Florida Shelf. J. Phys. Oceanogr., 13, 2201-2212.

Dewar, W. K., and J. M. Bane Jr., 1985: Subsurface energetics of the Gulf Stream near the CB. J. Physical Oceanogr., 15, 1771-1789.

He and Weisberg, 2002: West Florida shelf circulation and temperature budget for the 1999 spring transition *Continental Shelf Research* , 22, 719-748

Hoffmann, E. E., L. J. Pietrafesa, J. M. Klinck, and L. P. Atkinson, A time-dependent model of nutrient distribution in continental shelf waters, Ecol. Modell., 10, 193-214.

Hood, C. A. and J. M. Bane, Jr., 1983; Subsurface energetics of the Gulf Stream cyclonic frontal zone off Onslow Bay, North Carolina, J. Geophys. Res., 88(C8), 4651-4662

Hurlbert and Thompson, 1980: A numerical study of Loop Current Intrusions and eddy shedding, J. Phys. Oceanogr., 10, 1611-1651.

Hurlbert and Thompson, 1982: The dynamics of the loop current and shed eddies in a numerical model of the Gulf of Mexico. In the Hydrodynamics of the semi-enclosed seas, J.C. J. Nihoul, ed. Elsevier, Amsterdam, pp243-398.

Janowitz, G. S. and L. J. Pietrafesa, 1982: The effect of alongshore variation in bottom topography on a boundary current, Continental Shelf Res., Vol. 1, No. 2, 123-141

Knauss, J. A., 1969: A note on the transport of the Gulf Stream. Deep Sea Res., 16(Suppl.), 117-123.

Koblinsky and Niiler, 1980: Direct measurements of circulation on West Florida continental Shelf, Data Rep. 76, ref. 79-13. Oregon State University School of Oceanography.

Lee, T. N., et al, 1991: Gulf Stream Frontal eddy Influence on Productivity of the Southeastern U.S. continental shelf, J. Geophys. Res., 96, 22,191-22,105

Lee, T. N., E. Williams, J. Wang, R. Evans, and L. Atkinson, 1989: Response of South Carolina continental shelf waters to wind and gulf stream forcing during winter of 1986. J. Geophys. Res., 94, 10,715–10,754

Lee, T. N. and L. P. Atkinson, 1983: Low frequency current and temperature variability from Gulf Stream frontal eddies and atmospheric forcing along the Southeast U.S. outer continental shelf. J. Geophys. Res., 88(C8), 4541-4567

Lee, T. N., L. P. Atkinson, and R. Legeckis, 1981: Observations of a Gulf Stream frontal eddy on the Georgia continental shelf, April 1977, Deep Sea Research, Part A, 28(4), 347-378.

Lee, T. N. and D. A. Mayer, 1977: Low frequency current variability and spin-off eddies along the shelf off the Southeast Florida. J. Marine Res., 35, 193-220.

Legeckis, R. V., 1975: Application of synchronous meteorological data to the study of time-dependent sea surface temperature changes along the boundary of the Gulf Stream. Geophys. Res. Lett., 24, 435-438.

Legeckis, R.V., 1979: Satellite observation of the influence of bottom topography on the seaward deflection of the Gulf Stream off Charleston, South Carolina. J. Phys. Oceanogr., 9, 483-497

Levitus, S.,1982: Climatological atlas of the world ocean, NOAA Prof. Pap. 13, U.S. Govt. Print. Off., Washington, D. C.

Marmorino, 1982: Wind-forced sea level variability along the West Florida Shelf, J. Phys. Oceanogr., 12, 389-405

Marmorino, 1983: Variability of current, temperature, and bottom pressure across the West Florida Continental Shelf, winter 1981-1982. J. Geophys. Research. 88, 4439-4457.

Maul, G. A., P. W. deWitt, A. Yanaway, and S. R. Baig, 1978: Geostationary satellite observations of Gulf Stream Meanders: Infrared measurements and time series analysis, J. Geophys. Res., 83, 6123-6135.

Miller, J. L. and T. N. Lee, 1995a: Gulf Stream meanders in the South Atlantic Bight. 1. Scaling and energetics, J. Geophys. Res., 100(C4), 6687–6704.

Miller, J. L. and T. N. Lee, 1995b: Gulf Stream meanders in the South Atlantic Bight. 2. Momentum balances, J. of Geophysical Research, 100(C4), 6705-6724

Mitchum and Clarke, 1986: Evaluation of frictional wind-forced long-wave theory on the West Florida Shelf. J. Phys. Oceanogr., 16, 1029-1037.

Mitchum and Sturges, 1982: Wind-driven currents on the West Florida Shelf. J. Phys. Oceanogr., 12, 1301-1317.

Murphy et al. 1975: An explanation for the Florida east coast Gymnodinium breve red tide bloom of November 1972. Limnol. Oceanogr.. 20: 481-486.

Niiler, 1976: Observation of low-frequency currents on the west Florida continental shelf. Mem. Soc. R. Sci. Liege, 10, 331-358.

Olson, D. B., O. B. Brown, and S. R. Emmerson, 1983: Gulf Stream frontal statistics from Florida Straits to Cape Hatteras derived from satellite and historical data, J. Geophys. Res., 88(C8), 4569-4577

Orlanski, I., 1969: The influence of bottom topography on the stability of jets in a baroclinic fluid. J. Atmos. Sci., 45, 3253-3267.

Pietrafesa, L. J., J. O. Blanton, and L. P. Atkinson, 1978: Evidence for deflection of the Gulf Stream at the Charleston Rise, Gulf Stream, 4(9), 3 and 6-7

Pietrafesa, L. J., and G. S. Janowitz, 1979: A note on the identification of a Gulf Stream spin-off eddy from Eulerian data, Geophys. Res. Lett., 6, 549-552, 1979.

Pietrafesa, L. J., and G. S. Janowitz, 1980: On the dynamics of the Gulf Stream front in the Carolina Capes, in Proceedings of the Second International Symposium on Stratified Flows, pp. 184-197, Tapir Publications, Trondheim, Norway.

Pietrafesa, L. J., 1983; Survey of a Gulf Stream frontal filament, Geophys. Res. Lett., 10, 203-206.

Pietrafesa, L. J., G. S. Janowitz, K. S. Brown, F. Askari, C. Gabriel, and L. A. Salzillo, 1988: The invasion of the Red Tide In North Carolina Coastal Waters, UNC Sea Grant Publication UNC-SG-WP-88-1, August 1988.

Roberts 1979: Occurrence of Gymnodinium breve red tide along the west and east coast of Florida during 1976 and 1977, p199-202. In Toxic dinoflagellate blooms. Proc. 2nd Int. Conf. Elesvire.

Romanou, A, E. P. Chassignet, W. Sturges, 2004: Gulf of Mexico circulation within a high-resolution numerical simulation of the North Atlantic Ocean, J. Geophys. Res., 109, C01003, doi:10.1029/2003JC001770, 2004

Rooney, D. M., G. S. Janowitz and L. J. Pietrafesa, 1978: A simple model of deflection of the Gulf Stream by the Charleston rise, Gulf-stream, 4(11), 3-7

Rossby, 1987: Gulf Stream energetics, J. of Marine Research, 45, 61-94

Savidge, D. K., J. O. Blanton, T. N. Lee and R. H. Evans, 1992: Influence of an offshore shift in the Gulf Stream on water of the South Carolina continental shelf, J. Phys. Ocean., 22, 1085-1094.

Steidinger and Haddad, 1981: Biological and hydrographic aspect of red tides. BioScience 31: 814-819.

Steidinger, 1983: A re-evaluation of toxic dinoflagellate biology and ecology. Prog. Phycol. Res. 2: 147-188. Elsevier.

Sturges and Evans, 1983: On the variability of the Loop current in the Gulf of Mexico, J. Mar. Res., 41, 639-653.

Sun, L. C. and L. J. Pietrafesa, 1992: Baroclinic-barotropic instabilities and energy transfers in the Gulf Stream, Proceedings of the First World Congress of Nonlinear Analysts, Tampa, Florida, August 19-26, 1992

Tester and Fowler, 1990: Brevetoxin contamination of Mercenaria and Crassostrea virginica: A management issue, p499-503. In Toxic marine phytoplankton. Proc. 4th Int. Conf. Elsevier.

Tester, P. A. and K. A. Steidinger, 1997:Gymnodinium breve Red Tide Blooms: Initiation, Transport, and Consequences of Surface Circulation, Limnology and Oceanography, 42, 1039-1051.

Tester, P. A., R. P. Stumpf, F M. Vukovich, P. K. Flower, J. T. Turner, 1991: An expatriate Red Tide Bloom: Transport, Distribution, and Persistence, Limnology and Oceanography, 36, 1053-1061.

Weisberg et al., 1996: Seasonal modulation of the west Florida continental shelf circulation. Geophy. Research Letters, 23 2247-2250.

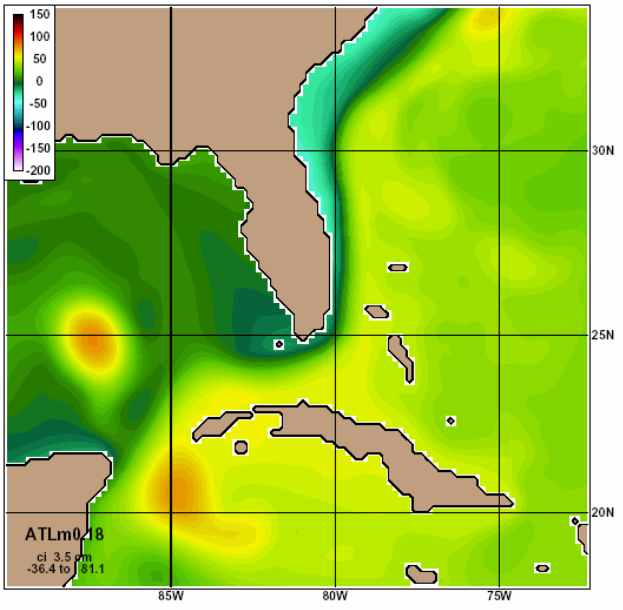
Weisberg, R.H., Z. Li, and F.E. Muller-Karger, 2001: West Florida shelf response to local wind forcing: April 1998. J. Geophys. Res., 106, 31239-31262.

Xie et al., 2006: Effect of bathymetry curvature on the Gulf Stream instability in the vicinity of the Charleston Bump, Journal of Phys. Oceano., accepted.

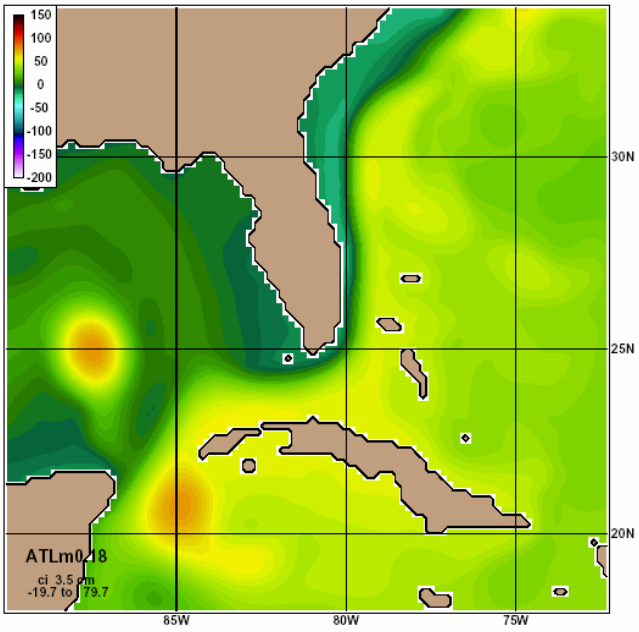
Xue, H., and G. Mellor, 1992: Instability of the Gulf Stream Front in the South Atlantic Bight, J. of Physical Oceanogr., 23, 2326-2350

Figure 1 Sea Surface Height in Simulation I for September 11, 15, 20 and 25

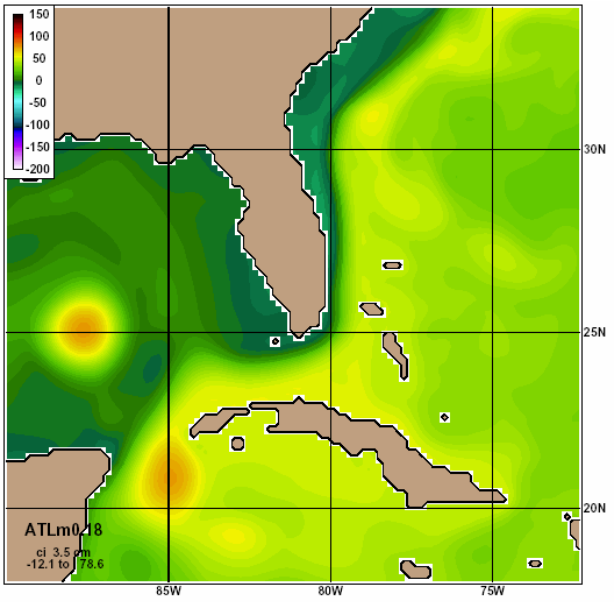
(a) Sea Surface Height, September 11, 1987



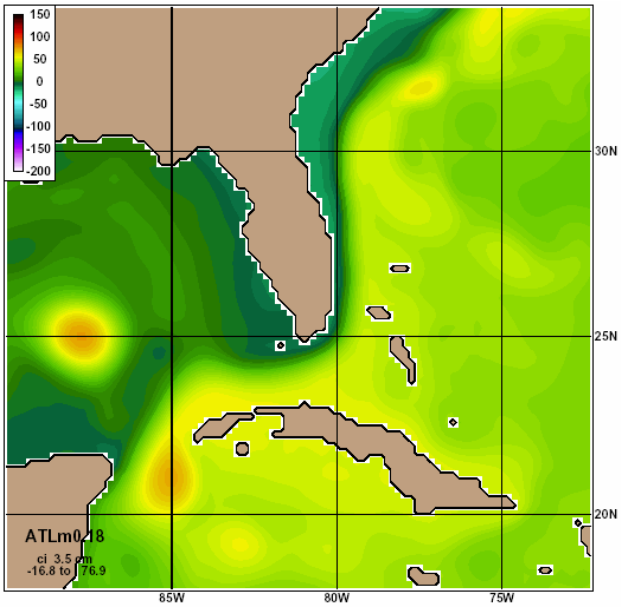
(b) Sea Surface Height, September 15, 1987



(c) Sea Surface Height, September 20, 1987



(d) Sea Surface Height, September 25, 1987



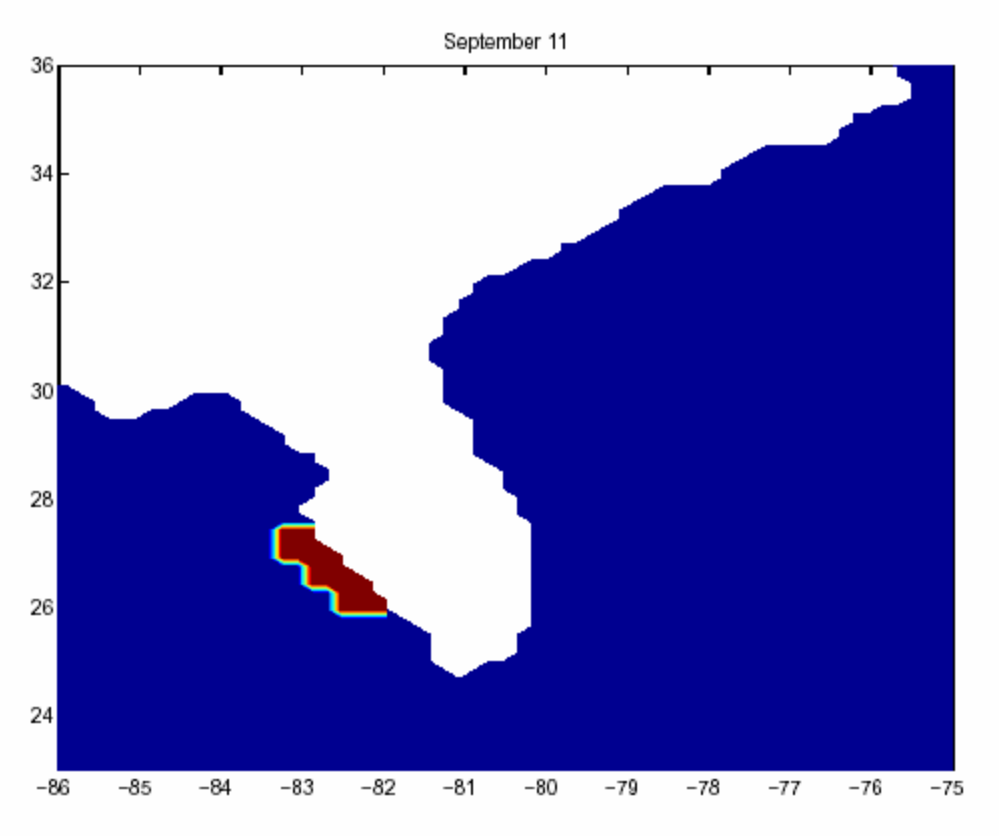


Figure 2 Initial condition of passive tracers

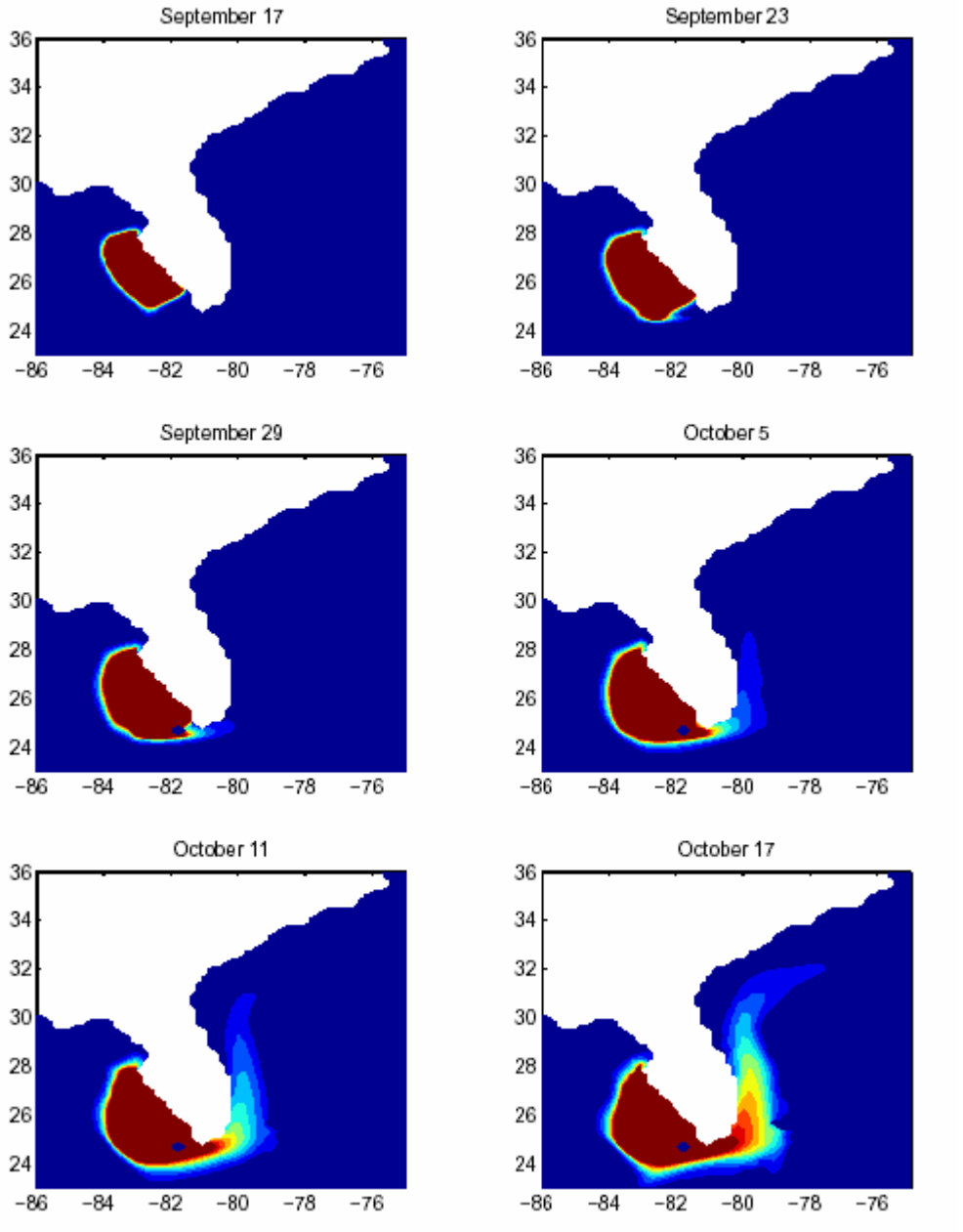


Figure 3 Passive tracer concentrations on September 17, 23, 29 and October 5, 11, 17.

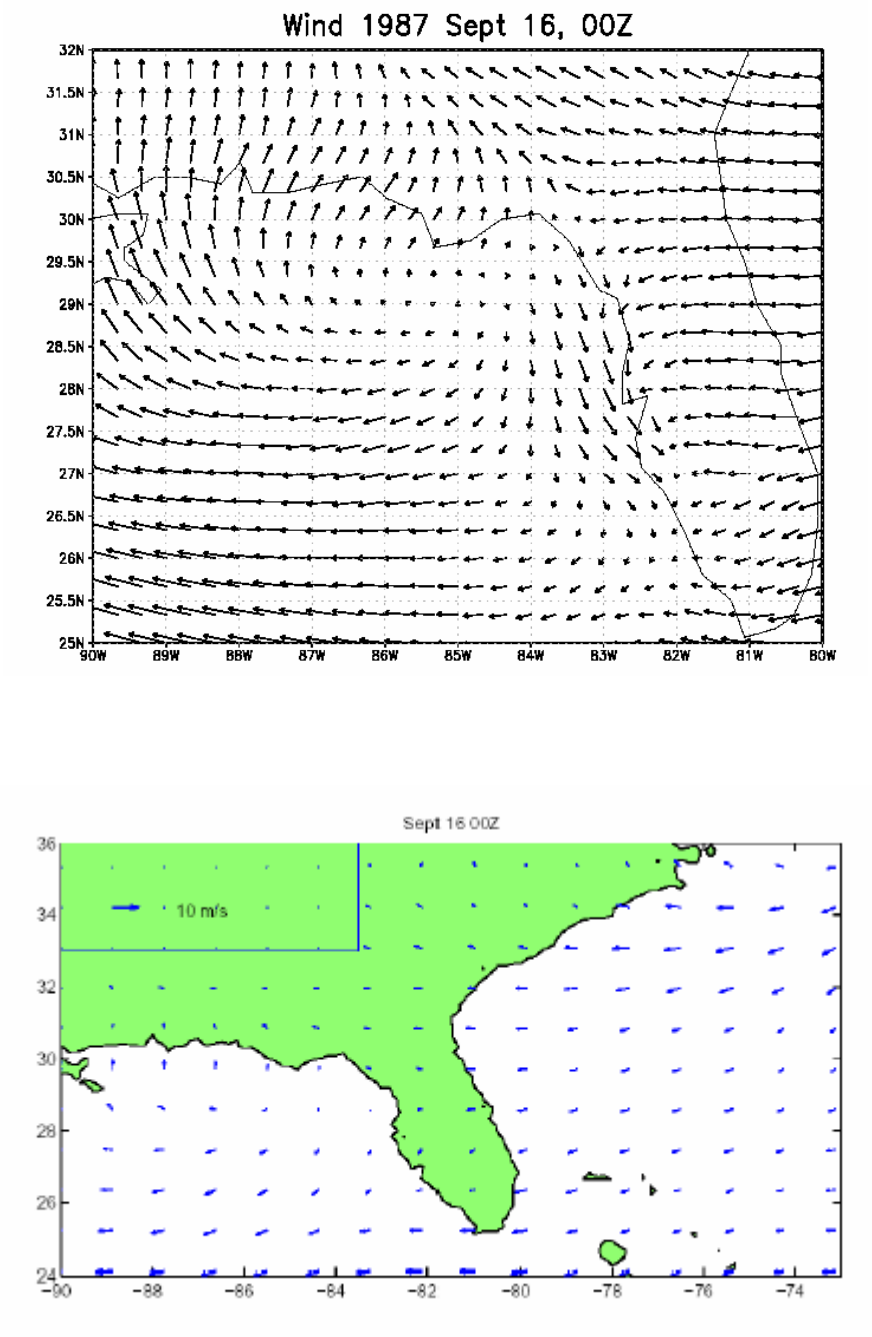


Figure 4 Wind on September 16 from NARR (upper) and ECMWF (lower)

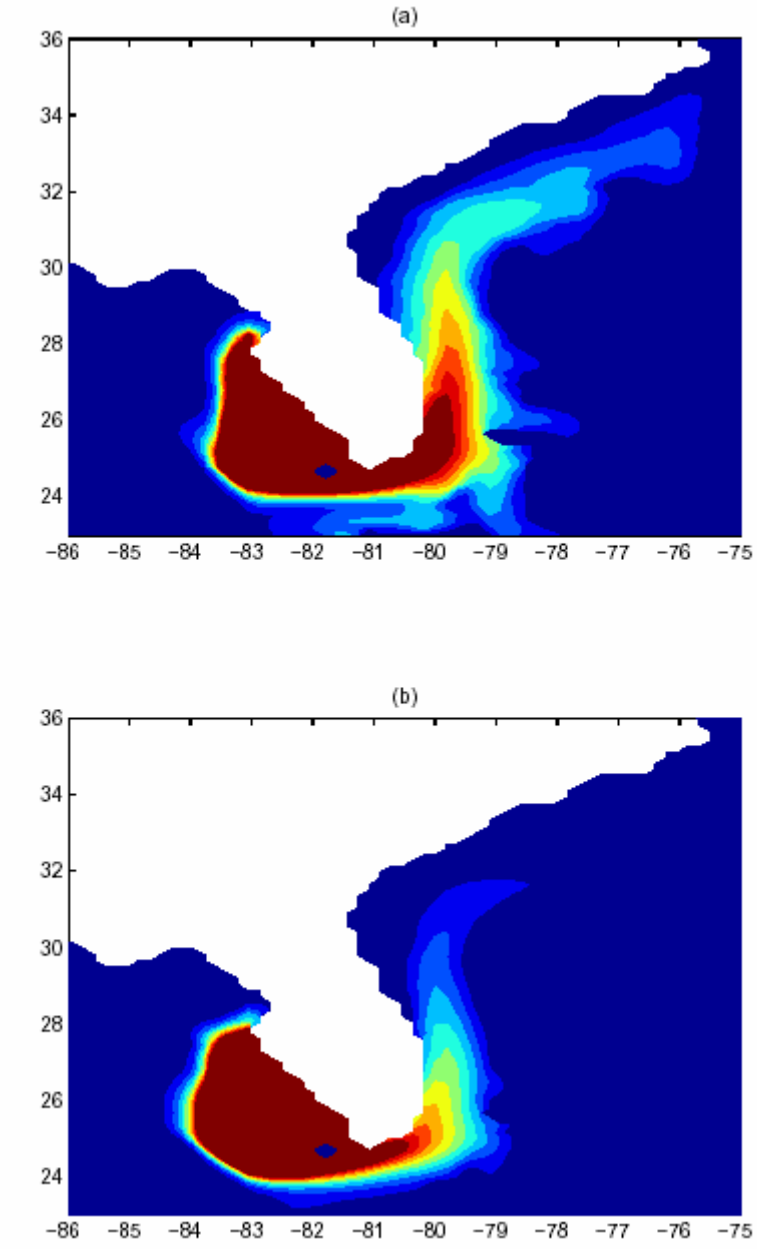


Figure 5 Passive tracer concentration on October 29 in (a) Simulation I, and (b) Simulation II.

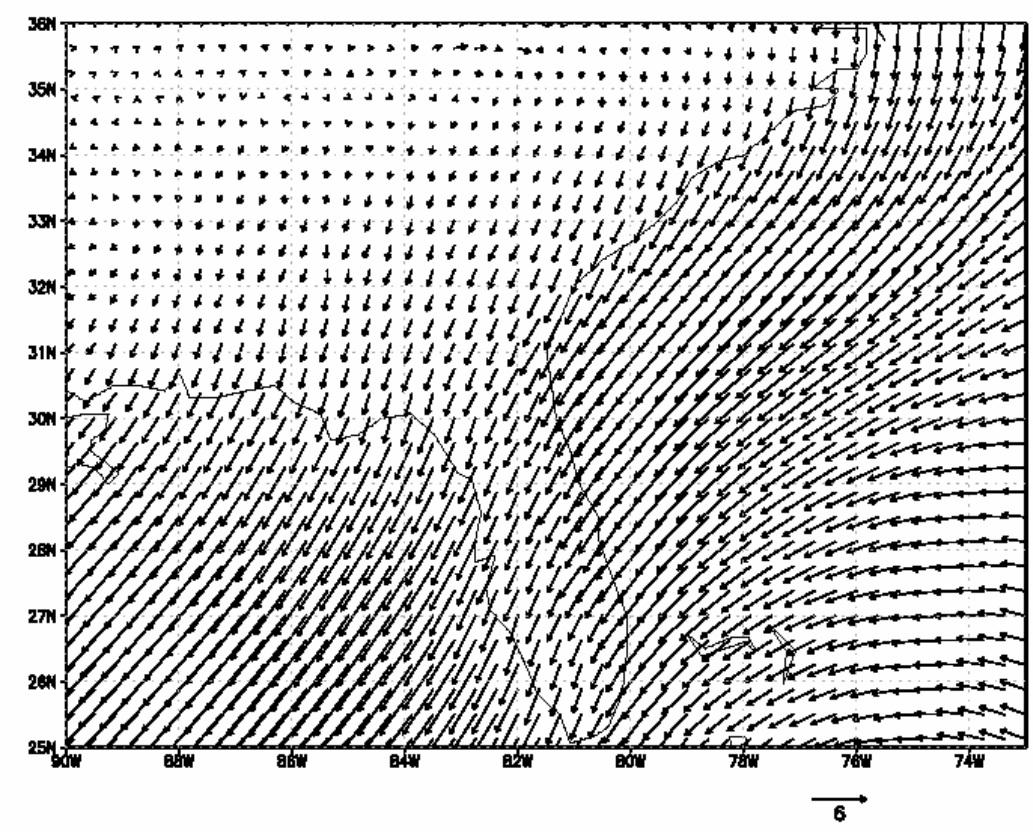


Figure 6 NARR monthly mean wind for October 1987.

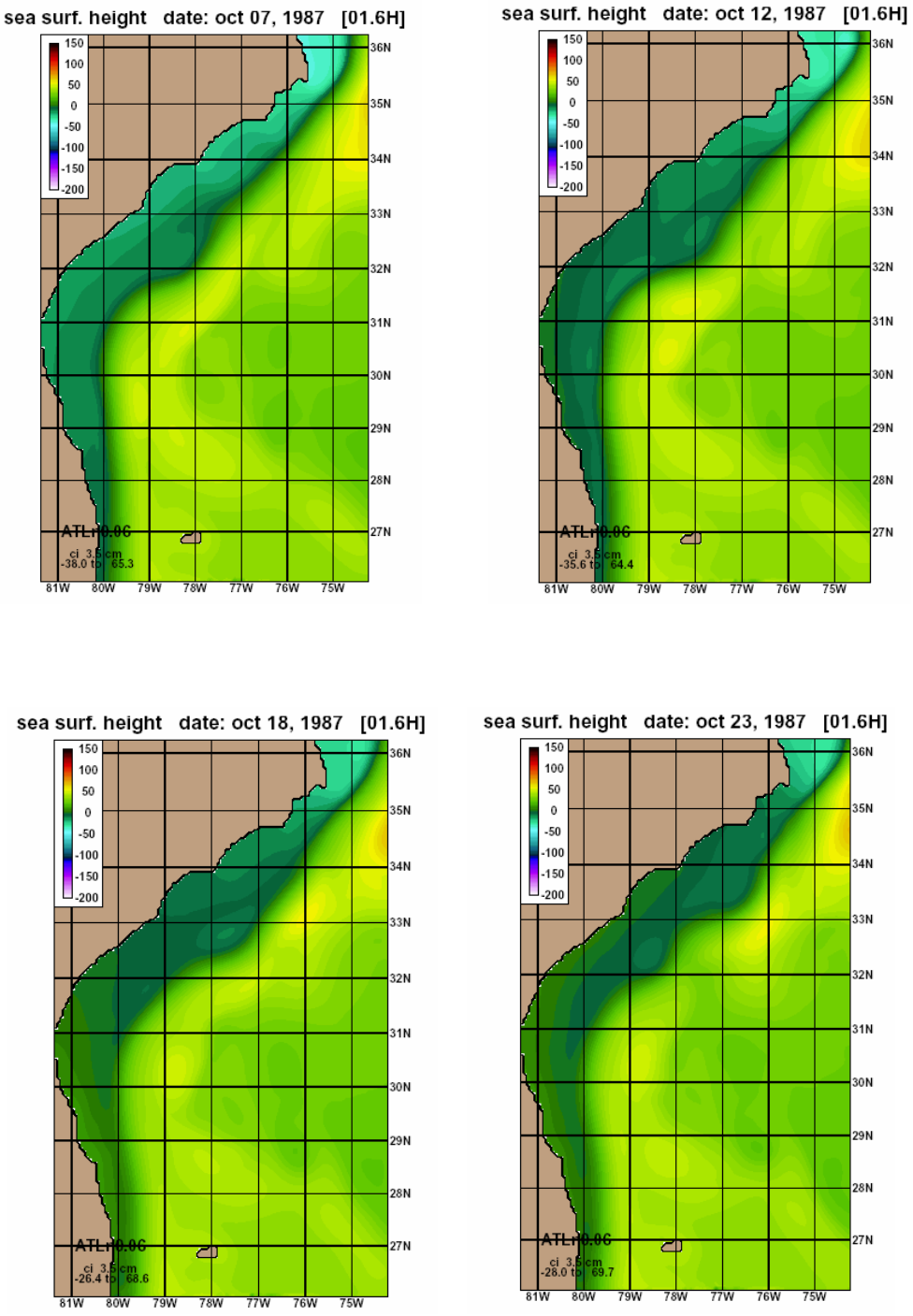


Figure 7 SSH on October 7, 12, 18 and 23 in Simulation III

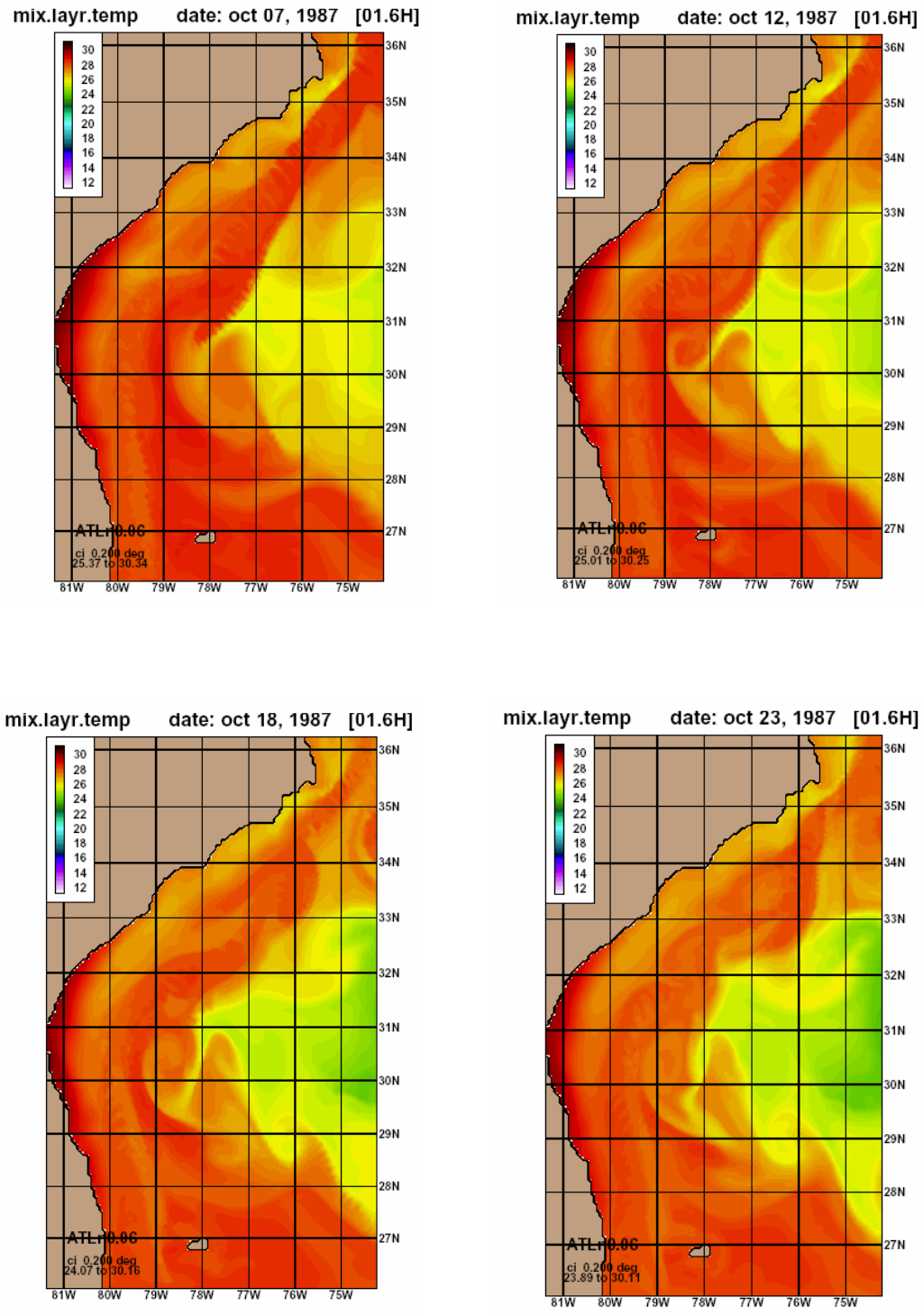


Figure 8 SST on October 7, 12, 18 and 23 in Simulation III

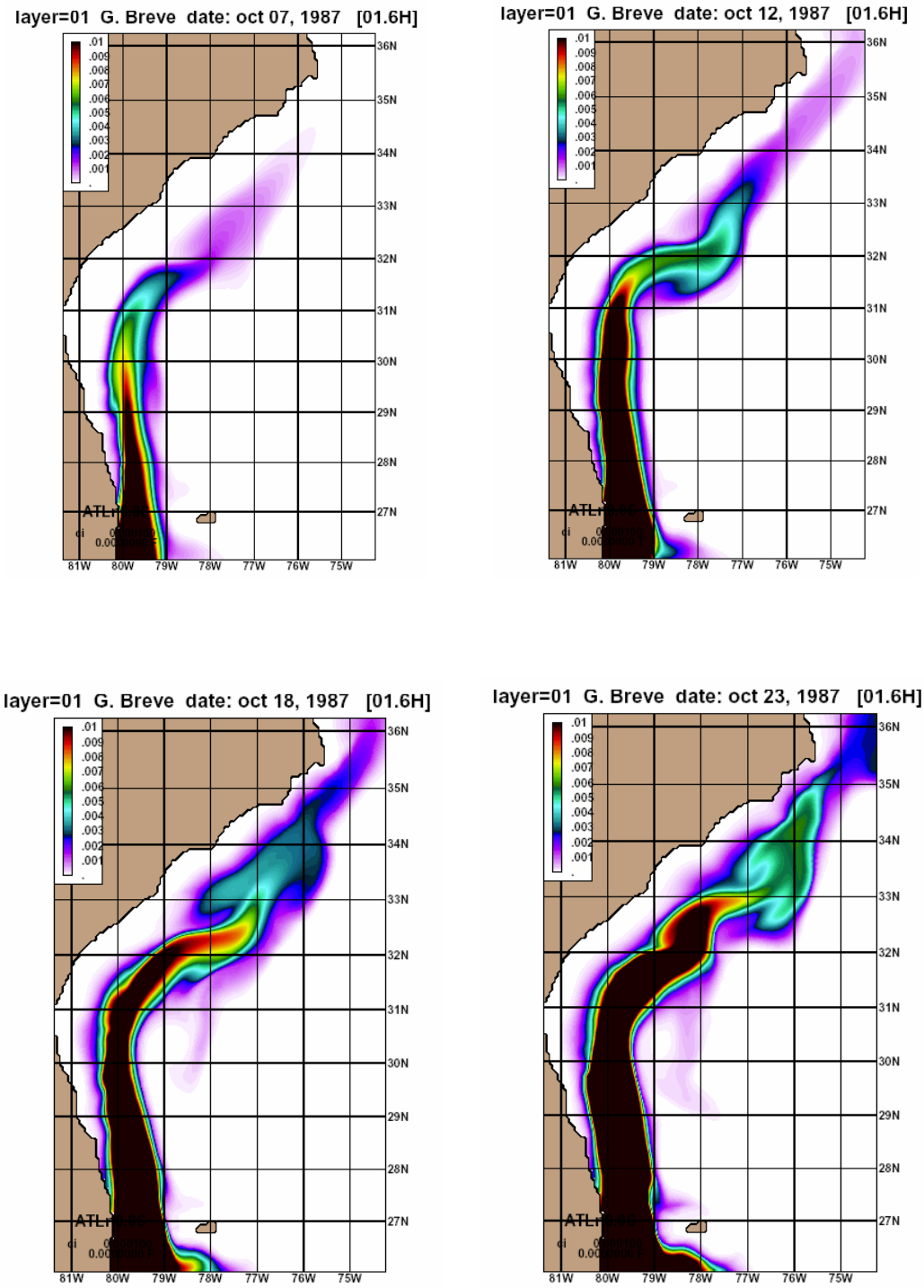


Figure 9 Passive tracer concentration on October 7, 12, 18 and 23 in Simulation III

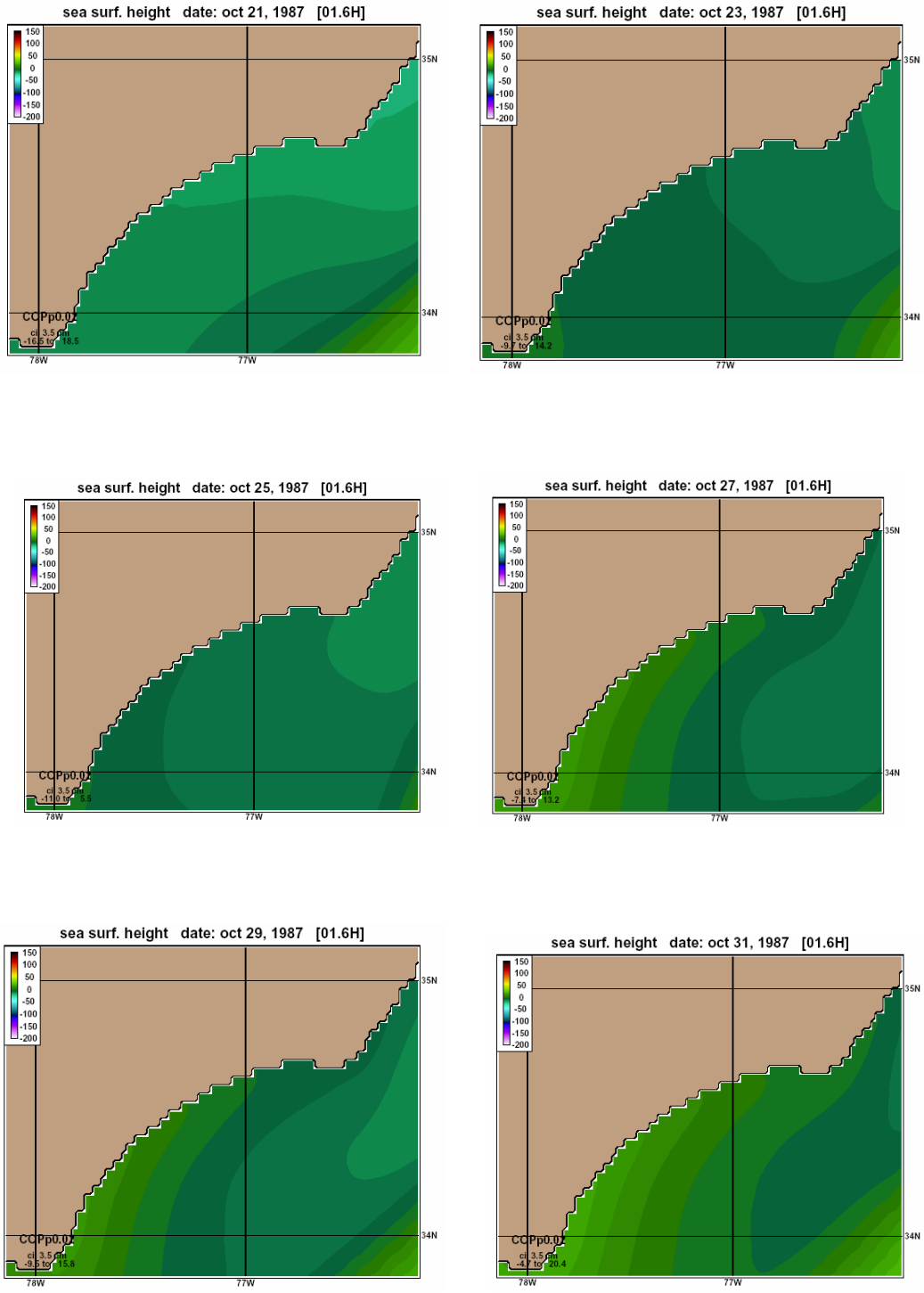


Figure 10, SSH on October 21, 23, 25, 27, 29 and 31 in Simulation IV

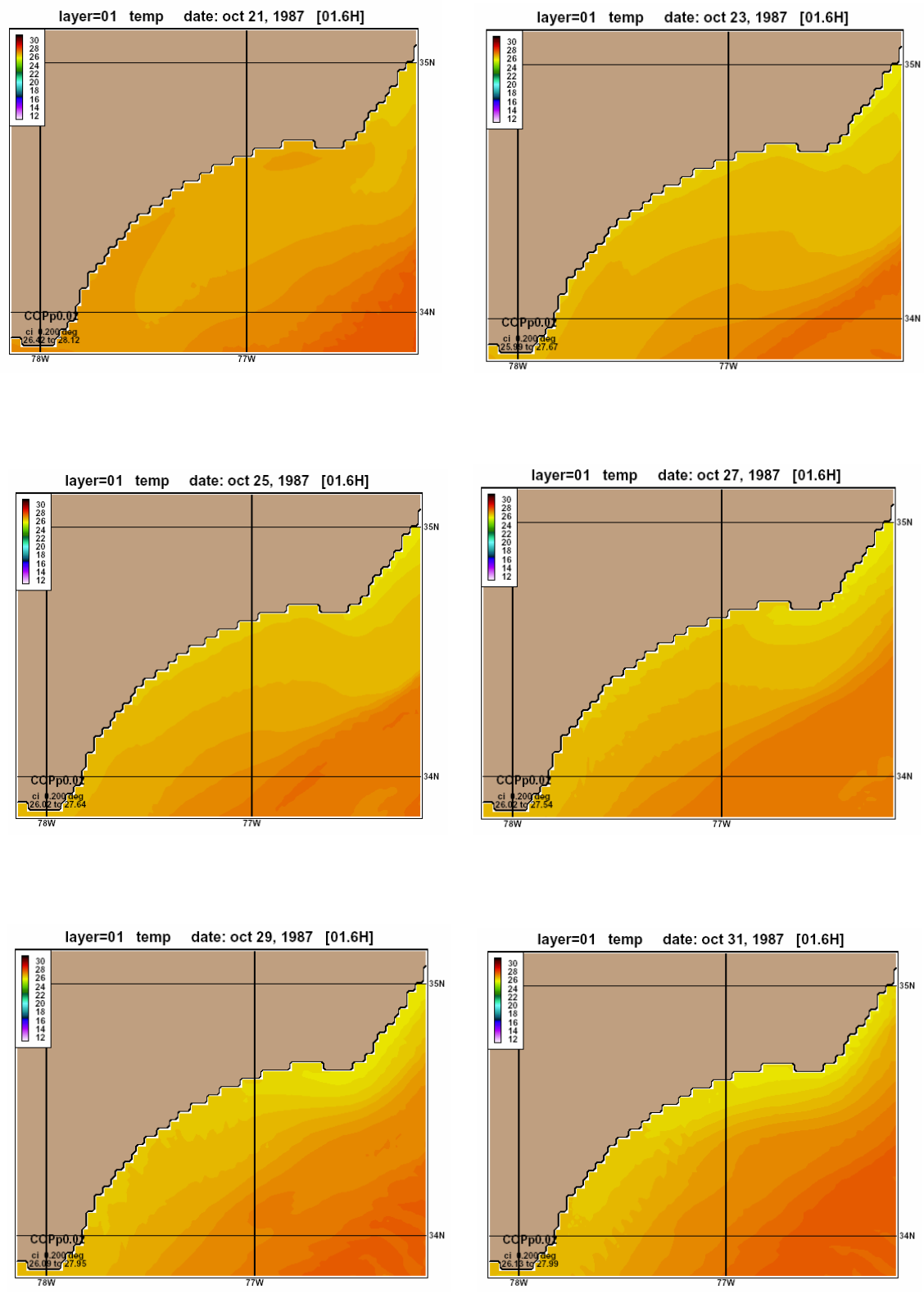


Figure 11 SST on October 21, 23, 25, 27, 29 and 31 in Simulation IV

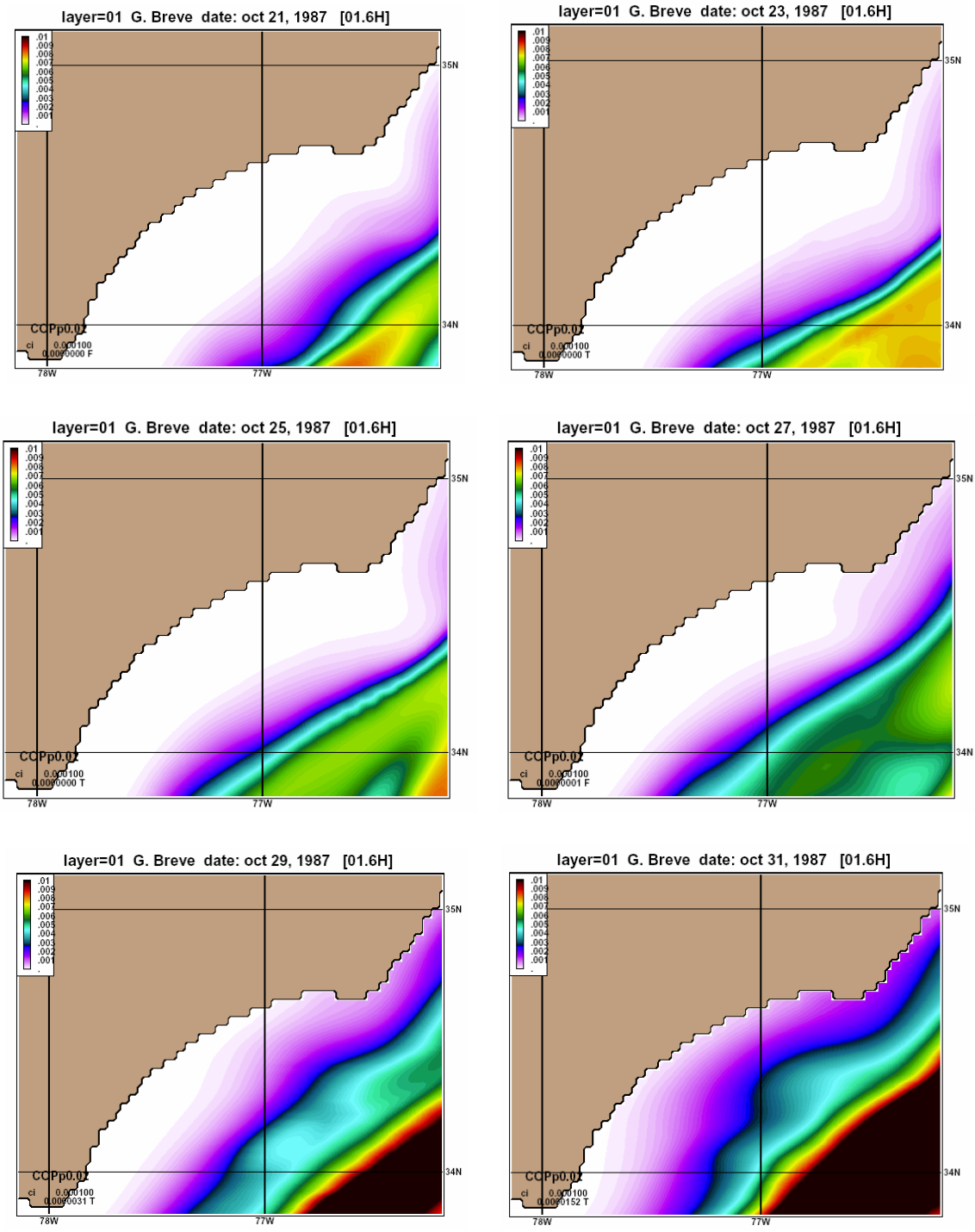


Figure 12 Passive tracer concentration on October 21, 23, 25, 27, 29 and 31 in Simulation IV

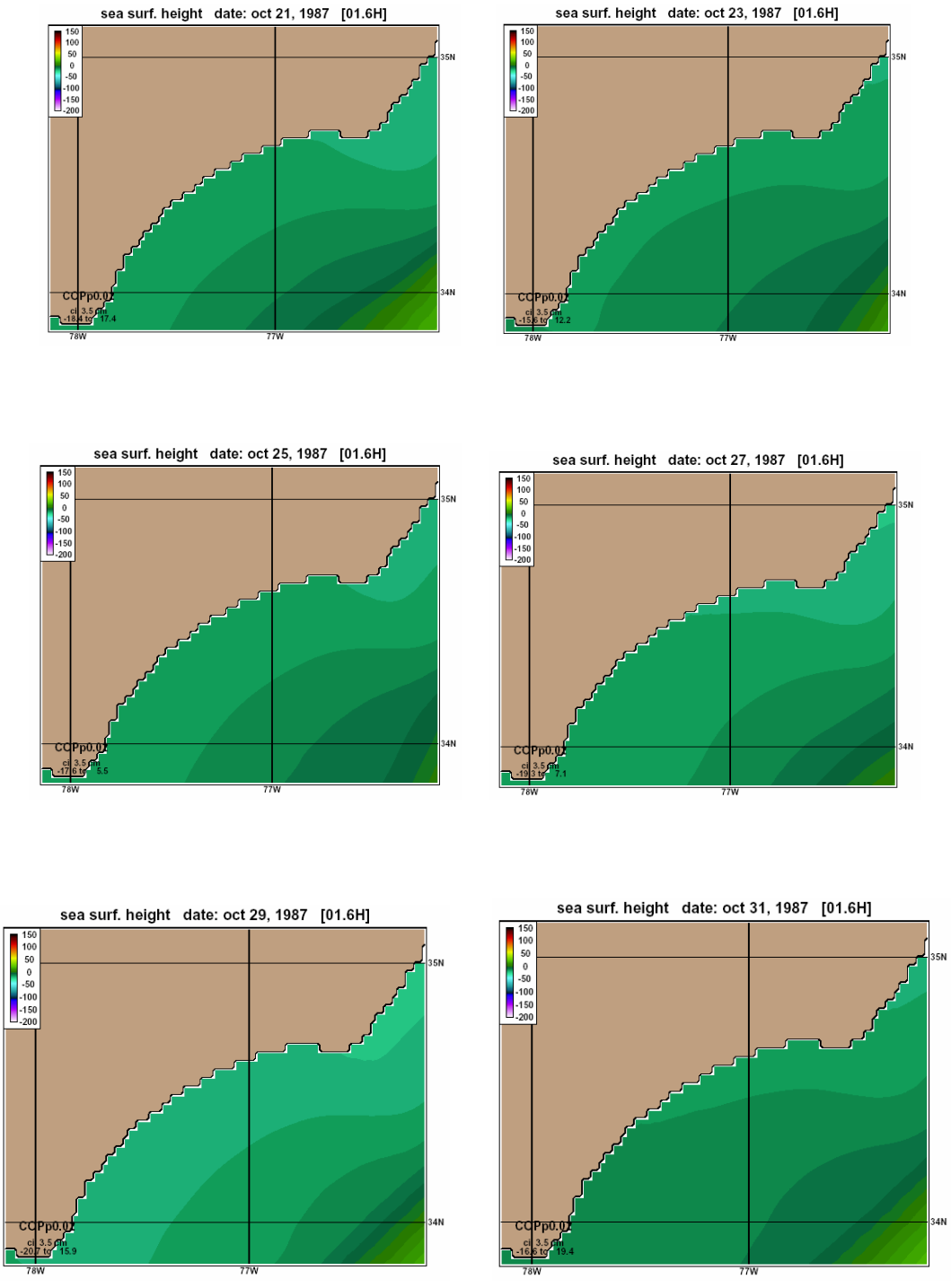


Figure 13 SSH on October 21, 23, 25, 27, 29 and 31 in Simulation V

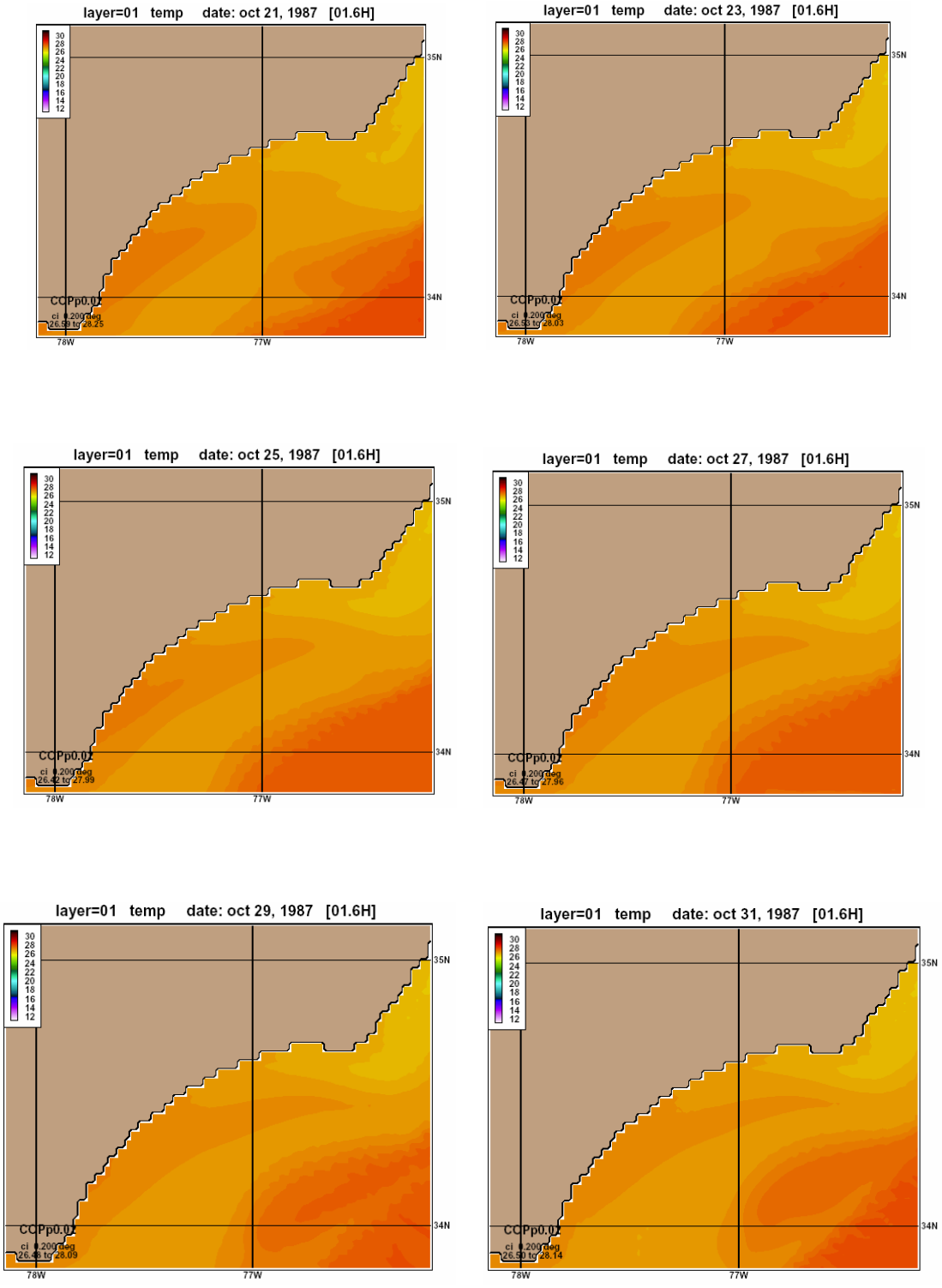


Figure 14 SST on October 21, 23, 25, 27, 29 and 31 in Simulation V

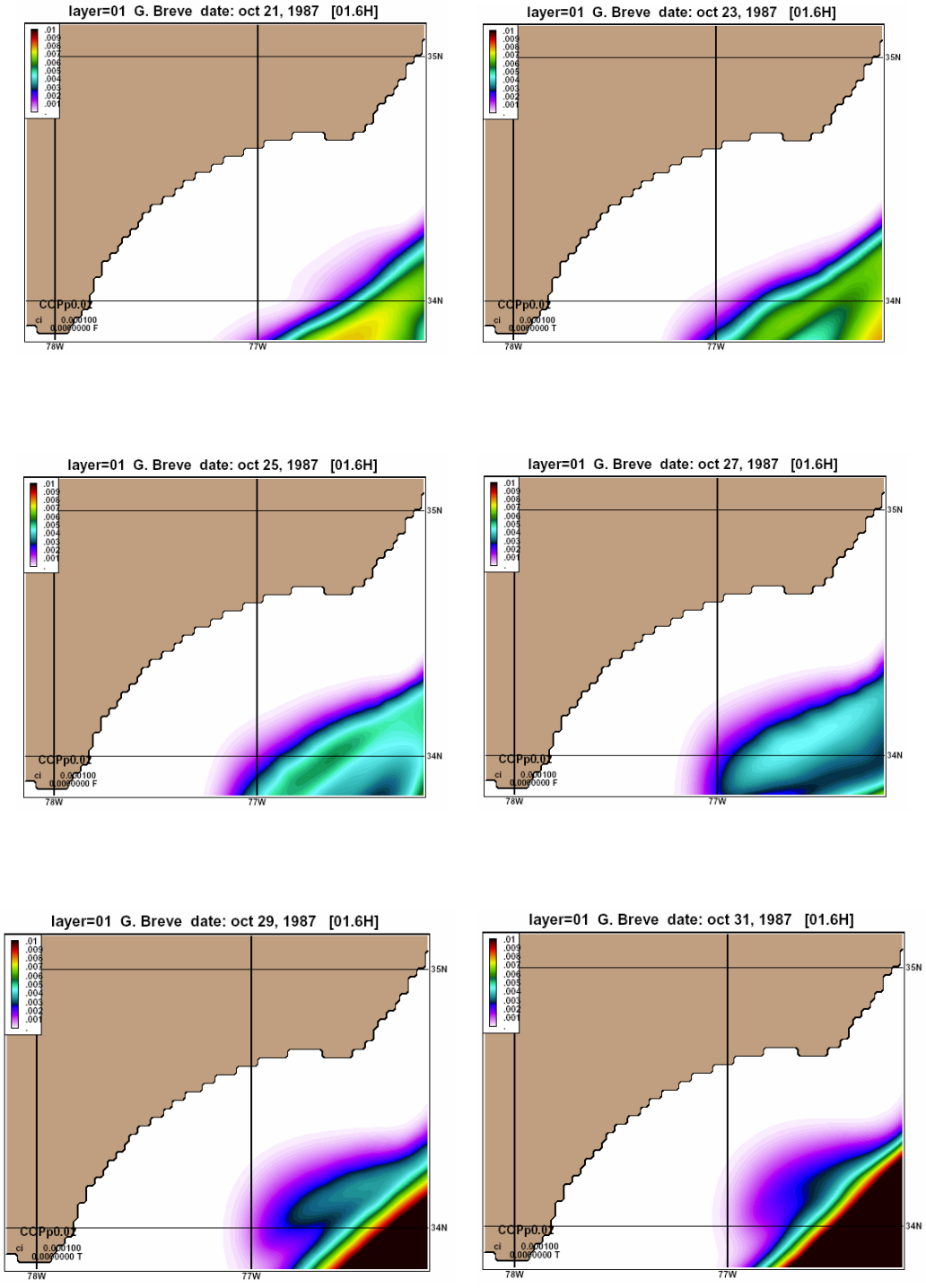


Figure 15 Passive tracer concentration on October 21, 23, 25, 27, 29 and 31 in Simulation V

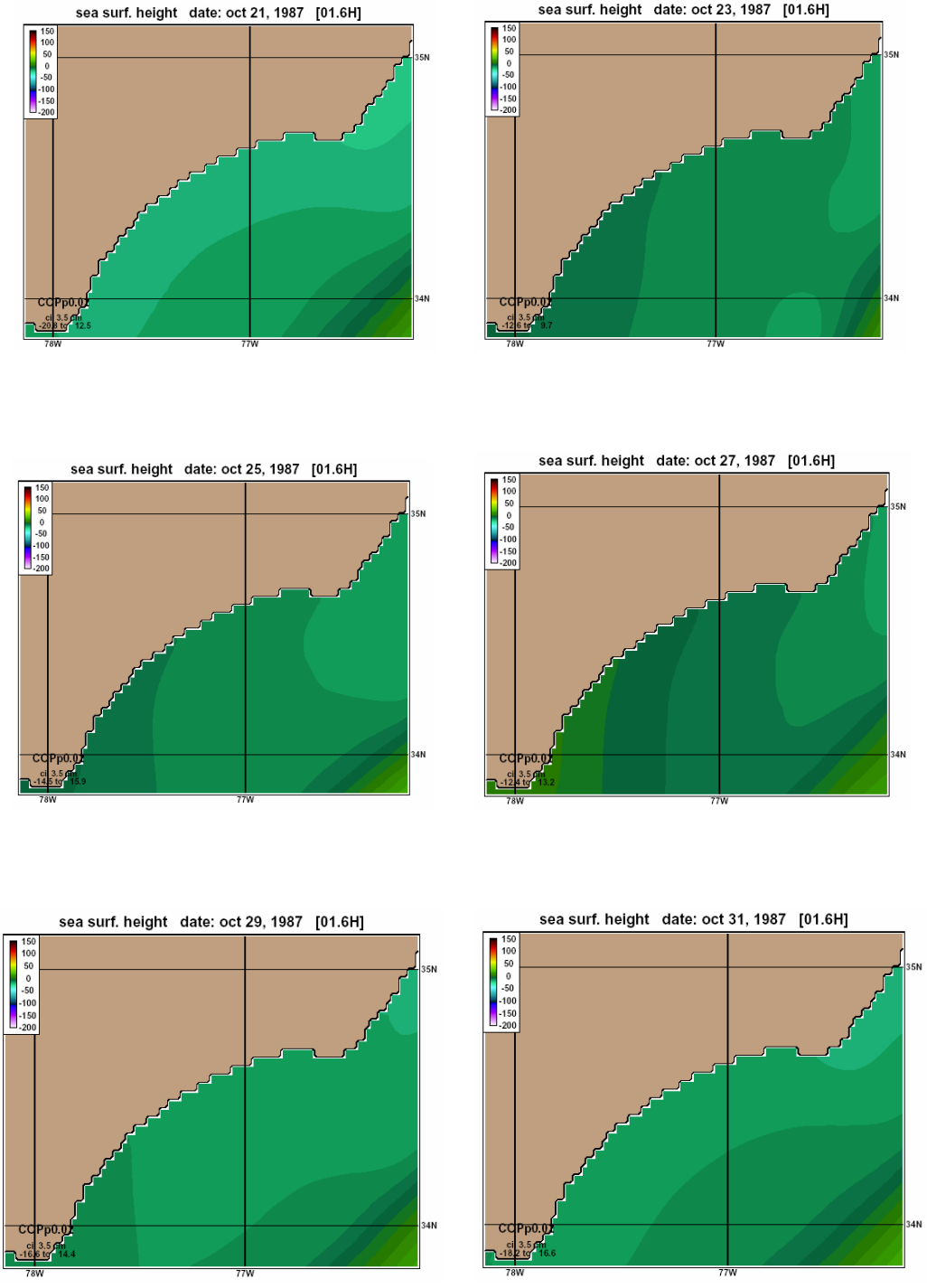


Figure 16 SSH on October 21, 23, 25, 27, 29 and 31 in Simulation VI

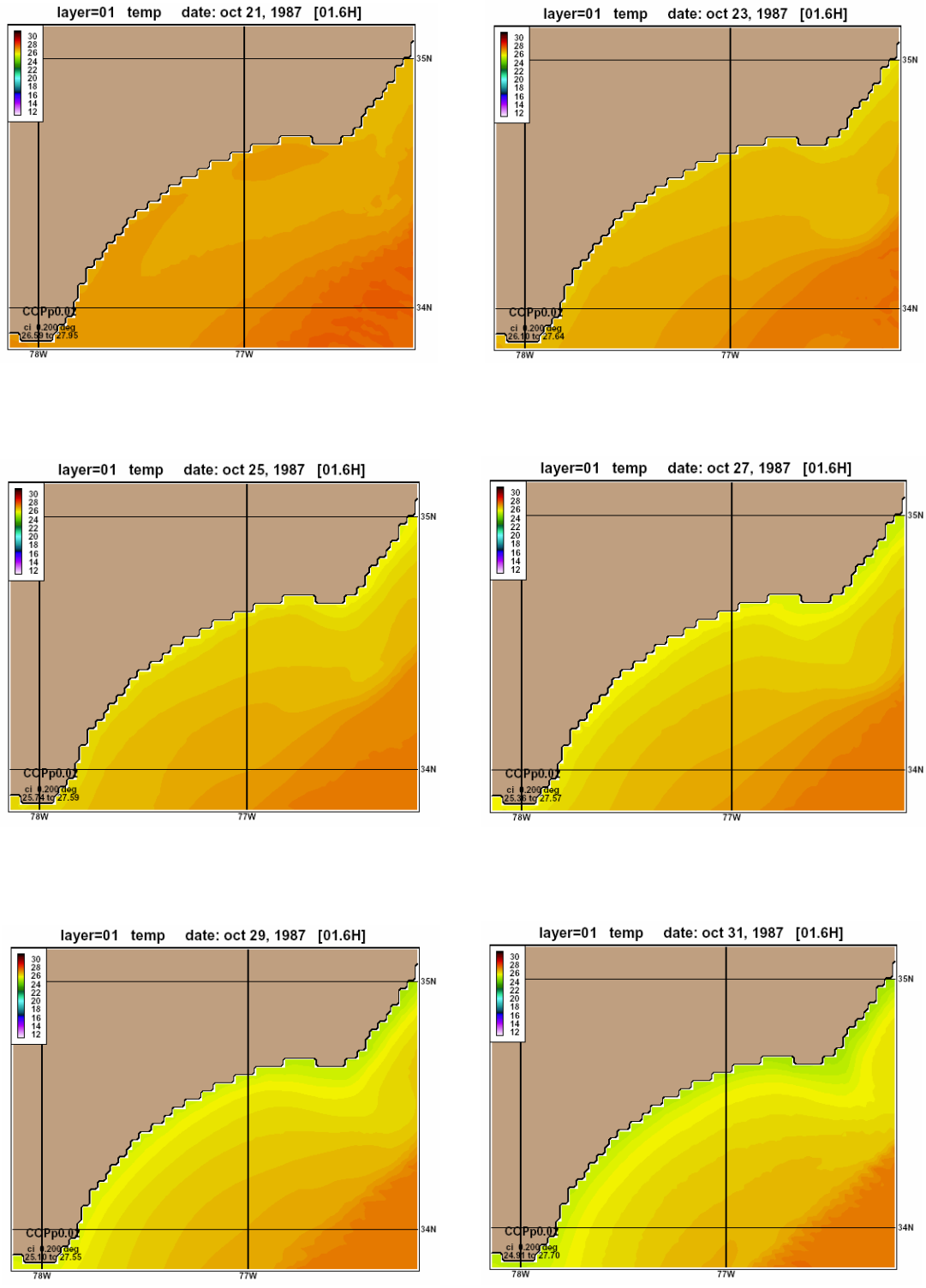


Figure 17 SST on October 21, 23, 25, 27, 29 and 31 in Simulation VI

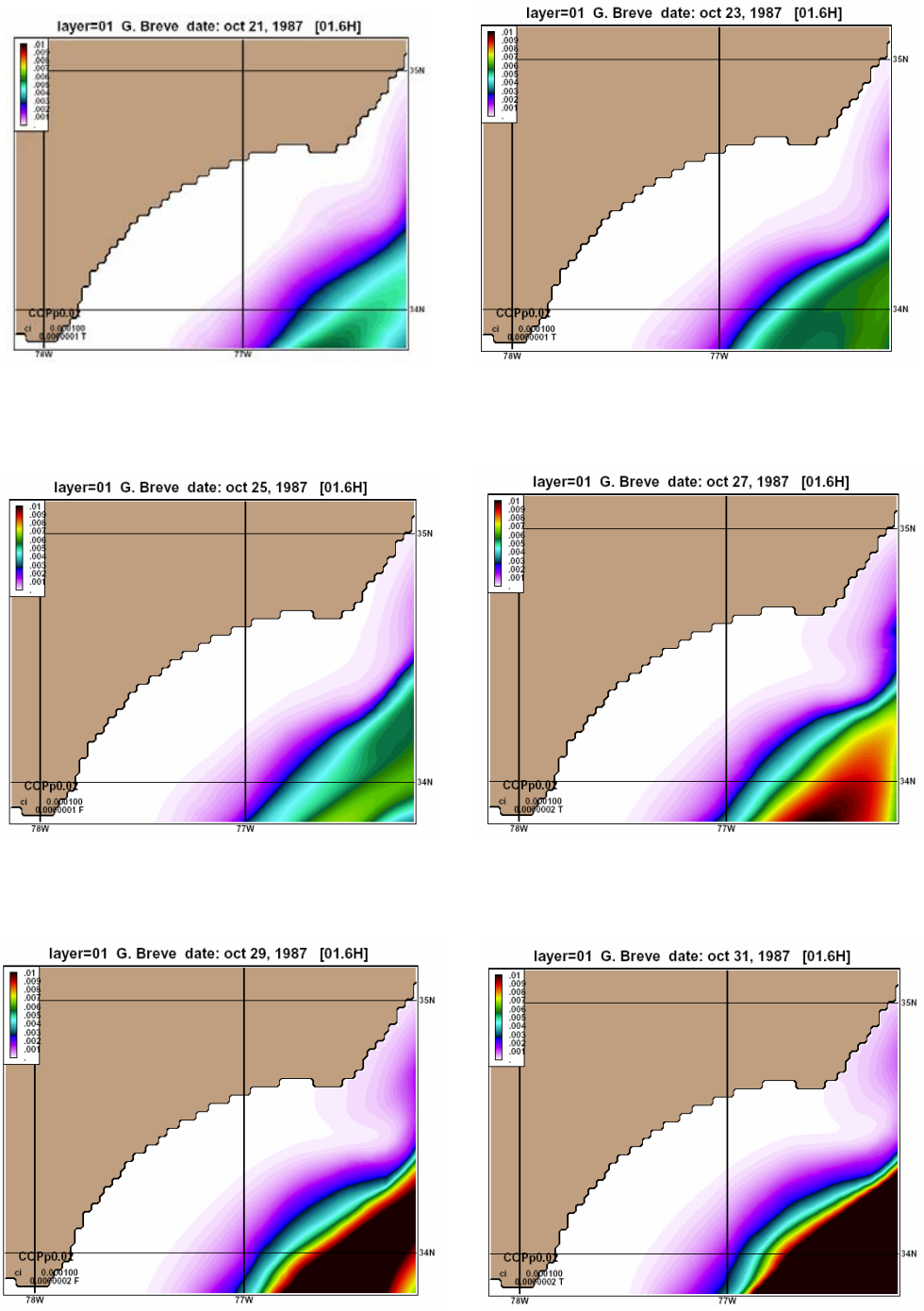


Figure 18 Passive tracer concentration on October 21, 23, 25, 27, 29 and 31 in Simulation VI

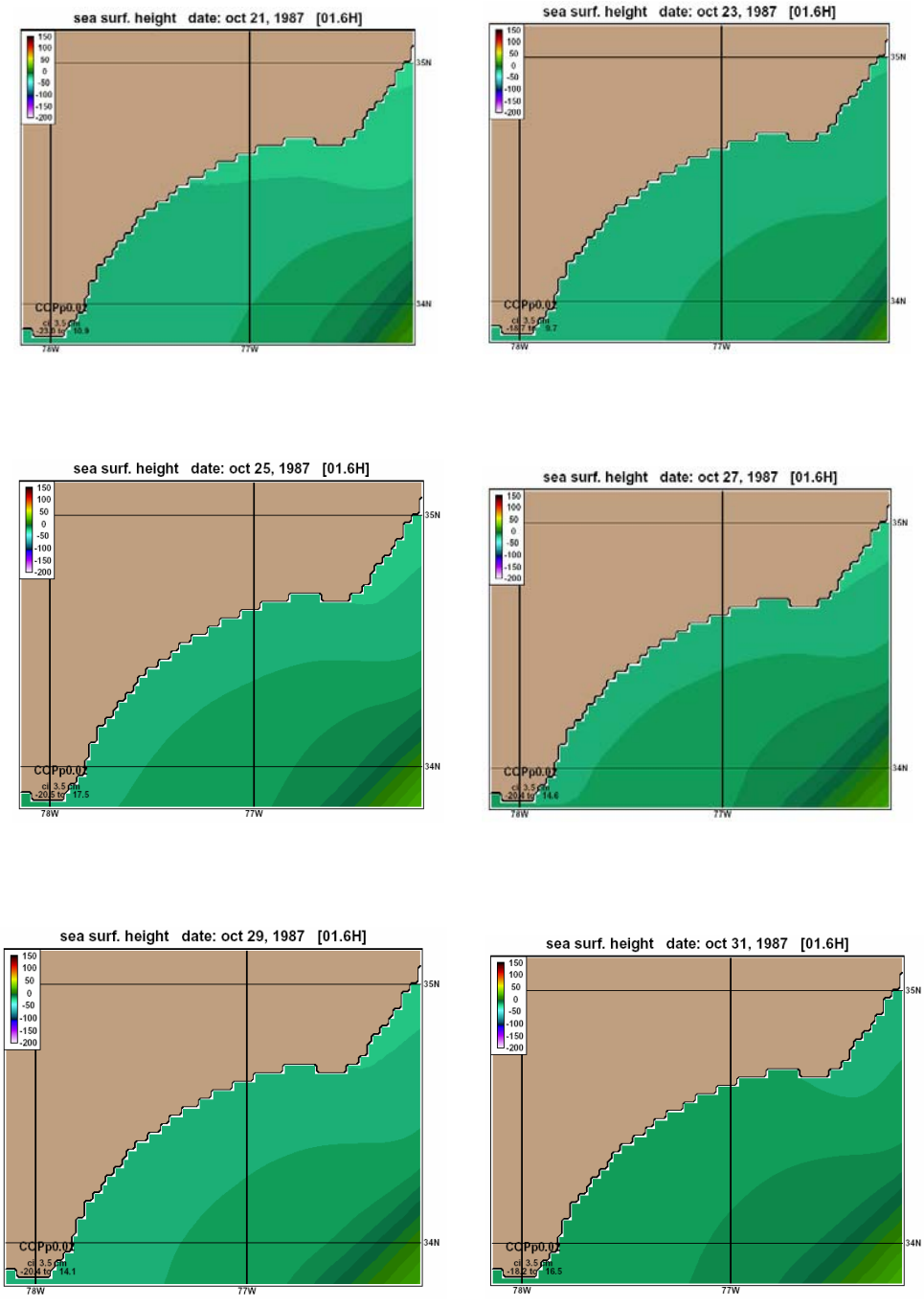


Figure 19 SSH on October 21, 23, 25, 27, 29 and 31 in Simulation VII

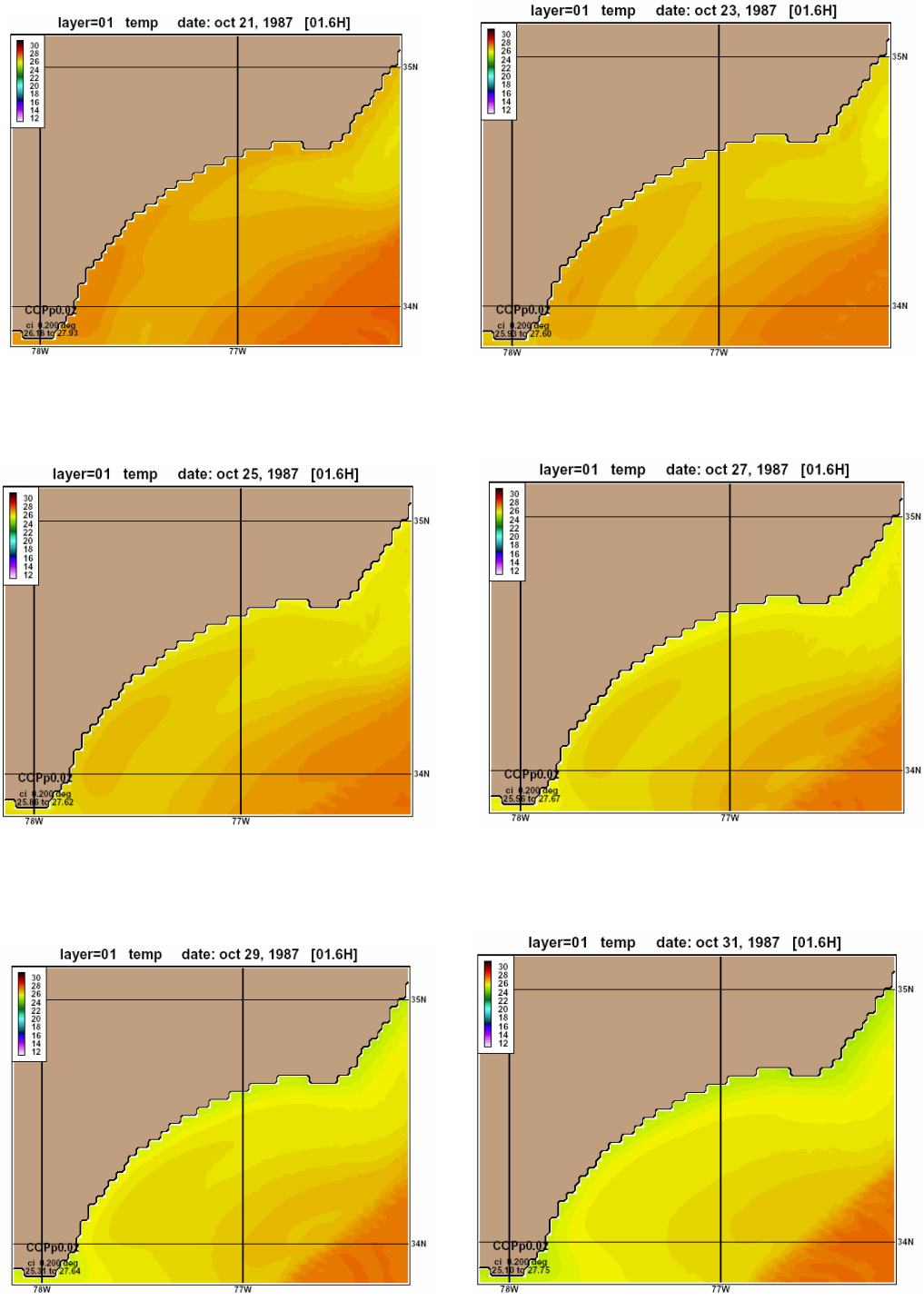


Figure 20 SST on October 21, 23, 25, 27, 29 and 31 in Simulation VII

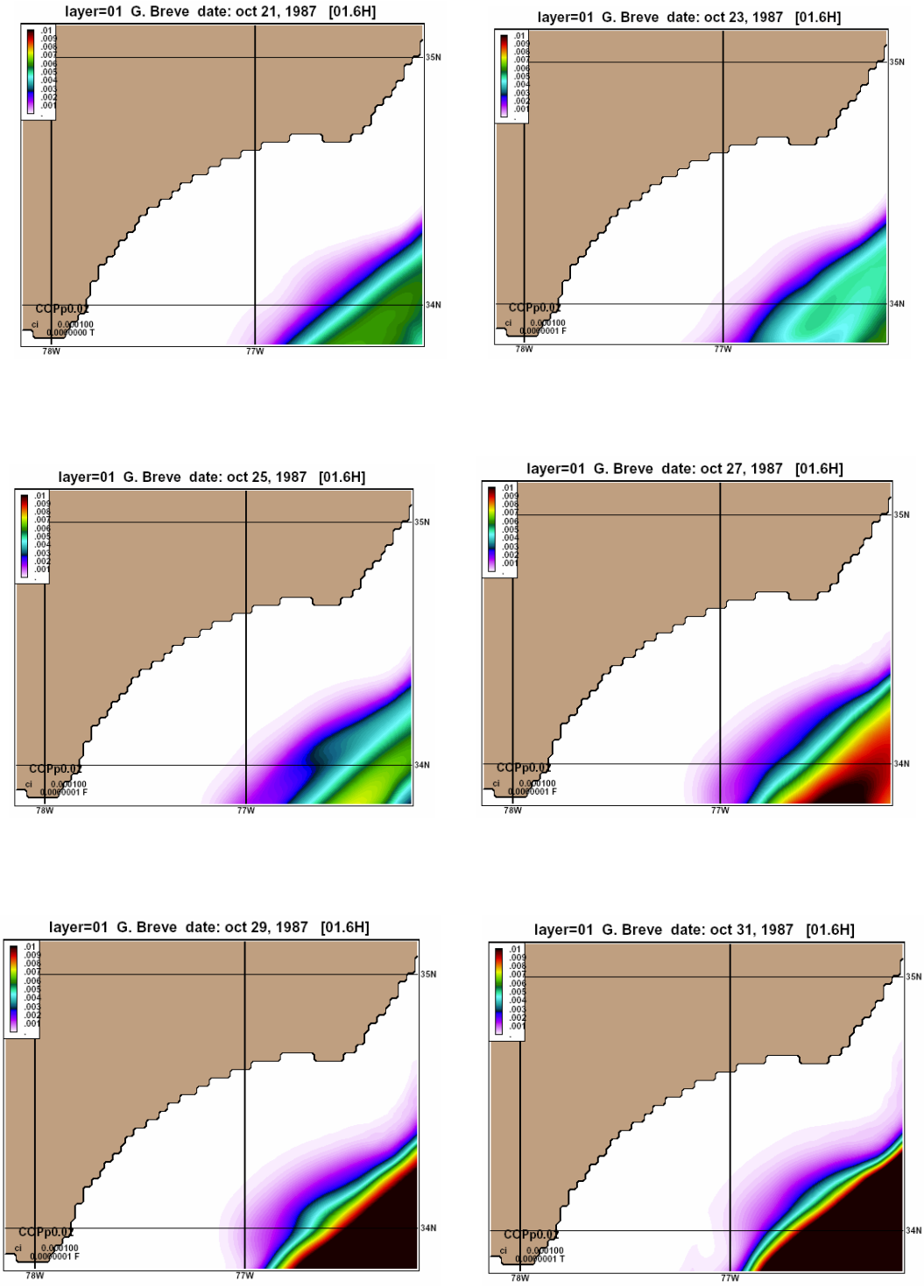


Figure 21 Passive tracer concentration on October 21, 23, 25, 27, 29 and 31 in Simulation VII

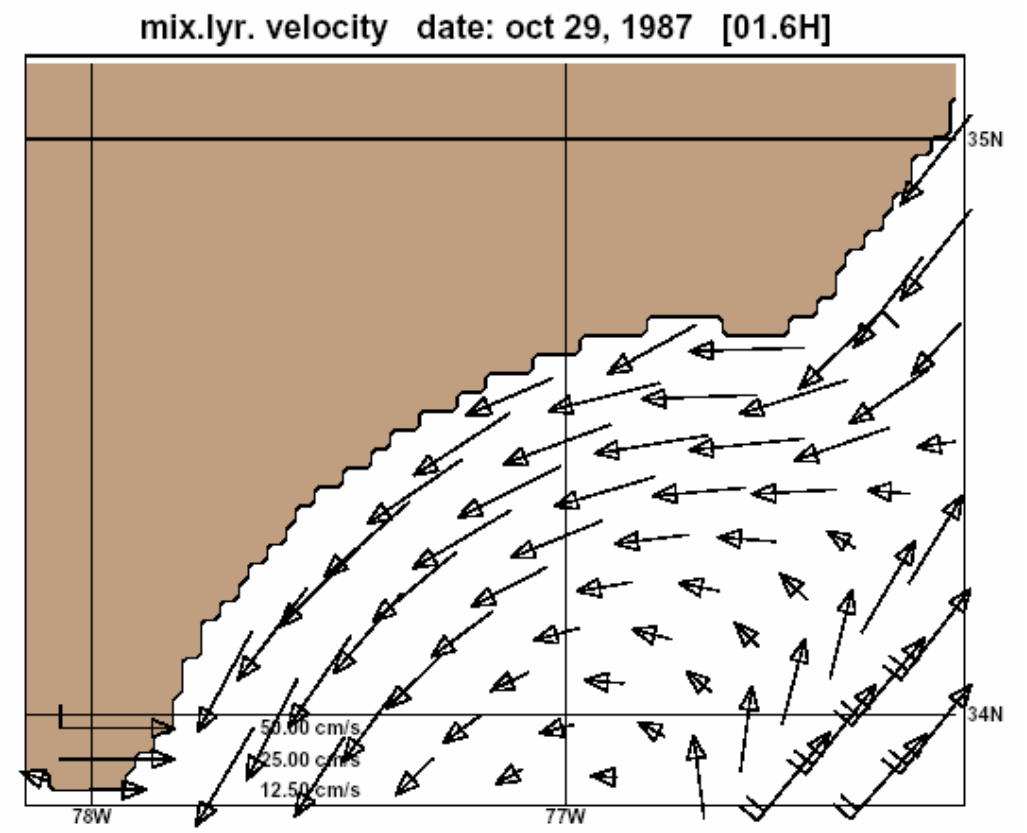


Figure 22 Mixed-layer horizontal velocity on October 29, 1987 in Simulation IV.

Chapter 6

Future Work

1. Data assimilation

Simulations of oceanic circulation can be improved by assimilating observations. Simulations without data assimilation contain errors due to inadequate knowledge of the ocean's initial/boundary conditions and its forcing by the atmosphere as well as those that are due to deficiencies in the model's dynamics. These errors can be corrected by assimilate available observations into model simulations. HYCOM has been a leader in the application of data assimilation techniques for operational ocean predictions. HYCOM is characterized by its treatment of the vertical coordinate. While conventional models employ as so-called z-coordinate with oceanic fields computed on a grid of points separated by fixed distances, HYCOM describes the ocean in terms of a stack of layers whose thicknesses and characteristics change dynamically as the flow evolves. For the bulk of the ocean the layers should correspond to water of specified densities in order to capture the well-defined stratification, while near the surface where the water is mixed, the layers are specified by their distances from the surface rather than density, and in shallow regions their thicknesses are proportional to the local water depth. Such a modeling strategy allows HYCOM to use the optimal coordinate system for each region and to transform naturally from one to the other.

The simplest method for assimilating data into HYCOM is optimal interpolation, where the corrections to the model state are based on the differences between the simulation and the observations with the size and influence of the corrections determined by the error covariances of both model and data. Current efforts toward at making HYCOM operational are centering on a data-assimilation package the Navy has developed for use with more conventional models. Ensemble Kalman Filter (Evensen, G. 1994) is an advanced data assimilation technique that is implemented in HYCOM. The EnKF is a sophisticated sequental data assimilation method. It applies an ensemble of model states to represent the error statistics of the model estimate, it applies ensemble integrations to predict the error statistics forward in time, and it uses an analysis scheme which operates directly on the ensemble of model states when observations are assimilated. The EnKF has proven to efficiently handle strongly nonlinear dynamics and large state spaces and is now used in realistic applications with primitive equation models for the ocean and atmosphere. Navy Research Library (NRL) in collaboration with the Nansen Environmental and Remote Sensing Center (NERSC), Bergen, Norway has implemented EnKF in HYCOM, and a version of EnKF code that is tailored for HYCOM can be downloaded at http://enkf.nersc.no/. The package has been downloaded and successfully compiled on the IBM Power 5 supercomputer at NSCU. However, further work needs to be done to prepare data input to run a case study.

2. Biological modeling

The process of red tide bloom is a complicated biological-physical process. Tester et al (1991) analyzed the cell count sampling during the red tide bloom event, along with

satellite SST images and observed wind. It is found that the transport of cells onto the inner continental shelf may have resulted from the large meanders of the Gulf Stream. The warm filament associated with this meander persisted on the continental shelf for at least 19 days, and inshore surface waters of both Onslow and Raleigh Bays were warmed. Both wind speed and direction are important in determining its distribution. It is concluded that the persistence of the filament in the inshore area for nearly 3 weeks in October-November 1987 is the key factor that could have provided ample time for cell division and bloom development. Therefore, the biological model needs to be coupled with the physical model to simulate this process.

The current version of HYCOM model contains the implementation of two ecosystem models with different compartments: Nutrient-Phytoplankton-Zooplankton (NPZ) and (Nutrient-Phytoplankton-Zooplankton-Detritus) NPZD. The NPZ (Nutrients-Phytoplankton-Zooplankton) model describes a simple food web system in which nitrogen is used as a tracer for the stable variables: dissolved nutrients are taken by the phytoplankton following Michaelis-Menten kinetics, phytoplankton are grazed by zooplankton with an Ivlev functional response and nutrients are regenerated from the source of the mortality of phytoplankton and zooplankton and egestion from zooplankton. A detailed description of NPZ model can be seen in Franks et al. (1986) and Franks and Chen (1996). NPZD model is an extension of the NPZ model in that one more component, detritus, is added.

A more advanced ten-compartment ecosystem model has been developed by Chai Fei (2002). This model contains compartments representing two size of phytoplankton, small phytoplankton cells (P1) and diatoms (P2), micro- and meso-zooplankton (Z1 and

Z2), nonliving detrital nitrogen and silica (DN and DSi), dissolved silicic acid (Si), two forms of dissolved inorganic nitrogen: nitrate (N1) and ammonium (N2), and total CO_2 (T CO_2). The one-dimensional version is ready for release, however, the 3D version that are coupled with HYCOM are under development and will be available in the future. Depends on the needs of biological application, one of the three different ecosystem models with different complexity can be selected to suit the requirement of a particular application.

3. Ocean Prediction

The long-term objective of this study is to develop a coastal ocean prediction system in SAB. At present, there are several coastal ocean observing and prediction systems in different regions along the U.S. coast. Along the east coast, for example, East Coast Ocean Forecast System (ECOFS), which covers the east coast of North America from Florida to New Foundland, Canada, is operated by NOAA. In the Gulf of Maine, Gulf of Maine Ocean Observation System (GoMOOS) numerical model is embedded in the ECOFS in that the ECOFS provides open boundary condition for the Gulf of Maine model. In the west coast, there is a Prince William Sound Nowcast-Forecast (PWSNF) in Alaska and JPL U.S. West coastal (USWC) in California. In the Gulf of Mexico, Coastal Ocean Monitoring and Prediction System (COMPS) covers the entire West Florida Shelf, with an offshore boundary stretching from the Mississippi Delta to the Florida Keys. Since SAB is one of the most important coastal region along the U.S. coast, a coastal ocean prediction in the SAB will great benefit its economy and environment.

4. References

Atkinson, L.P., Hydrography and nutrients of the southeastern U.S. continental shelf, in Oceanography of the Southeastern U.S. Continental shelf, Coastal and Estuarine Sci., vol. 2,AGU, Washington, D.C., 1985

Blaha, J., and B. Lunde, 1992: Calibrating Altimetry to Geopotential Anomaly and Isotherm Depths in the Western North Atlantic, Journal of Geophysical Research, 97, 7465-7477.

Bleck, R., An oceanic general circulation model framed in hybrid isopycnic-Cartesian coordinate, Ocean Modeling, 4, 55-88

Chin, T.M., A.J. Mariano and E.P. Chassignet, 1999: Spatial regression with Markov Random Fields for Kalman filter approximation in least-squares solution of oceanic data assimilation problems. Journal of Geophysical Research, 104, 7991-8014.

Cooper, M. and K. Haines, 1996: Altimetric assimilation with water property conservation. Journal of Geophysical Research, 101,1059-1077

Dunstan, W.M., and L.P. Atkinson, Source of new nitrogen for the South Atlantic Bight, in Estuarine Processes, Uses, Stresses, and Adaptation to Estuary, vol. 1, edited by M. Wiley, pp. 69-78, Academic, Orlando, Fla., 1976

Evensen, G. 1994: Sequential data assimilation with a nonlinear quasi-geostrophic model using Monte Carlo methods to forecast error statistics. Journal of Geophysical Research, 99, 10143-10162.

Fox, D.N, W.J. Teague, C.N. Barron, M.R. Carnes and C.M. Lee, 2001: The Modular Ocean Data Assimilation System, Journal of Atmospheric and Oceanic Technology (accepted).

Franks, P.J.S, NPZ models of plankton dynamics: their construction, coupling to physics and application, Journal of Oceanography, vol. 58, pp. 379-387, 2002

Gavart, M. and P. De Mey, 1996: Isopycnal EOFs in the Azores Current Region: A statistical tool for Dynamical Analysis and Data Assimilation, Journal of Physical Oceanography, 27, 2146-2157

Hulbert, E.M., Some notes on the phytoplankton of the southeastern coast of the United States, Bull. Mar. Sci., 17, 330-337, 1967

Hurlburt, H. E., D. N. Fox and E. J. Metzger, 1990: Statistical inference of weakly-correlated subthermocline fields from satellite altimeter data. Journal of Geophysical Research, 95, 11375-11409.

Kelly, K. A., and S. T. Gille, 1990. Gulf Stream surface transport and statistics at 69~W from the GEOSAT altimeter, J. Geophys. Res. 95, 3149--3161.

Koblinsky, C. J., R. Ray, B. D. Beckley, Y-M. Wang, L. Tsaoussi, A. Brenner and R. Williamson, 1999: NASA Ocean Altimeter Pathfinder Project, Report 1: Data Processing Handbook, NASA/TM-1998-208605, (http://neptune.gsfc.nasa.gov/ocean.html).

Lee, T, et al, Gulf Stream Frontal eddy Influence on Productivity of the Southeastern U.S. continental shelf, JGR, 96, 22,191-22,105, 1991

Lozier, M. S., W. B. Owens and R. G. Curry, 1996. The climatology of the North Atlantic, Progress in Oceanography, 36, 1--44.

Mariano, A.J. and O.B. Brown, 1992: Efficient objective analysis of dynamically heterogeneous and nonstationary fields via the parameter matrix. Deep-Sea Research, 39 (7/8), 1255-1271.

Marshall, H.G., Composition of phytoplankton off the southeastern coast of the United States, Bull. Mar. Sci., 21, 806-825, 1971

Newberger, P.A., et al, Analysis and comparison of three ecosystem models, JGR, vol. 108, No. C3, 3061, 2003

Paffenhoffer, G.A. et al., Summer upwelling on the southeastern continental shelf of U.S.A. during 1981, Abundance, distribution and patch formation of zooplankton, Progress of Oceanography, 19, 403-436, 1987

Paffenhoffer, G.A. et al., The relation of concentration and size distribution of suspended particulate matter to hydrography in Onslow Bay, North Carolina, Deep Sea Res., 27, 435-448, 1980

Paffenhoffer, G.A., Aboundance and Distribution of Zooplankton on the southeastern Shelf of the United States, in Oceanography of the Southeastern U.S. Continental shelf, Coastal and Estuarine Sci., vol. 2,AGU, Washington, D.C., 1985

Pham, D.T., J. Verron and M.C. Roubaud, 1998: A singular extended filter for data assimilation in oceanography. Journal of Marine Systems, 16, 323-340.

Wang, Y.M., 2000: The satellite altimeter data derived mean sea surface GSFC98, Geophysical Research Letters, 27, 701-704.

Yoder, J.A., et al., Effect of upwelling on phytoplankton productivity on the outer southeastern U.S. continental shelf, Continental Shelf Res., 1, 385-404, 1983

Yoder, J.A., et al., Phytoplankton dynamics within Gulf Stream intrusions on the southeastern United State continental shelf during summer, 1981, Cont. Shelf Res., 4, 611-635, 1985